NRSP-2
01-36

TILSO

"Tianjin InSAR Land Subsidence Observation" Demonstration Project

A. ten Katen
B.M. Kampes
R. van Bree
R.F. Hanssen
L.M.Th. Swart
Jia Youliang
Lu Xu

BELEIDSCOMMISSIE REMOTE SENSING

TILSO

"Tianjin InSAR Land Subsidence Observation" Demonstration Project

A. ten Katen
EARS Remote Sensing
B.M. Kampes
Delft Institute of Earth Oriented Space Research,
Delft University of Technology (DEOS)
R. van Bree
Netherlands Organization for Applied
Scientific Research, Physics and Electronics
Laboratory (TNO-FEL)
R.F. Hanssen
L.M.Th. Swart
Delft Institute of Earth Oriented Space Research,
Delft University of Technology (DEOS)
Jia Youliang
Lu Xu
Tianjin Control Landsubsidence Office (TCLO)

NRSP-2 report 01-36
NRSP-2 project 3.1/DE-32

ISBN 90 54 11 379 0

October 2001

This report describes a project carried out in the framework of the National Remote Sensing Programme (NRSP-2) under responsibility of the Netherlands Remote Sensing Board (BCRS)

CONTENTS

Preface

The body of this report was written by R. van Bree, B. M. Kampes, A. ten Katen and L. M. Th. Swart. The text in section 2.1 "SAR interferometry" is copied from a paper by R. Klees and R.F. Hanssen as was written for a summer school, parts of this paper that were not relevant have been removed; Figure 6 was replaced by an image of Tianjin area. There i0s no principal author, please regard this report as a writing by all people mentioned above.

The processing was done on Alpha / HP workstation with operating platform UNIX. PC based computers were used operating on NT and RedHat Linux.
Following software was used: ESARP, Getorb, Doris, cpxfiddle, GMT, Latex, GhostScript, Aladin, Matlab, Microsoft Office.

The final version of this report was made with Microsoft Word.
The number of color images in this report is limited to the figures 42, 43, 51, 30-35, 39, 44, 47 and 49; the color versions can be found in appendix D. To obtain a full color version, this document is also made available via the website of the DIG (Dutch Interferometry Group): www.geo.tudelft.nl/fmr/research/insar/dig/dig.html

Abstract

This report is the reflection of a demonstration project on the measurement of subsidence using satellite data. The target area consists of the coastal areas of Tianjin province, China, this area includes one of China's major cities named Tianjin. Calculations have been made on basis of 25 radar images acquired by the ERS-1 and ERS-2 satellites. With these data it is possible to obtain land surface deformations over a period of several months at an accuracy of less then a centimeter.
Two methods have been applied. Interferometric SAR processing (InSAR) and Permanent Scatterer SAR processing (PS-method). The InSAR method was only successful in urban areas. It was shown that InSAR results could be used to enhance and/or replace part of the traditional subsidence measurement as is done by conventional leveling. The PS-method was only successful for simulated data; no reliable subsidence figures were obtained. Though it is mentioned that, already during the final editing of this report, further research into the PS-method showed successful measurements outside the urban areas in Tianjin. The over all conclusion of the report was that in the near future large parts of the leveling work can be replaced by interferometric measurements, provided that research is continued.

Summary

This report is the reflection of a demonstration project on the measurement of subsidence using satellite data. The target area consists of the coastal areas of Tianjin province, China, it includes Tianjin city. With 6 million inhabitants, Tianjin city is one of the major cities in China. Subsidence is a major problem in the coastal areas of Tianjin province. The subsidence exists due to the combination of groundwater extraction and the presence of thick unconsolidated sediment layers in this area. The subsidence is monitored by leveling along an extensive network throughout the coastal areas. In this project it was investigated and demonstrated to what extend radar interferometry might improve the present monitoring.

The project was carried out in co-operation between the following partners

- Tianjin Control Landsubsidence Office (TCLO), Tianjin, China.
- Netherlands Organization for Applied Scientific Research, Physics and Electronics Laboratory (TNO-FEL), The Hague, The Netherlands.
- Delft Institute of Earth Oriented Space Research, Delft University of Technology (DEOS), The Netherlands.
- HOFUNG, Beijing, China.
- EARS Remote Sensing, Delft, The Netherlands.

HOFUNG acted as intermediary, this was essential for a smooth preparation and progress of the project. DEOS and TNO-FEL concentrated on the processing of radar imagery and the evaluation of the results. EARS, the principal contractor, carried out a cost-effectiveness study of the methodology, in co-operation with the end user TCLO. The benefits of the methodologies have been assessed.

In radar interferometry the phase of at least three images is combined to create certain interferometric effects that can be used to measure surface deformations. The use of Synthetic Aperture Radar (SAR) as an interferometer is rather new due to the stringent requirements on the stability of the satellite orbit. InSAR offers the possibility to map the Earth's land and ice topography and to measure small displacements over large temporal and spatial scales with sub centimeter accuracy, in general independently of the sun's illumination and the cloud coverage. These properties make InSAR a unique technique that combines the high accuracy of classical geodetic techniques such as DGPS and leveling with the imaging property modern remote sensing techniques. Recent examples have demonstrated that InSAR can be applied to study a variety of deformation processes, e.g. land subsidence due to the withdrawal of water, gas, and oil, the co-seismic and post-seismic displacement field related to earthquakes etc.

For the measurement of subsidence in Tianjin two methods have been applied: a) InSAR and the b) PS-method.

a) Subsidence measurement using InSAR
Temporal decorrelation is a major limiting factor if one wants to apply InSAR. Already after a time span of only 35 days, most of the (rural) area is decorrelated due to plant growth etc. Only urban parts, mainly the cities of Tianjin and Tangu, remain coherent. Therefore, we have selected the city of Tianjin as primary target area for the InSAR processing. Topographic signal can be neglected for this area, since the maximum

topographic difference is only 10 meters. Another limiting factor, besides temporal decorrelation, is atmospheric disturbance. This can be a significant signal over larger areas, depending on the weather conditions during the acquisitions (may be approximately 1 fringe over Tianjin area). In order to show this effect an interferogram was processed with a small perpendicular and temporal baseline. Averaging over a number of interferograms has reduced the atmospheric signal in the final deformation map. It was concluded that reliable deformation maps can be formed for urban areas. Unwrapping problems arise at the edges of the coherent areas. A different unwrapping algorithm may be able to improve this, although the real noisy parts can never be unwrapped. Using larger temporal baselines can improve the results, since the deformation signal is relatively larger in that case. The drawback is that temporal decorrelation also will be larger

b) Subsidence measurement using the PS-method
With the use of the PS-method almost all interferograms from ERS-1/ERS-2 over a certain area can be used. For this method uniform baseline coverage, in time as well as spatial, is preferred. Contrary to the usual InSAR method large temporal baselines are no problem for the PS-method. If a topographic correction with accuracy of about 10m height can be applied, large perpendicular baselines can be accepted as well. Despite the effort made to calculate proper subsidence figures, the method was only successful for simulated data. Already during the final editing of this report further research into the PS-method by the TU-Delft showed positive result outside the urban areas in Tianjin, note that this work was not done under the contract of this project and is not included here.

Conclusions
Following statements summarize the results achieved.
- The demonstration of the conventional InSAR in Tianjin was successful in the urban areas. It was made clear that in the urbanized areas of Tianjin interferometry is useable to reduce the cost of the leveling campaign and improve its results. It is possible to reduce the amount of benchmarks of the leveling network, to simplify the interpretation of the leveling results into contour maps and to indicate where extra leveling measurements might be required. Outside the urban areas coherence was lost, and consequently conventional InSAR is of no use.
- The demonstration of the relatively new method of "Permanent Scatterers" (PS) on the Tianjin data was not satisfactory. Despite this, it is expected that in the near future this technique will provides individual measurements over the whole SAR image, even for scenes showing decorrelation in the classical approach, and therefore be a highly valuable tool.
- A major drawback at present is the decreased availability of SAR data. During the project the orbit of the ERS-2 satellite became less stable; the future ERS data are therefore less applicable for interferometry. At the moment the only other satellite available is RADARSAT. In the coming years several other radar satellites will be launched that can be used for interferometry like ENVISAT (autumn 2001) and RADARSAT2 (April 2003).
- The cost for implementing an InSAR system for measurement of subsidence in Tianjin does not have to be very high. Commercial software is expensive but the use may be justified when compared to the total cost of the leveling campaign. The low budget set up within this project works well and may well be preferred above commercial packages for reason of higher level of user control and better performance.

1 INTRODUCTION

1.1 Problem definition

The Tianjin municipality is situated on the coast of China on 117°15″ East, 39°10″ about 200 km South East of Beijing. It covers an area of about 3000 square km. Tianjin is a major Chinese city ("city province") with 9 million inhabitants. It is the main harbor for Beijing and the north of China. After the Shanghai and Beijing municipalities, Tianjin is economically the third most important center of China. The climate is moderate. Temperatures vary between –2 degrees in winter and 26 in summer. The rainfall is concentrated in summer, the annual precipitation is about 600 mm. The humidity in the area varies from about 50% in winter up to 75% in summer.

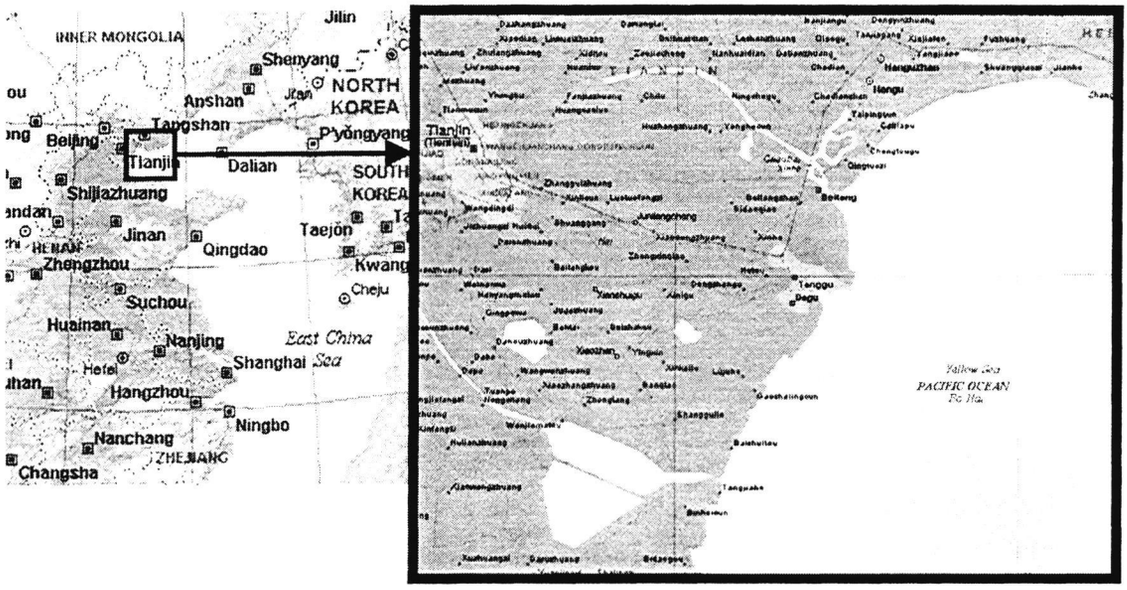

Figure 1 Tianjin area (the enlarged section is comparable with the ERS radar image coverage).

Subsidence due to groundwater extraction has become a major problem in this municipality. This problem has been acknowledged since 1959. Since 1985 a yearly leveling campaign is carried out. The total stretch measured each year is 3000 km. The leveling measurements have shown that since 1959 the total subsidence in this area can be as high as 3 meter. Subsidence speeds in the order of 50 mm/year are common. Governmental regulation has resulted in a decreased subsidence. In the coastal areas outside Tianjin the subsidence rate is still high.

The local government has paid much attention to the subsidence problem. In 1969 the Tianjin Control Land subsidence Office (TCLO) was established to study and monitor this. The tasks of the organization include policy making, implementation and management. The yearly leveling surveys are stored in a database. The leveling data consist of point measurements with a density of approximately one point per four square kilometer. Continuous subsidence maps are produced by interpolation between the points. The

collection of this information puts very high demands on financial resources: in the order of 1 million US dollar per year. For this reason the TCLO has actively been considering the potential of new technologies to improve the cost to benefit ratio of their work. One of these new techniques is the use of the U.S. Global Positioning System (GPS). In 1998 a GPS measuring network has been established in part of the area. Another relatively new technique with a high potential in this respect is SAR interferometry (InSAR). This report contains a study on the application of this technique.

The use of InSAR techniques can give a more detailed view of the subsidence areas [Haynes et al., 1997]; [van der Kooij et al, 1997]; [Stow et al., 1997]; [Wegmuller et al., 1998]. The technique can also isolate local subsidence pits, which are easily missed by the GPS/leveling network. The main restriction when using InSAR is that one needs a coherent area over a reasonable period of time, say, one or two years. The best coherent areas are mostly urban areas with manmade structures, or very dry desserts with very little vegetation. The area under study is partially covered with urban areas but most of it is agricultural (rice fields) or bare land with or without vegetation. Using the InSAR technique could give a good result for the coherent areas as mentioned above. To overcome the 'coherent area' restriction effort was made to apply a new technique called "the Permanent Scatterer technique". This technique is developed by [Ferretti et al., 1999] and was used successfully [Ferretti et al., 2000].

1.2 Objective

The objectives of the project are

- To demonstrate the InSAR subsidence monitoring technology, as developed in the Netherlands, for practical ground subsidence monitoring applications to the Tianjin Control Landsubsidence Office.
- To investigate the potential of InSAR subsidence monitoring technology for commercial market development by a Dutch consortium consisting of a university, an organization for technological research and a remote sensing company.
- To demonstrate the possibilities of a new development within the InSAR technology referred to as 'Permanent Scatterers' (PS).

1.3 Project set up

In August 1998 a delegation from Tianjin municipality visited EARS Remote Sensing in Delft, the Netherlands to be informed about the InSAR technology that has been developed in the Netherlands, in particular by TNO-FEL and Delft University of Technology-DEOS. The delegation was also informed about the application of this technology to subsidence monitoring in the Netherlands, where the conditions are not very different from Tianjin. The idea of co-operation between Dutch and Chinese parties, to test the technology for practical implementation in Tianjin, was born. November 1998, EARS made a return visit to China where a follow-on meeting took place and further project preparation was done.

The present project proposal is the result. The project was carried out in co-operation between the following partners

- Tianjin Control Landsubsidence Office (TCLO)
- Netherlands Organization for Applied Scientific Research, Physics and Electronics Laboratory (TNO-FEL)
- Delft Institute of Earth Oriented Space Research, Delft University of Technology (DEOS)
- HOFUNG, Bussum, Beijing
- EARS Remote Sensing, Delft

The partners have complementary qualities. TCLO is the end-user of the technology. TNO-FEL and DEOS have carried out scientific research and development in this field since the beginning of the 1990's. EARS is a remote sensing value added company interested in the commercialization of radar interferometry for ground subsidence monitoring. HOFUNG is a Dutch company specialized in technology transfer from Europe to China.

HOFUNG acted as intermediary, this was essential for a smooth preparation and progress of the project. DEOS and TNO-FEL concentrated on the processing of radar imagery and the evaluation of the results. EARS, in co-operation with the end user TCLO finally carried out a cost-effectiveness study of the methodology. The benefits of the methodologies have been assessed. Conclusions have been drawn on the economic feasibility of partially or totally replacing the ground data collection by the InSAR technology. Subsequently the user requirements for the InSAR methodology have been discussed and established.

2 BASIC PRINCIPLES

2.1 SAR interferometry

2.1.1 Introduction

The purpose of this section is to introduce the basic principles of SAR Interferometry (IN-SAR). This introduction into InSAR does not intend to serve as a reference. In order to avoid an exhaustive list of references it is limited to some review papers.

It is about 40 years ago that it was observed that a side-looking imaging radar operating on wavelengths in the order of centimeters can be used to map the Earth's surface with a resolution of some meters without requiring huge antennas. Already NASA's Seasat-A, launched in 1978, and, since 1991, ESA's ERS-1, showed a wide variety of applications of this technique, which is called Synthetic Aperture Radar (SAR). The use of SAR as an interferometer is rather new due to the stringent requirements on the stability of the satellite orbit. InSAR offers the possibility to map the Earth's land and ice topography and to measure small displacements over large temporal and spatial scales with sub centimeter accuracy, independently of the sun's illumination and the cloud coverage. These properties make InSAR a unique technique that combines the high accuracy of classical geodetic techniques such as GPS and leveling with the imaging property of classical remote sensing techniques. Recent examples have demonstrated that InSAR can be applied to study a variety of deformation processes, e.g. land subsidence due to the withdrawal of water, gas, and oil, the co-seismic and post-seismic displacement field related to earthquakes etc. The interferometric processing of SAR signals allows not only to infer surface changes from the radar images but also to derive high-resolution digital elevation maps.

Basic theory

In this section a brief review of the basic principles of InSAR for topographic mapping and deformation monitoring is given. First, the geometry of imaging radar will be outlined, followed by a discussion of the interferometric approach. For issues related to radar system operation and signal processing the interested reader may consult a general text on radar remote sensing, e.g. [Curlander, McDonough, 1991].

Imaging SAR geometry

A SAR is an imaging radar device that records the radar backscatter of the Earth's surface. An antenna, mounted on a spacecraft transmits periodically pulses in a side-looking direction with respect to the spacecraft's direction of motion. A part of the radar pulse energy is backscattered from the surface of the Earth and received a fraction of a second later at the same antenna. The brightness (*amplitude*), the round-trip time (*slant range*), and the *phase* relative to a stable reference oscillator are measured and recorded to construct the image. The typical size of the illuminated area is about 100-500 km for today's spacecraft systems. The nominal resolution in the direction of illumination, the so-called *range direction*, is about 9m, and in the direction of the spacecraft's motion, the *azimuth direction*, it is about 5m. The resolution on the ground depends on the look angle θ. Assuming $\theta=23^{\circ}$,

which corresponds to the mean look angle of the ERS-satellites, we obtain a resolution cell of about 25 x 5 m^2.

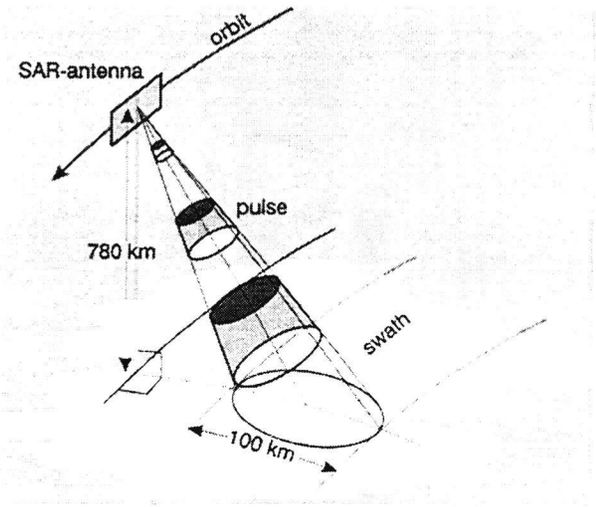

Figure 2 Geometry of a spaceborn imaging radar.

Usual applications of SAR make only use of the amplitude information in just *one* image. InSAR, however, makes use mainly of the *phase* measurements in *two or more* SAR images of the same scene, acquired at two different instants and/or at two slightly different locations. This is made possible since SAR is a coherent imaging system retaining phase information in the radar echo during data acquisition and subsequent processing. By interference of the two images, we can infer very small slant range changes in two SAR images of the same surface. These slant range changes can be related to topography and/or surface deformations. Since SAR is an imaging system, this information is available for each pixel. One full scene (100 x 100 km) contains roughly 10^8 pixels, meaning that SAR provides an almost continuous picture of the topography and/or the deformation field within the scene.
The relation between the total phase Φ and the distance between antenna and pixel, the *slant range* r is given by the simple formula (Figure 3).

$$\Phi = -2\pi \frac{2r}{\lambda} + \Phi_{scat} \qquad \textbf{(Equation 1)}$$

That means the total phase Φ at each point is equal to the sum of a *propagation part*, proportional to the round-trip distance 2r, and a *scattering part* Φ_{scat} due to the interaction of the wave with the ground. The radar wavelength is denoted by λ, which is, e.g., 5.66 cm for the ERS SAR. The scattering part Φ_{scat} cannot be determined and remains unknown. Therefore, when making use of just one image, it is never possible to infer the slant range from the measured phase due to the unknown phase shift Φ_{scat}.

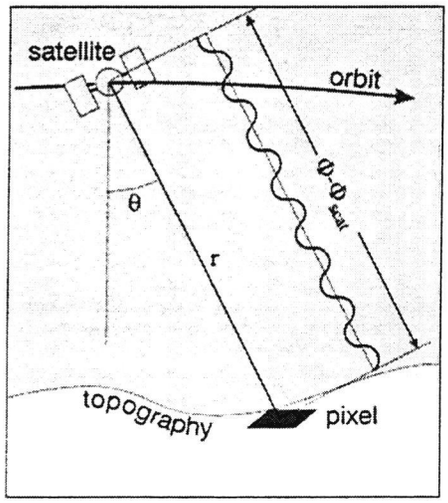

Figure 3:Slant range - phase relation

It is assumed that we take two images of the same scene at two distinguished time instants, t_1 and .t_2, from exactly the same location in space (Figure 4:Geometry of zero-baseline SAR Interferometry.).

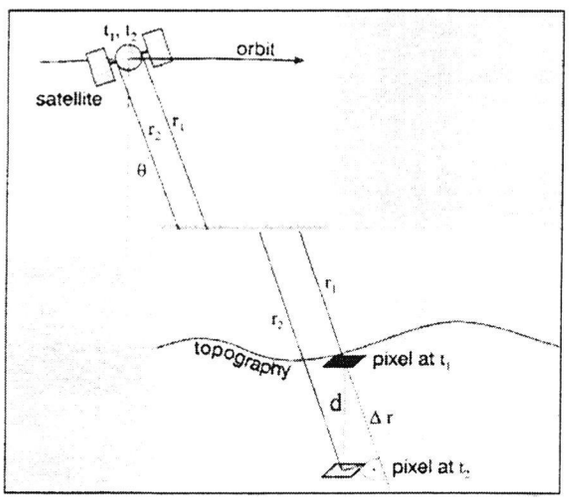

Figure 4:Geometry of zero-baseline SAR Interferometry.

If the elementary scatterers within each pixel are undisturbed in the time between the two image acquisitions, the scattering part Φ_{scat} does not change. Thus, the phase difference (for simplicity reasons the notation Φ is used again) is independent of the scattering mechanism, and becomes a measure of the line-of-sight component

$$\Delta r = r_1 - r_2$$

of the target displacement vector over the time interval (t_1, t2):

$$\Phi = 2\pi \frac{2\Delta r}{\lambda} \qquad \textbf{(equation 2)}$$

So, given the phase difference Φ, the component of the displacement in *range direction* can be determined pixel-by-pixel. The phase can be measured with an accuracy of a fraction of the radar wavelength, i.e. accurate to a few millimeters for today's satellite SAR systems. A second image of the same scene can be obtained in various ways (Figure 5) One possibility is to mount two physical antennas on a single platform. Only one antenna transmits the signals but both antennas receive it. Another possibility is to use two different passes of the same satellite. In our case the latter configuration using ERS satellites was chosen.

InSAR Geometry

In the following the term SAR Interferometry (InSAR) is used for all methods that employ the phase of the SAR signals in at least two complex-valued SAR images in order to derive information about the geometry and deformation of the Earth's surface. The usual configuration of this so-called across-track space borne InSAR is shown in Figure 6: two SAR systems fly on ideally parallel tracks and view the terrain from slightly different directions. The separation of the flight paths is called baseline, its component perpendicular to some look direction the perpendicular or effective baseline, and its component parallel to some look direction the parallel baseline. This implies that in reality the second image is not taken at exactly the same location as the first one (which is different from the zero-baseline configuration of Figure 4), and the phase difference Φ contains not only the radar line-of-sight component of the displacement vector but also some range differences due to the side-looking geometry and the topography.

It is assumed that the geometry of the reference surface is flat (Figure 5). For space borne sensors this flat geometry will usually not be accurate enough, but similar expressions as given next using a curved geometry may be derived easily.

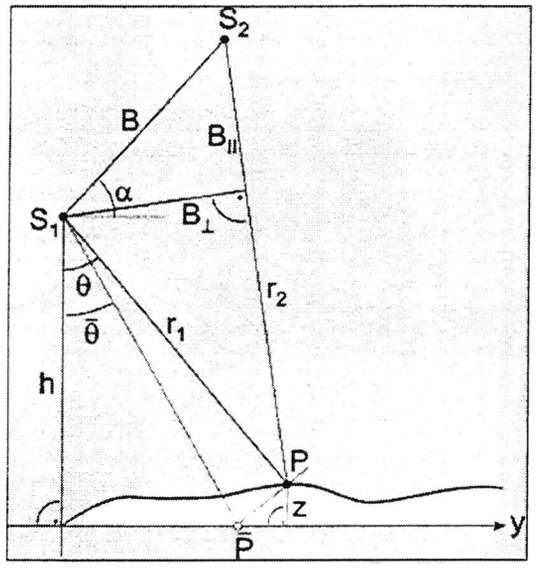

Figure 5: Geometry of across-track InSAR. The flight paths are perpendicular to the plane. The SAR illuminates the same pixel on ground from positions S_1 and S_2. The measured interferometric phase is proportional to the range difference $\delta r = r_1 - r_2$, which in turn is approximately equal to the parallel baseline, according to equation (5). It can be determined to a small fraction of a wavelength. Note that the SAR image acquired at S_1 does not allow to separate point P from since both have the same distance 'r_1 to the SAR sensor S_1.

Forming the interferogram means computing the complex product of two complex-valued SAR images u_1 and u_2:

$$u_{\text{int}}(.) = u_1.u_2^* = |u_1(.)|e^{i\Phi_1}.|u_2(.)|e^{i\Phi_2} = |u_1(.)||u_2(.)|e^{i(\Phi_1-\Phi} \quad \textbf{(equation 3)}$$

The total interferometric phase $\Phi := \Phi_1 - \Phi_2$ then becomes

$$\Phi = \arctan\left[\frac{\text{Im}(u_1(.)u_2^*(.))}{\text{Re}(u_1(.)u_2^*(.))}\right] = \varphi - 2\pi.\omega, \omega \in Z, \quad \textbf{(equation 4)}$$

where $\varphi := W\{\Phi\} = \text{mod}((\Phi+\pi),2\pi) - \pi \in [-\pi,\pi)$, is called the wrapped (fractional) interferometric phase. W denotes the so-called wrapping operator. Of course, φ is still ambiguous to within integer multiples of 2π, and the phase ambiguity 2π . ω, $\omega \in Z$ first has to be determined pixel by pixel in order to determine the absolute or unwrapped interferometric phase Φ. This process is called phase unwrapping. Φ is directly proportional to the distance difference $\delta_r = r_1 - r_2$:

$$\Phi_1 = -\frac{4\pi}{\lambda}r_1 + \Phi_{scat,1}, \Phi_2 = -\frac{4\pi}{\lambda}r_2 + \Phi_{scat,2}$$

$$\Rightarrow \Phi = -\frac{4\pi}{\lambda}\delta r + (\Phi_{scat,1} - \Phi_{scat,2}).$$

InSAR thus uses the phase information of two SAR images to measure the distance difference δr (note that this is unlike stereo photogrammetry, where homologous points need to be identified, and parallaxes have to be measured directly). Once δr has been measured, the location of a point in a plane perpendicular to the (parallel) flight paths is found as the intersection of the circle r = constant and a hyperbola defined by δr = constant. δr is related to the look angle θ:

$$r_2^2 = r_1^2 + B^2 - 2r_1 B\cos\left(\frac{\pi}{2} - (\theta - \alpha)\right)$$

$$\delta r \approx B\sin(\theta-\alpha) - \frac{B^2}{2r_1}\cos^2(\theta-\alpha) + O\left(\frac{B^3}{r_1^2}\right)$$

$$\delta r \approx B\sin(\theta-\alpha), B << r_1 \quad \textbf{(equation 5)}$$

Equation (5) shows that the distance difference δr is approximately equal to the parallel baseline. Moreover, it varies even for flat terrain due to the side-looking SAR. For constant slant-range r the look angle θ depends also on the terrain height of the pixel above the reference surface:

$$\cos\theta(z) = \frac{h-z}{r} = \cos\bar{\theta} - \frac{z}{r},$$

where $\bar{\theta} = \theta(z = 0)$, and h is the height of the radar sensor above the reference surface. When inserting this equation into equation (5), and making a Taylor series expansion, δr is obtained as function of the terrain height z

$$\delta r(z) = B\sin(\bar{\theta}-\alpha) + \frac{B\cos(\theta-\alpha)}{r\sin\bar{\theta}}z - \frac{B\cos\alpha}{2r^2\sin^3\bar{\theta}}z^2 + O\left(\left(\frac{z}{r}\right)^3\right).$$

Using $\Phi = -\frac{4\pi}{\lambda}\delta r$, the equation, which describes the variation of the interferometric phase due to topography and deformations up to terms of order $O((z/r)^2)$, is obtained:

$$\Phi(z) = -\frac{4\pi}{\lambda}(B_{\|} + \frac{B_{\perp}}{r\sin\bar{\theta}}z + \Delta r), \qquad \textbf{(equation 6)}$$

where Δr denotes the line-of-sight component of the deformation vector,

$B_{\|} = B + \sin(\bar{\theta} - \alpha)$ the parallel baseline and $B_{\perp} = B + \cos(\bar{\theta} - \alpha)$ the perpendicular baseline. Equation (6) shows that the total interferometric phase is the sum of three components: first, a component proportional to the parallel baseline for the reference surface, due to the viewing geometry, second, a component that expresses the range difference due to topographic height variations relative to the reference surface, and third, a component that is proportional to the line-of-sight surface displacement. Note that the effect of topography on the interferometric phase is scaled by the perpendicular baseline $\boldsymbol{B}_{\perp}$. The effect of the side-looking geometry of the reference surface is determined by the parallel baseline $\boldsymbol{B}_{\|}$.

The wrapped interferometric phase image is called *interferogram*. It shows pixel-by-pixel the wrapped interferometric phase of the complete scene. An example is given in Figure 6 .It shows the area of Tianjin city. The top left panel is the amplitude image. In order to interpret the amplitude image correctly it may be assumed as a rule of thumb that calm water (river) and smooth surfaces show up in black, while surface variations near the radar wavelength are bright, as for urbanized areas or wind-roughened water surfaces. Hills are mapped bright on one side and dim on the other; mountains look like `lying down', and steep topography and small look angles makes this worse. The upper right panel shows the wrapped interferometric phase, coded on a color wheel. One run through the color wheel corresponds to a complete rotation of 2π or 360° in interferometric phase. The dominant frequency is associated to the side-looking imaging geometry, i.e. due to the term $\Phi_{ref} = -\frac{4\pi}{\lambda}B_{\|}$; topography and line-of-sight deformations show up as local modulations of the dominating phase term Φ_{ref}. When subtracting the term Φ_{ref} a much smoother interferogram is obtained, displayed bottom left, which in the absence of topography shows in line-of-sight deformations (Figure 6, bottom panels).

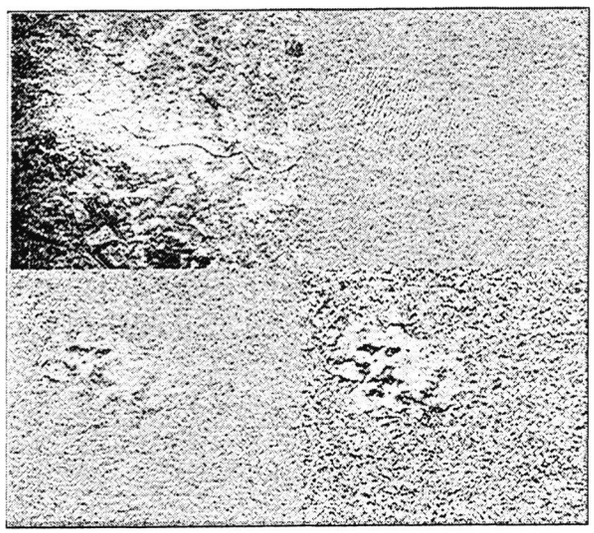

Figure 6: From top left to bottom right: amplitude image, total interferogram, flat phase corrected interferogram and an enhanced flat phase corrected interferogram of Tianjin city. Temporal baseline=1050 days, Perpendicular baseline=50m. Because of the flat topography and the small baseline the resulting interferogram, after flat phase correction, is dominated by subsidence and some atmospheric influence. Note that the high frequency fringes in the upper right panel are caused by the side-looking geometry, whereas the bottom panels only show the low frequency fringe pattern of the subsidence movement in that area. Outside the city the phase images are not coherent. In these areas interferometry is possible only by PS as discussed in the next chapter.

The height sensitivity of the interferometric phase is given by

$$\frac{\partial \Phi(z)}{\partial z} = \frac{4\pi}{\lambda} \frac{B_{\perp}}{r \sin \bar{\theta}} \qquad \textbf{(equation 7)}$$

The height difference resulting in a phase change of one fringe (2π) is called the height ambiguity, $z_{2\pi}$:

$$z_{2\pi} = \left| \frac{\lambda}{2} \frac{r \sin \bar{\theta}}{B_{\perp}} \right| \qquad \textbf{(Equation 8)}$$

An interferogram is more sensitive to topography if the height ambiguity is smaller. Since λ is a system parameter and r and θ vary only slightly over a full scene, the sensitivity is obviously scaled by the perpendicular baseline $\boldsymbol{B}_{\perp}$. The sensitivity increases with increasing perpendicular baseline, thus decreasing height ambiguity. Figure 7 shows the relation between the height of ambiguity and the perpendicular baseline. For the ERS satellites, the height ambiguity can be as low as 10 meters. Note that the sensitivity with respect to deformations is independent of the baseline and only depends on the radar wavelength λ.

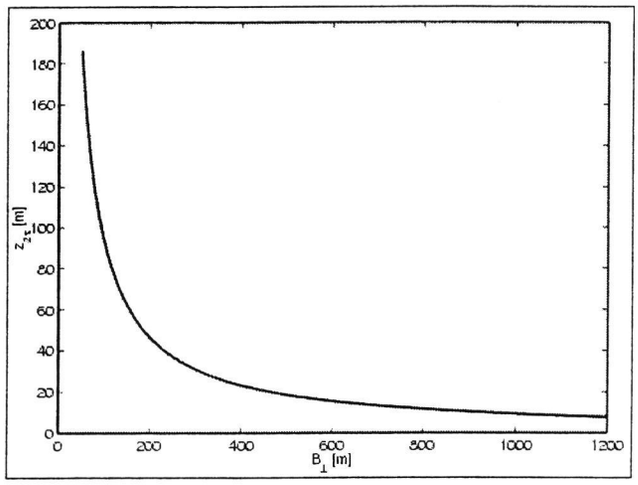

Figure 7: Relation between the perpendicular baseline $B_\perp$ and the height of ambiguity $z_{2\pi}$, equation (8). The larger the perpendicular baseline the more sensitive the interferometric phase with respect to height variations. Note that the maximum perpendicular baseline is limited.

2.1.2 The functional model

In this section the observation equations for InSAR are formulated. For more details the interested reader may consult (Hanssen, 2001).
Equation (6) describes approximately the relation between the total interferometric phase and both the topography and the deformation. In terms of the theory of parameter estimation in linear models it may be considered as an observation equation connecting the observed (fractional) interferometric phase with the primary unknowns `topography' and 'line-of-sight deformation'. In reality this model has to be extended by at least two terms describing the slant atmospheric delay at the time epoch of the first and second image acquisition, respectively. Moreover, one has to take into account that the total interferometric phase can only be measured modulo 2π. When assuming that the reference surface term is first wrapped and then subtracted from the wrapped interferometric phase φ,

$$\psi_k := \varphi_k - W\{kB_{ll,k}\} \qquad \textbf{(Equation 9)}$$

Where ψ is called the flattened interferometric phase, the observation equation for pixel k may be written as

$$\psi_k = -k\frac{B_{\perp,k}}{r_k \sin\bar{\theta}_k} z_k + k\Delta r_k + kS_{k,t_1} - kS_{k,t_2} - 2\pi\omega_k, \qquad \textbf{(equation 10)}$$

where $k = \frac{4\pi}{\lambda}$. Equation (10) relates the flattened interferometric phase related to pixel k to 5 unknowns: the topographic height z_k, the deformation in slant-range direction Δr_k, the slant atmospheric delay during acquisitions t_1 and t_2, S_{k,t_1} and S_{k,t_2}, respectively, and the

integer ambiguity number $\omega_k \in Z$. Therefore, the parameter estimation problem is underdetermined. In order to get a unique solution more observations may be added to the model, e.g. by making use of more than two SAR images of the scene, or a priori information may be introduced, e.g. by making certain assumptions about the unknown parameters.
For topographic mapping it is usually assumed that (1) no deformation in slant-range direction is present within the data acquisition interval and (2) atmospheric effects can be neglected. Both may for instance be justified if the two SAR images are acquired simultaneously (single-pass interferometry, see Figure 4) or if the SAR images are selected carefully. Then, the observation equation (10) reduces to

$$\psi_k = -k \frac{B_{\perp,k}}{r_k \sin \bar{\theta}_k} z_k - 2\pi\omega_k . \qquad \textbf{(equation 11)}$$

Provided that the integer ambiguities ω_k have been solved successfully, equation (11) provides the topographic height for every pixel.
For deformation studies the contribution of topography to the interferometric phase has to be modeled and removed; this requires information about the topography. This information may be either a high-resolution digital terrain model or a third or even fourth radar image of the scene. The former is referred to as *two-pass* InSAR, the latter *three-pass* and *four-pass* (differential) InSAR, respectively. If a digital elevation model of the terrain is available the first term on the right-hand side of equation (10) can be computed.

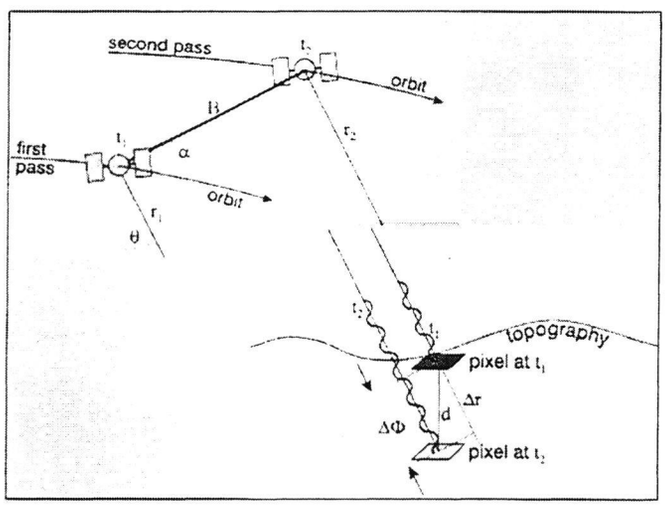

Figure 8: Two-pass InSAR for deformation monitoring. In order to extract the phase $\Delta\Phi$ caused by a deformation between image acquisition at t_1 and t_2, the contribution of topography to the interferometric phase has to be eliminated. This requires a digital elevation model to be available.

Three-pass interferometry uses three SAR images, acquired at time epochs t_i : i = 1,2,3 to form two interferograms: interferogram ***I***, making use of the SAR images acquired at t_1 and t_2, and interferogram ***II***, making use of the SAR images acquired at time epoch, say, t_1 and t_3. Assuming that interferogram ***I*** has successfully been unwrapped, and no significant deformation occurred during the time interval between t_1 and t_2, one may estimate the topography from interferogram ***I***, which is called the topography pair, according to

$$z_k = (-\Phi_{k,I} + kS_{k,t_1} - kS_{k,t_2}) \frac{r_{k,I} \sin \bar{\theta}_{k,I}}{kB_{\perp,k,I}}.$$

When inserting this equation into the observation equation for the second interferogram, the deformation pair,

$$\psi_{k,II} = -k \frac{B_{\perp,k,II}}{r_{k,II} \sin \bar{\theta}_{k,II}} z_{k,II} + k\Delta r_{k,II} + kS_{k,t_1} - kS_{k,t_3} - 2\pi\omega_{,II},$$

one obtains

$$\psi_{k,II} = -b_k \Phi_{k,I} + k(1-b_k) S_{k,t_1} + kb_k S_{k,t_2} - kS_{k,t_3} + k\Delta r_{k,II} - 2\pi\omega_{k,II},$$

where $b_k \approx \frac{B_{\perp,k,II}}{B_{\perp,k,I}}$ denotes the baseline ratio. If no suitable SAR images are available to form the topographic pair, one may also use another suitable interferogram to extract the information about the topography. This is called four-pass (differential) InSAR. Assuming that interferogram ***I*** formed by images acquired at time epoch t_1 and t_2 is the topographic pair, the following observation equation is obtained in order to extract the deformation signal:

$$\psi_{k,II} = -b_k \Phi_{k,I} + kb_k (S_{k,t_1} - S_{k,t_2}) + kS_{k,t_3} - kS_{k,t_4} + kd_{k,II} - 2\pi\omega_{k,II}.$$

It is important to note that the baseline scaling factor b_k affects the atmospheric contribution. Usually, the topographic pair is chosen to have a large baseline (i.e. small b_k) in order to increase the sensitivity with respect to topography. Correspondingly, the deformation pair, interferogram ***II***, is chosen to have a small baseline, in order to make it less sensitive with respect to residual errors in the topographic information, extracted from interferogram ***I***. A zero-baseline deformation pair would make the topographic pair superfluous, and would have normal, i.e. non-scaled, atmospheric contributions. In practice, other factors may influence the choice of the topographic pair as well, such as relief, vegetation, temporal decorrelation and atmospheric conditions. Moreover, the baseline cannot be chosen arbitrarily large.

Neglecting the atmospheric terms and assuming the phase unwrapping was successful, the fundamental equation for deformation monitoring using three-pass or four-pass InSAR is obtained:

$$\Delta r_{k,II} = \frac{1}{k}(\Phi_{k,II} - b_k \Phi_{k,I}), \qquad b_k = \frac{B_{\perp,k,II}}{B_{\perp,k,I}}.$$

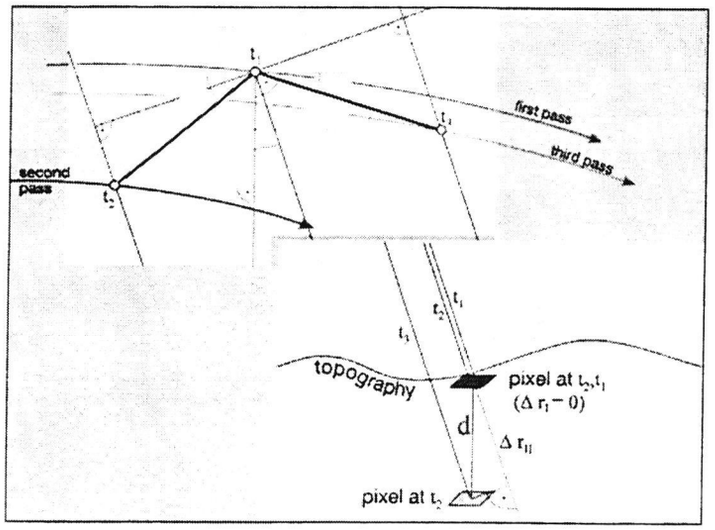

Figure 9: Three-pass SAR interferometry. Images acquired at t_1 and t_2 form interferogram I, which is used to determine the topography (`topographic pair'). Images acquired at t1 and $t_3$ form interferogram II, which is used to determine the line-of-sight deformation component $\Delta r$ (`deformation pair'). Note that a deformation Δr_I in time interval $[t_1, t_2]$ cannot be separated from a deformation Δr_{II} in time interval $[t_1, t_3]$. Only the sum of both can be inferred from the interferometric phase. Therefore, images at t_1 and t_2 are usually selected such that Δr_I can be neglected.

Some remarks concerning this equation should be made (Dixon, 1995):

1. The phase difference provides only the line-of-sight component of the three-dimensional surface displacement vector. When using images of both the ascending and descending passes of the satellite, it is possible to extract two components, since, then, the two interferograms represent views of the same scene taken in two different directions.
2. A phase comparison of the two images cannot be done in all cases but depends on the nature of the change. For instance, random motions of the scatterers within a pixel introduce noise in the measured phase difference. When the root mean square motion exceeds the radar wavelength (typically some centimeters), the noise may exceed the signal, meaning that a pixel-by-pixel phase comparison between the two images is not possible. However, if the entire surface within a pixel moves in the same way, while the relative motion of the elementary scatterers is small compared to the radar wavelength, the information on the deformation can be extracted from the phase difference.
3. The radar-scattering characteristics within each pixel must not change strongly over the time interval the images are acquired. Only then, the unknown phase shift Φ_{scat}, which is caused by the interaction of the electromagnetic wave with the ground, is constant over the time interval $[t_1, t_3]$, and drops out when forming the phase difference. When this condition is not met, it is termed *temporal decorrelation*. It constitutes one of the major problems for InSAR. Vegetation, wind effects, soil moisture, snow fall, farming activities etc. may preclude or hamper the phase comparison of the two SAR images.
4. As mentioned before, one can measure the total interferometric phase Φ only moduloπ. Therefore, a proper interpretation of the deformation field requires that the interferometric phase has to be unwrapped pixel by pixel. The problem of phase unwrapping is comparable to the problem of ambiguity estimation in GPS phase

measurements. Phase unwrapping is a rather difficult step that depends, e.g., on the imaging geometry, the terrain, and the phase noise level. Phase unwrapping is not addressed in these lecture notes; the interested reader may consult e.g. [Ghiglia and Pritt, 1998]. Note also that if no digital elevation model is available, and two image pairs are used to extract the target displacement, a phase unwrapping of each of the two interferograms is mandatory, unless an appropriate integer combination of the interferograms drastically reduces the topographic contribution.

5. Not any arbitrarily large displacement can be detected with InSAR. There are some limits with respect to the displacement gradient and the spatial scale of the deformation process.
6. Measuring the surface displacement field as a fraction of the radar wavelength, i.e., to some millimeter accuracy, requires a priori information about the topography in the region. Since the topography may be poorly known, the question arises how sensitive the interferometric phase Φ is to topography? Simple calculations show that a topographic height error of σ_z meters in the digital elevation model will produce an interferometric phase error of $\frac{\sigma_z}{z_{2\pi}}$, where the height ambiguity $z_{2\pi}$ is given by equation (8). Typical errors in digital elevation models are between 10 and 30 meters. Using the nominal ERS SAR parameters $\lambda = 5.66$ cm, $r = 850$ km, $\theta = 23°$, and assuming a perpendicular baseline of $\boldsymbol{B}_\perp = 100$ meters, which gives a height ambiguity of $z2\pi = 94$ meters, phase errors between 0.1 and 0.3 cycles are obtained, which is equivalent to errors in the line-of-sight component of deformation between 3 and 9 millimeters. Since the contribution of topographic errors to the interferometric phase errors grows inversely proportional to the height ambiguity and proportional to the perpendicular baseline $\boldsymbol{B}_\perp$, image pairs with short perpendicular baselines (large height ambiguity) should be preferred to reduce the effect of the un-modeled topography on the deformation.

2.1.3 The stochastic model

Introduction

The major limiting factors for topographic mapping and deformation monitoring using InSAR are (1) the limited measurement accuracy of the interferometric phase (phase noise), (2) the accuracy of the imaging geometry (orbit errors), and (3) the variation in the wave propagation conditions over the data acquisition period (atmospheric signal). In this Section the three major limiting factors are briefly discussed. For more details the reader should consult [Bamler and Hartl, 1998] and [Hanssen, 2001].

Phase noise

Figure 10 shows the height error as function of the phase noise for various perpendicular baselines. The perpendicular baseline length and the phase noise determine the height error. For $\boldsymbol{B}_\perp = 200$ meters a height error of about $\sigma_z = 0.13$ meters per degree of phase error is obtained. Phase errors in the order of 40° result in about 5 meter height errors. A smaller perpendicular baseline results in larger height error. The phase noise statistic is determined by the response of a resolution cell to the radar pulse, which in turn depends on the

scattering mechanism. Two scattering mechanisms are of interest in InSAR: distributed scattering (Gaussian or Rayleigh scattering) and point scattering.

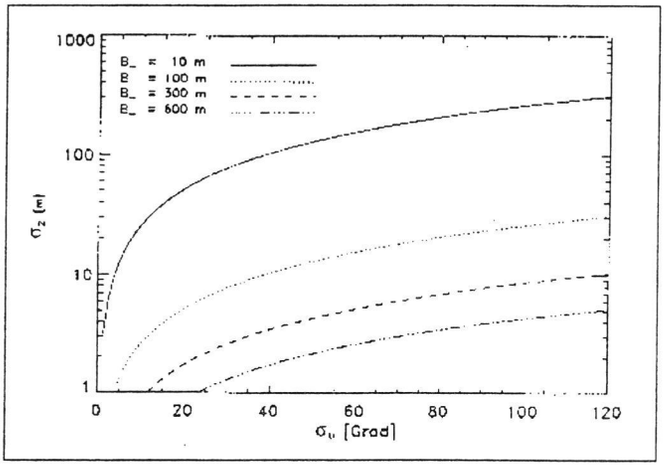

Figure 10: Height error σ_z as function of phase noise $\sigma_\varnothing$ for various perpendicular baselines $B_\perp$.

For SAR systems a resolution cell is many wavelengths long in the slant range direction, hereby introducing a very large range of total phase shifts. When folded into the principal interval $[-\pi,\pi)$ this results in a uniformly distributed phase from $-\pi$ to π. Furthermore, it is assumed that no single scatterer dominates the others in a resolution cell, that the phases of the individual scatterers are uncorrelated, and that the amplitude and phase of every scatterer are uncorrelated. Then, the central limit theorem applies and the SAR image pixel is a complex circular Gaussian random variable. For resolutions of tens of meters the Gaussian assumption is true for many natural scatterers such as forests, agricultural fields, soil and rock surfaces [Bamler and Hartl, 1998].

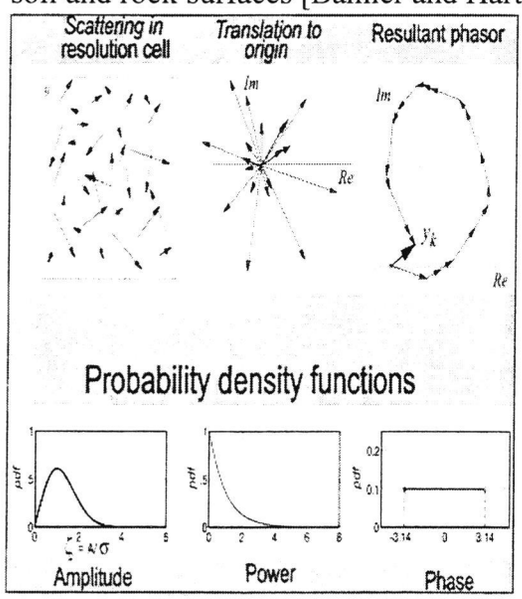

Figure 11 Single pixel scattering statistics. Top panels from left to right: The distribution of many individual phasors within a resolution cell; all phasors translated to the same origin (scaled); the phasor sum of all scatterers. The fat arrow indicates the (scaled) sum, which is the complex observable. Bottom panels from left to right: Probability density functions for amplitude, power, and phase. Note that the phase of the radar data is uniformly distributed

Under ideal conditions, SAR imaging is a deterministic process, i.e. identical imaging conditions yield the same result. Under real conditions, a number of disturbances occur, which degrade the coherence (decorrelation). The reasons are

- thermal noise within the radar system (γ_{SNR})
- errors induced by the SAR processing (γ_{proc})
- temporal variations of the backscatter (γ_{scene})
- different observation geometries at the two data acquisitions (γ_{geom})

As a result, the coherence γ can be written as the product of various terms,

$$\gamma = \gamma_{SNR} \cdot \gamma_{proc} \cdot \gamma_{scene} \cdot \gamma_{geom}$$

For instance, γ_{scene} stands for the temporal scene coherence and is defined as the ratio of temporarily stable scattering contributions to the total scattering intensity transferred to the SAR images. If the two SAR images have been acquired at different times, the structure of the scatterers may have changed in the meantime. The contribution γ_{geom} is the geometric decorrelation, caused by the perpendicular baseline $\boldsymbol{B}_{\perp}$. It causes a shift of the two image spectra. If this shift exceeds the system bandwidth, it results in complete loss of correlation. Therefore, there is a maximum perpendicular baseline, which never must be exceeded. For ERS-satellites this is about 1.1 km for flat terrain. In practice no ERS SAR-image pairs with perpendicular baselines larger than 600m should be used due to the increased noise level.

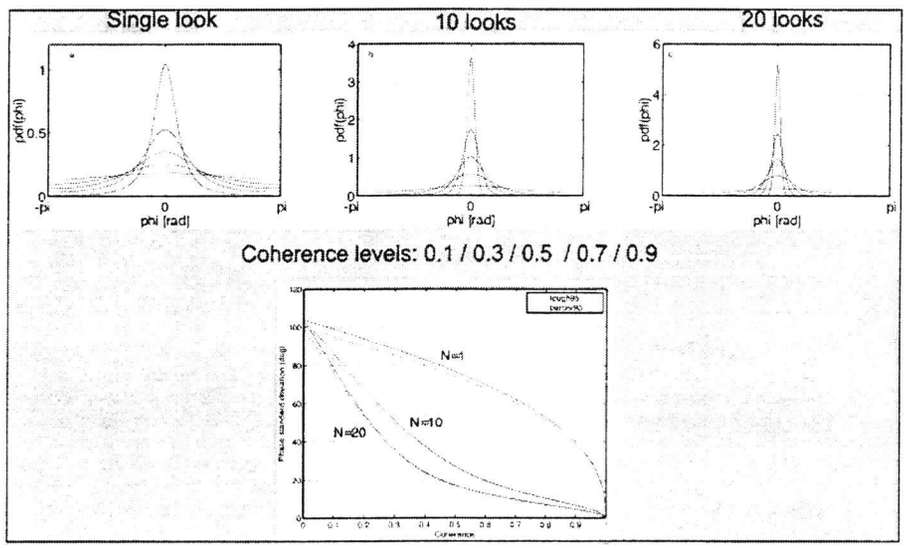

Figure 12: Interferometric phase statistics. Top panel: Probability density functions for different coherence levels (narrow curves correspond with higher coherence). From left to right: single look, 10 multilook level, 20 multilook level. Multilooking means that the average of a number of pixels is taken; this improves the phase statistics. Bottom panel: Standard deviation of the interferometric phase as function of coherence for three multilook levels

Orbit errors

The extraction of topography and deformation from interferograms and the proper referencing of topographic and deformation maps to a specific coordinate system require information about the satellite coordinates during the few seconds of SAR image

acquisition. As along-track errors are usually corrected for during the co-registration of the SAR images only radial and across-track errors propagate into the interferogram. Estimated radial and across-track errors in the ERS orbits provided by the Delft Institute for Earth-Oriented Space Research (DEOS) are on the order of 5 cm and 8 cm, respectively. The orbit errors result in a residual interferometric phase, which can be erroneously interpreted as topography or deformation. The orbit-error induced fringe pattern depends on the orientation of the baseline error vector, which cannot be predicted. As an example, Figure 13 shows the maximum residual fringes in a 100 x 100 km interferogram as function of the radial and across-track errors. One fringe or less corresponds to rms values of 5 and 10 cm residual fringes in the interferogram. Expected maximum rms values are 80 and 160 centimeters in radial and across-track direction.

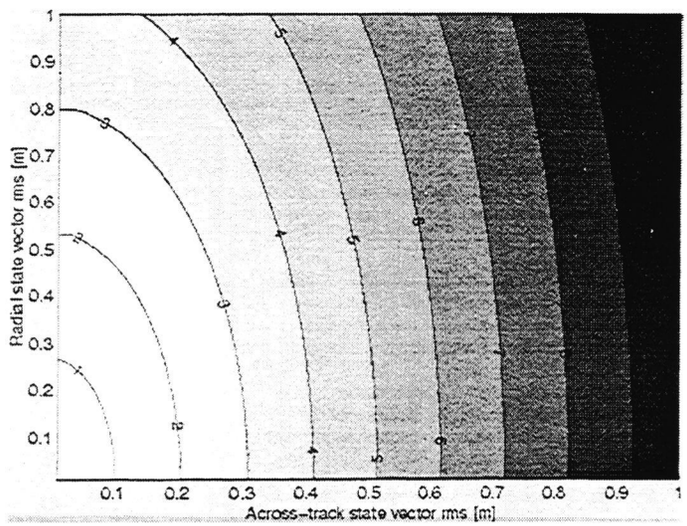

Figure 13: Maximum amount of residual fringes in an interferogram as a function of the radial and across-track state vector accuracies. With a 95% confidence, the maximum number of fringes is less then shown here.

In practice tie points distributed over the scene may be used to correct for the orbit error induced fringe pattern in the interferogram. At least 4 tie points with different known heights are necessary in order to solve for the baseline error vector. Practical problems with tie points may happen if the interferogram is corrupted by atmospheric signal. In addition, long-wavelength fringe patterns may also be caused by a deformation process or by errors in the topographic model, and this signal would be attributed to the orbit error when the latter is estimated using tie points. Finally, if the interferogram suffers from decorrelation, it may be difficult to identify a long-wavelength phase pattern, which is typical for orbit errors, and to attribute it to orbit errors.
The effect of (residual) orbit errors on topography (see equation 11) can be described by:

$$dz = \frac{dB_{\perp}}{B_{\perp}} z,$$

where $d\boldsymbol{B}_{\perp}$ is the perpendicular baseline error. Thus, the (perpendicular component of the) baseline error results in an erroneous scaling of the topographic height with factor $\frac{dB_{\perp}}{B_{\perp}}$.
For instance, in order to map a mountain with an elevation of 1000m with an accuracy of about 1m the relative accuracy in the perpendicular baseline must be better than 10^{-3}. If the error is, say, $d\boldsymbol{B}_{\perp} = 0.20$ meters, a perpendicular baseline of $\boldsymbol{B}_{\perp} > 200$ meters is needed.

Atmospheric path delay

The determination of surface changes using InSAR is based on the assumption that the radar signal propagates unaffected in the atmosphere. This, however, is not the case. Path delays occur in both the ionosphere and the troposphere. Ionospheric path delay is caused by variations in the Total Electron Content (TEC) along the path and by Traveling Ionospheric Disturbances (TID). Both effects can generally be ignored for mid-latitude sites. Since 1) the interferogram is only sensitive for relative variation, not for delays which effect the entire image, and 2) ionospheric variations can be neglected within a 100 x 100 km SAR area.

The most severe atmospheric effect is due to the troposphere. Its path delay consists of two components, a dry part (about 2.3 meters in vertical direction) and a small but highly variable wet part. The latter is dominated by the strong temporal and spatial variability of the water vapor concentration. It can take on magnitudes up to 30cm.

Artifacts in interferograms have been reported quite often and some of them have been assigned to atmospheric perturbations. These effects can cause misinterpretation of deformation fields derived by InSAR in the order of centimeters. For instance, a differential interferometry chart of the Kilauea volcano system, generated by data of the April and October mission of SIR-C in 1994 was interpreted firstly as a demonstration of a volcanic lift of several centimeters, but turned out later to be just an atmospheric effect as was reported by a JPL team on several occasions. Especially in wet regions SAR images exhibit artifacts due to the temporal and spatial variations of atmospheric water vapor. Other tropospheric variations, such as pressure and temperature, as well as ionospheric perturbations induce distortions as well, but the effects are smaller in magnitude and more evenly distributed throughout the interferogram than the wet tropospheric term.

Figure 14 shows an interferogram of the area of Groningen, The Netherlands. The images have been acquired during the ERS-1/2 tandem mission on two successive days and show the fringe pattern, which is due to convective cells. More than 4.5 fringes corresponding to a line-of-sight path delay of 12.6 centimeters can be counted showing that atmospheric effects can have a very large influence on the interferogram. Since these effects are independent of frequency at microwave wavelengths, the contamination of the signal cannot be mitigated by dual-frequency measurements such as those commonly utilized for ionospheric corrections.

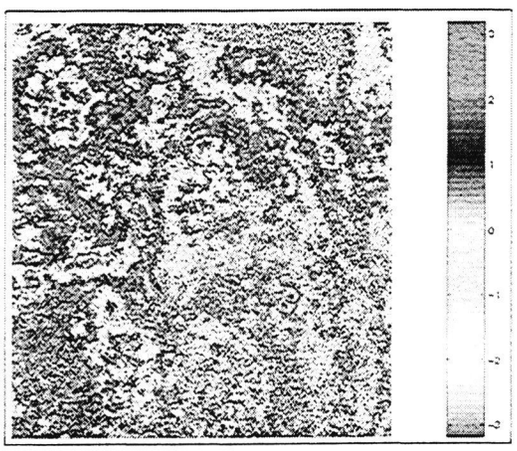

Figure 14: Interferogram of the Groningen area taken over one day. The fringe patterns indicate the influence of convective cells during the data acquisition. Up to 4.5 fringes corresponding to 12.6 centimeters line-of-sight propagation delay can be counted (from Hanssen, 1998).

Not only lateral variation in refractivity can cause atmospheric artifacts in SAR interferograms. Also vertical stratification, which is the result of different vertical refractivity profiles during the two SAR acquisitions, may lead to significant distortions in mountainous areas.

2.2 "Permanent Scatterers" method

2.2.1 Introduction

Within the frame of this project a new processing approach called the Permanent Scatterer technique was studied. It is developed and used successfully by [Ferretti et al., 1999], [Ferretti et al., 2000]. This technique uses points that stay coherent in time instead of areas (collection of points). The advantage is that if such a point (a 'PS') is identified, a reliable estimation of the subsidence can be given relative to another PS. In the conventional methods, a coherence estimation to identify such points was used. In the case of one stable point surrounded by noise it could be missed in the coherence estimation window. This disadvantage of coherence windows results in subsidence measurements of almost only urban areas. With the new technique reliable measurements in the non-urban areas can be used, for example backscatter from railroads, farms, fences, or any manmade structures with a size of one pixel or less. Some assumptions are made using the Permanent Scatterer method (referred to as "PS-method"). With these assumptions we deviate from [Ferretti et al, 1999/2000] otherwise it was not possible to produce a satisfactory result within the time of the project.

2.2.2 Simulation of PS-technique

Delft University of Technology-DEOS, and TNO-FEL developed the simulation algorithm described in the following section. The procedures were composed in Matlab (common used matrix processing software). In lack of real data a set of simulated interferograms were produced with an a-priori known deformation. These interferograms were used in the deformation algorithm of Permanent Scatterers.

Generation of simulated interferograms

For the testing of the deformation algorithm the input consists of a set of interferograms with a known subsidence. The noise and the atmosphere of the interferogram had to be simulated to investigate their effect on the algorithm.
The simulated interferograms must be generated with the same temporal baselines as the 24 real radar images that are to be collected later on in the project.

Some properties of the interferograms depend on the baseline. One of these is the topography and is coupled to the interferometric phase equation (7) [Pristi, 1990]:

$$\Delta\phi_{topo} = \frac{4\pi B_{\perp}}{\lambda H \tan\theta}\Delta h_{topo} \qquad \textbf{(Equation 12)}$$

With '$B_{\perp}$ 'the perpendicular baseline, 'θ' the incidence angle, 'H' the height of the platform. The topographic phase difference is proportionally to the perpendicular baseline

so topography can best be measured with an interferogram with a large baseline, but not too large because of baseline de-correlation.

The vertical deformation is coupled to the interferometric phase as:

$$\Delta\phi_{defo} = \frac{4\pi \cdot \cos\theta}{\lambda} \cdot \Delta h_{defo} \qquad \textbf{(Equation 13)}$$

Phase difference caused by a height change, with θ the incidence angle and λ the wavelength. As can be seen this phase difference is independent of the baseline of the interferogram. The best baselines for measuring deformation are small baselines between 10 and 100 meters.

In our simulation no topography is added for two reasons:

1) In the Tianjin area the topography is almost flat (comparable to the north and west parts of the Netherlands)
2) It is a simplification in the PS-method algorithm described later. This saves a lot of time and will presumably have no effect on the result.

One side effect of this is that we do not want to use interferograms with baseline larger than 600 meters because a building with a height of 15 meters results in phase differences of 7 radians (one fringe). This favors to look at sites with no high buildings (i.e. the countryside). The baseline criterion leads to the selection of 14 out the 20 interferograms. (If we could have corrected for the DEM we could have been using more images).

For the generation of the interferograms a 200 by 200 pixels image is made. In this image the deformation rate is inserted as illustrated in Figure 15.

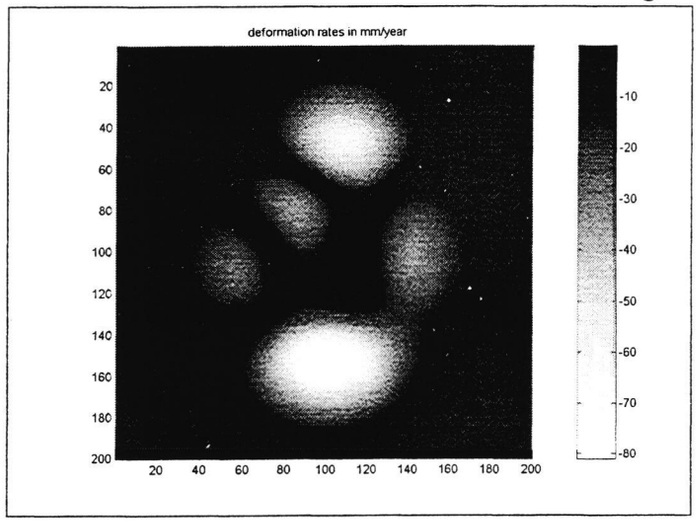

Figure 15: Input deformation rate. Bowl ranging from 0 to -82 mm/year

Using the temporal baselines of the 20 interferograms we can generate a set of interferograms, as they would look like with the deformation rates given by Figure 15. Assumed is that the deformation rate is constant in time.

Noise is added to the interferograms to simulate different types of decorrelation (baseline decorrelation, temporal decorrelation). This is done by adding a random number between {-0.15π, +0.15π}, leading to a noise ranging from {–/+ 0.47 radians}. The last added to the interferograms is atmosphere [van Bree et al. 1999], [Hanssen, 1998]. For each image an atmosphere is simulated using a fractal-based simulator in Matlab. This simulator describes the atmosphere with power models. It creates an isotropic 2 dimensional fractal surface with a power law behavior, which corresponds with the [-2/3, -8/3, -5/3] power law. The strength of the atmosphere can be set with the P_0 parameter [Hanssen, 1998]. For the simulations one master atmosphere is created and 20 slave atmospheres. They are all combined with simulated atmospheres, deformations and noise. The result of the 20 simulated interferograms is plotted in the next figure.

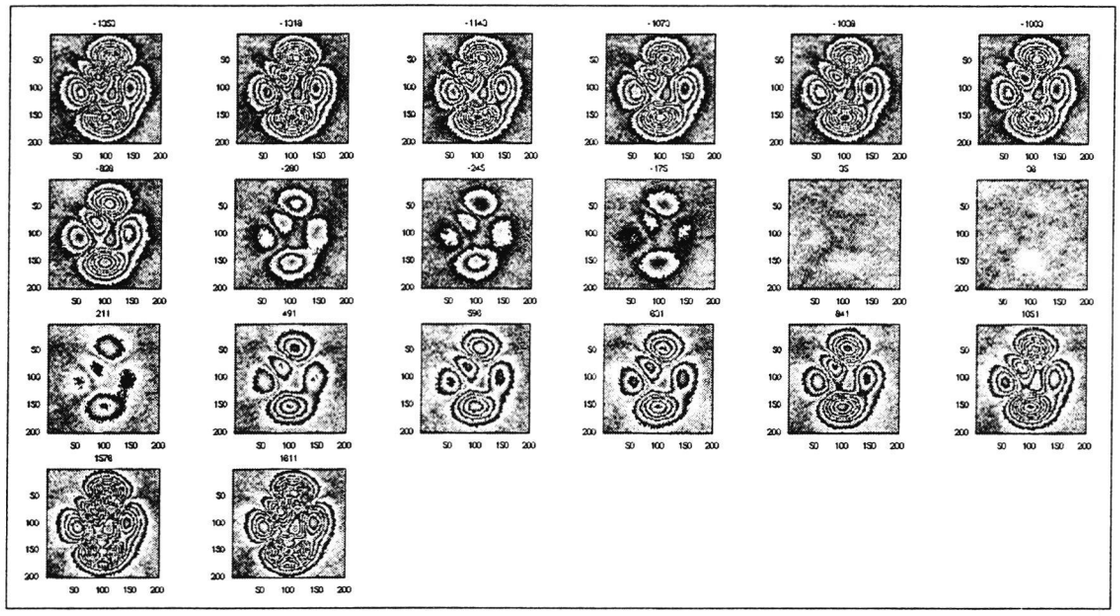

Figure 16: Twenty interferograms with atmospheres (P_0=40), noise and deformation. Temporal baselines are in the titles (nr. of days).

2.2.3 Algorithm for subsidence estimation using Permanent Scatterer points

Introduction

In this section the methodology and the algorithm are described. The main idea using permanent scatterers comes from [Ferretti et al., 1999] of the "Dipartimento di elettronica e informazione – politecnico de Milano". The effect of temporal decorrelation and atmospheric in-homogeneities strongly effects the quality of the interferograms and with that the ability to use them for deformations measurements. The PS-points work like "natural GPS" points and with the analysis of the temporal behavior of the phase of such a PS point, deformation information can be extracted.

Selection of PS-candidates

To extract the PS-points in an interferogram PS-candidates are selected. In the simulation this is done by taking the top 0.5-5% of the highest amplitudes. High amplitudes are considered to be an indicator of stable points in time. A single scatterer cell contains the

contributions of a lot of scatter points; the sum of these individual scatter points is what we record as the signal. If we have a high backscatter point within a cell, the phase of this cell is usually more constant over time compared to a cell with only low backscatter points. This can best be illustrated with a sketch in the complex plane.

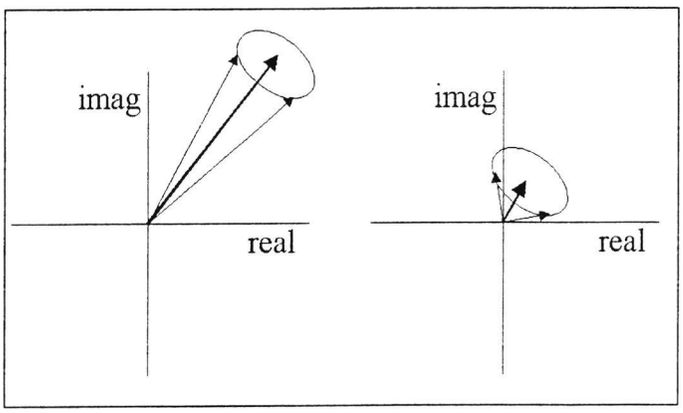

Figure 17: Left: high amplitude with noise; Right: low amplitude with noise

With high amplitude the variance in the phase (angle of the vectors with the x-axis) is less compared to low amplitude, when the same amount of speckle is present. This amplitude can be the amplitude of the interferogram as well as the amplitude of the SLC image. The 0.5-5% highest amplitudes are randomly selected as PS-candidates and in the simulation the number lies around 350 PS (0.9%). The next plot shows the randomly selected PS-candidates.

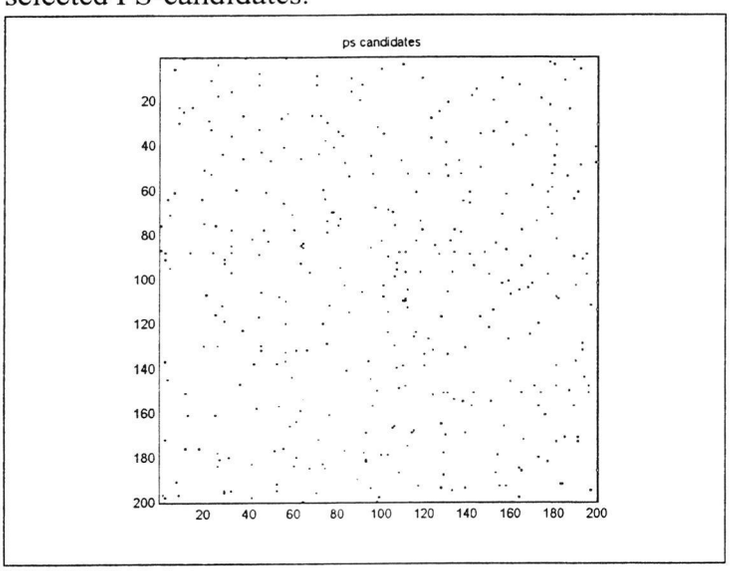

Figure 18: 375 randomly selected PS-candidates

Deformation rate estimation

A window of a given size is laid over the first PS-candidate with this candidate as the center of the window. The size of this window was taken 5x5 km because atmospheric delay is assumed nearly constant within this size [Hanssen, 1998]. The phase of this central, or reference pixel, is subtracted from the entire window. This window is subtracted from each interferogram in the stack each with it's own reference phase. This is done to make it possible to compare all the other PS-candidates in the window region with the reference

pixel, which now has a phase of zero. We have to take the same reference point for all compared points.
From all the PS-candidates in the window, with respect to the reference pixel, the phase behavior in time is compared with wrapped deformation rates in the same time interval. These linear deformation-rates run from –70 mm/year to +70 mm/year with a 1 mm/year step, so 141 deformation rates are calculated and compared with the data values. For each deformation rate the residue, mean distance from calculated to observed value, is calculated and the three lowest residues are selected. If the minimal residue is above a certain value (adjustable) the PS-candidate is rejected. For linear subsidence the behavior of the phase of such a point cannot be properly fitted by one of the subsidence rates and is therefore rejected. This can also be the case if the atmosphere distorts points too much and there are not enough data points to compensate for that distortion. If two or three points in a stack of five points are heavily distorted by atmosphere, it is not possible to fit a reliable deformation rate through those points. On the other hand if you have only 3 distorted points out of 20 points this will not cause a problem. Other –non linear– curves might fit; however this is beyond the scope of this project. The method is visualized in the Figure 19.

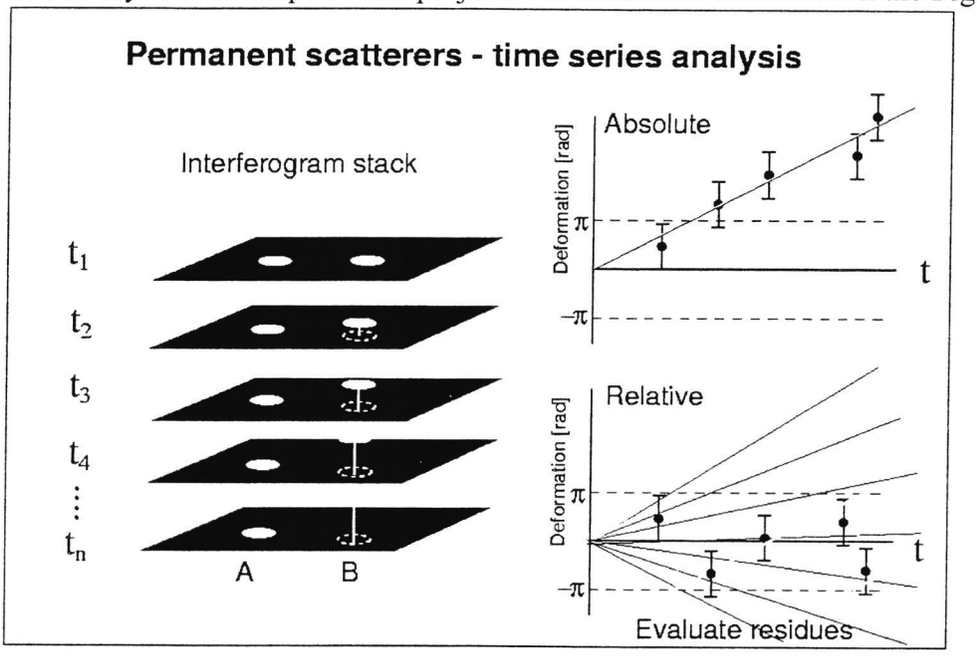

Figure 19: Visualization of analysis method. Left: *A* is the reference pixel and *B* is the PS-candidate. Right: Residue fit to wrapped deformation phases.

For each pair of PS-candidates in the window a deformation rate is estimated using that deformation rate which had the lowest residue. If the deformation rate is between +2/-2 mm/year the PS-candidate is rejected. Fluctuating data values caused by noise or by "deformation zero" points could cause these deformation rates. The former are bad selected PS-candidates and must be rejected, the latter are of interest but the danger of adding false noise pixels to the data set is to high. We cannot make a clear distinction between noise points and zero deformation. Perhaps this can be done using values of the residues.

The results of all the deformation rates of the PS-candidates in a window are stored in a matrix, which has the reference point numbers as the column numbers and the PS-candidate numbers as the row numbers. This step is repeated for all the PS-candidates. To make this clearer the matrix mentioned is plotted in Figure 20. All PS-candidates are numbered. On

the left axis the "from point" number is plotted and on the bottom axes the "to point" number is plotted. In this matrix all 'in between' estimated deformation rates are plotted.

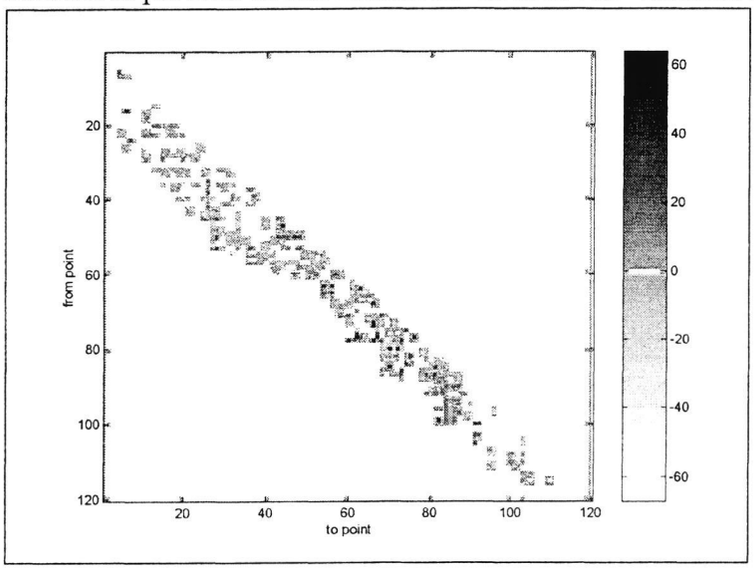

Figure 20: Matrix with in-between deformation rates of all PS-candidates

The matrix is symmetrical; the values in the upper right corner are the same as in the lower left, the sign excluded. So half of the matrix is thrown away and the rest is put in a Matlab function, which resolves the redundancy in the data set. The algorithm is using a Cholesky factorization. The input for the algorithm is the points from the matrix described above and an error value of each observation from this matrix. The result is a deformation rate for each point. This part of the deformation algorithm does not always work because there is not always a solution to the redundancy problem. A solution is found depending on which points are used, and how high or low the errors are. Experience has learned if the average number of pairs in a window is above 15, a solution can be found.

2.2.4 Results of simulation

The solution for the twenty interferograms from Figure 16, including atmosphere and noise is plotted in Figure 21.

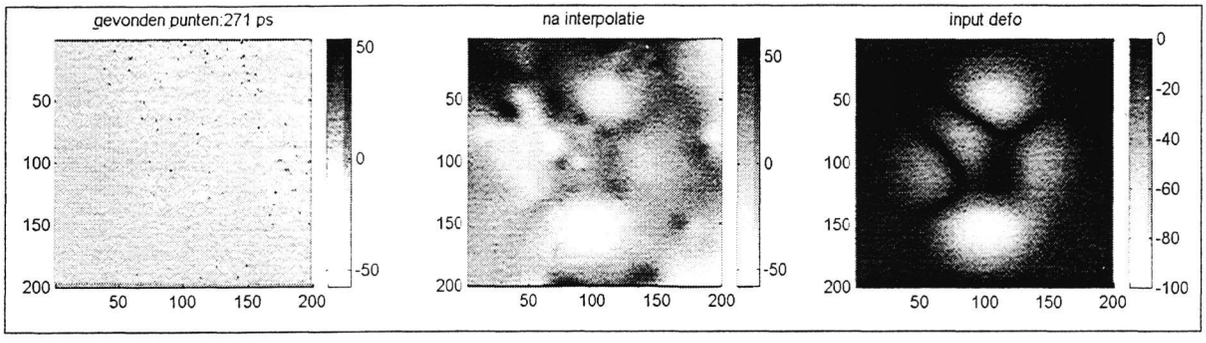

Figure 21: Left: Output of 271 points with certain deformation rates. Middle: A bi-cubic interpolation of found points. Right: Input deformation rates as reference.

The window size in this example is 29x29 pixels and the pixel spacing is 160 meters. So the scene measures 32x32 km and the window 4.6x4.6 km. The number of input PS-candidates is 362 and finally 271 PS-candidates are marked point scatterers.

The solution is not really satisfactory and is contaminated by the atmosphere. As said before the three lowest residues were stored. Using the a-priori information that over a window of size 29x29 points (in this example) the maximal in-between deformation rate lays around 30 mm/year (from the input deformation), a limit can be set in the result matrix (Figure 20). Each result is evaluated and checked if its value is beyond this limit. Points that are lying above the limit are changed in the nearest lowest (second) residue deformation value, if this value also lies above the limit the third lowest residue deformation value is picked. If that number is still above the limit the point is removed from the matrix and is labeled unreliable and set to zero.
In our example we set the limit to 30 mm/year over a window of 29 pixels. The results are illustrated in Figure 22

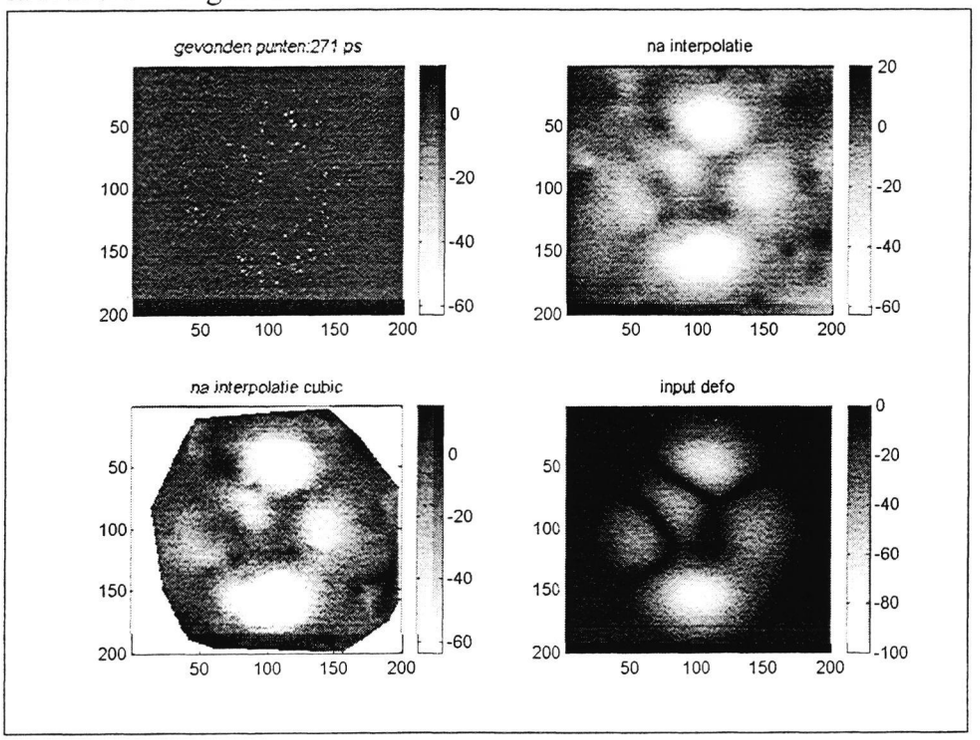

Figure 22: Result based on 20 interferograms. Top left: The 294 points found; top right: bi-cubic interpolation, bottom left; bi-cubic interpolation using Delaunay triangulation, bottom right; Reference (input) deformation rates.

The reason why the second or third smallest residue give a better result than the smallest residue is that the minima in residue are close together. Often the differences are of the same magnitude as the atmospheric distortion. If not enough interferograms are available to level the atmospheric influences; the multiple residue selection method leads to better reproduction of the initial deformation pattern. The result in Figure 22: Result based on 20 interferograms.", has an offset in deformation rate [-60 / +20 mm/yr]. The offset is a consequence of the algorithm; it solves the redundancy in the data set without an absolute calibration. This could be overcome if one ground truth point is included.

In advance of the results of the next chapter, it is also interesting to look at the results with 14 interferograms.

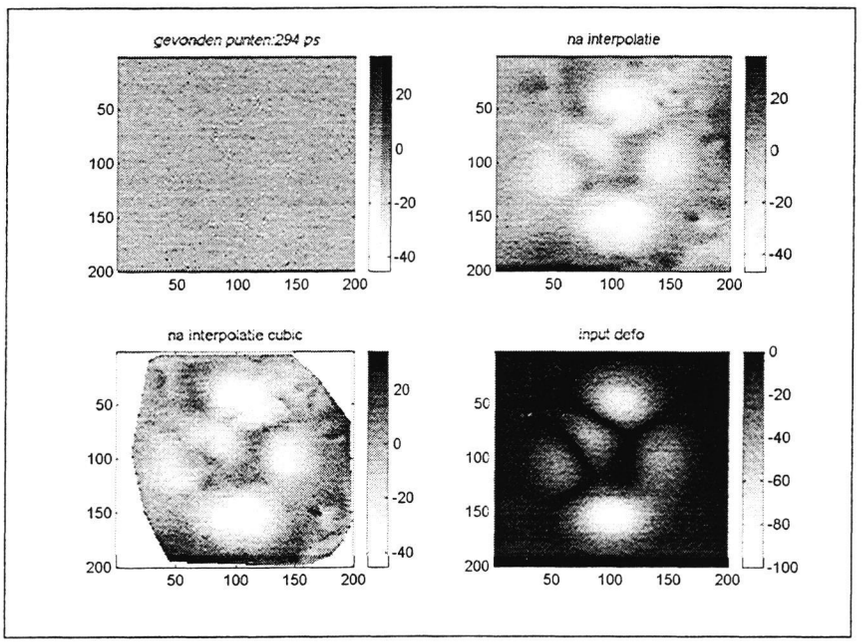

Figure 23: Result based on 14 interferograms. Top left: The 294 points found; top right: bi-cubic interpolation, bottom left; bi-cubic interpolation using Delaunay triangulation, bottom right; Reference (input) deformation rates. Result based on 14 interferograms. Top left: found deformation rates. Top right: bi-cubic interpolation of found points. Bottom left: bi-cubic interpolation using Delaunay triangulation. Bottom right: reference (input) deformation rates.

The parameters, window size and subsidence limit, are the same as in Figure 22. The result is worse compared to the twenty-interferogram case, but the pattern is still visible with a little more distortions on the sides.

2.2.5 Conclusions on the simulation results

These simulation results give good confidence in the algorithm and method. Assuming that:

- The deformation is linear in time
- There is no disturbance from topography
- The atmosphere is constant over a 5x5 km range.

Apart from an offset, the subsidence pattern is found with matching amplitude. The only worrying points are the absence of a topographic correction and the atmospheric distortion. The influence of these factors is limited. The topography in the Tianjin area is rather flat, though especially in urban areas high buildings may cause artificial elevation problems. The atmospheric phase delays in the simulations is in general less than one phase cycle provided that the weather conditions are not too bad (e.g. Thunderstorms may result in distortions of a few cycles).

3 DATA GATHERING

In this section detail is given on GPS and leveling data gathering, as well as on the satellite data gathering.

3.1 GPS and leveling

3.1.1 Organizational structure

A consortium of companies in Tianjin is responsible for the data gathering and map production. The Tianjin Construction Union (TCU) is the governmental organization involved in the leveling. Under this organization following three companies are active:

1) Tianjin Control Landsubsidence Office (TCLO)
2) Tianjin Geology and Mining bureau (TGM)
3) Tianjin Survey and Mapping bureau (TSM).

The fourth company that is connected to the measurement of subsidence is the National Deformation Monitoring Center (NDMC). NDMC is part of the National Earthquake Bureau, another governmental organization.
The organization of the measurement campaign is governed by TCLO. The leveling measurements are done by TGM, TSM and NDMC. The GPS measurements are done by TSM and NDMC. After the measurement campaigns all data are handed over to TSM. They update the subsidence database and contour maps and make them available to TCLO. TCLO will use this information to control and execute the regulations on the issue of subsidence, as set by the provincial government.

3.1.2 GPS

At present the GPS data is gathered only for testing purposes. The procedures for processing these subsidence measurements do not yet apply to GPS data. The data of 17 GPS points are just used to compare with leveling measurement result. The accuracy in z direction is about 10 mm.

3.1.3 Leveling data

For monitoring the subsidence every year a measurement campaign is held. The duration of a campaign is 12 weeks and takes place in the period October-December. This type of data collection started in 1984.

Figure 24 Leveling network with coastline; note that Tianjin city is not included here

The survey covers about 1400 leveling benchmarks. The network has a total length of 3000 km, covering the whole Tianjin municipality (approximately 12.000 km^2). At present the working procedure is as described above. For the first degree leveling measurement the maximum error between fore measurement and back measurement is plus or minus $1.8K^{1/2}$; for the second degree leveling measurement this error is plus or minus $4K^{1/2}$ mm where K is the length of measurement in km (Source: TCLO).

3.1.4 Satellite radar data acquisition

The acquisition of radar data is governed by specific requirements. These requirements result in a number of steps when gathering data.

1) Choice of satellite
2) Obtain a list of available data
3) Select and order desired imagery

Ad 1) as a consequence of the sensitivity of radar interferometry to the input data it is required that the focused input data are similar to a high degree. This requires that the data should be derived from identical satellites, the orbits of the different captures should be similar, and the RAW imagery should be processed into SLC format using the same SAR-processor. Furthermore for acquiring subsidence measurements with a precision of a few millimeters, the wavelength of the radar should be less then a few centimeters at a high S/N ratio. For this reason it was decided to acquire raw data from the ERS-1 and ERS-2 satellites.

Ad 2) As the ERS satellite operates discontinuously in SAR mode, first a list of available data should be obtained. This can be done using the DESCW software provided by the ESA.

Ad 3) the next step in data acquisition is to determine which data will be useful for interferometric measurements. The primary factors in this procedure are the orbital parameters "temporal" and "perpendicular baseline". These should be within certain limits. For the baseline a maximum of 1000m is a common restriction. For the maximum difference in acquisition time a few years is acceptable, depending on the type of terrain. These data can be obtained using the "getorb" software provided by DEOS (http://www.deos.tudelft.nl/ers/precorbs/software/). An extra criterion is the atmospheric influence during data capture. The usability of the data is decreased seriously if the atmospheric circumstances are bad. This is often problematic if, for instance, heavy cloud cover of the type "cumulonimbus" is present. This can be checked by evaluation of meteorological data, e.g. weather reports / satellite imagery.

As the meteorological data were not available the choice under step three was based on the orbit criteria only. The following radar satellite data were ordered:

1	E1 23710/2817 27 Jan 1996
2	E1 32728/2817 18 Oct. 1997
3	E1 12554/2817 14 Sep 1997
4	E2 13055/2817 19 Oct. 1997
5	E2 16061/2817 17 May 1998

Due to a policy change of ESA, the price of ERS data for research and development usage decreased significantly. Therefore it was possible to obtain all other available ERS data for the Tianjin area. This would increase the likeliness of a good result using the PS method. As the temporal and baseline requirements are of lesser importance for this method, all available ERS data were ordered. Of the 29 images ordered 4 did not become available for unknown reason. The RAW data received were processed to SLC. The following table lists the available SLC data.

NR.	Slave orbit	ERS satellite	Date slave (dd-mm-yyyy)	B⊥ (m)	B_{temp} (days)	PS
1	04328	1	14-05-1992	-222.5	-1353	+
2	04829	1	18-06-1992	-320.5	-1318	+
3	07334	1	10-12-1992	+150.0	-1143	+
4	08336	1	18-02-1993	+381.0	-1073	+
5	08837	1	25-03-1993	+88.5	-1038	+
6	09338	1	29-04-1993	+751.0	-1003	-
7	11843	1	21-10-1993	+612.0	-828	-
8	19702	1	22-04-1995	-271.0	-280	+
9	20203	1	27-05-1995	-217.0	-245	+
10	21205	1	05-08-1995	+219.0	-175	+
11	24122	1	02-03-1996	+476.5	+35	+
12	04538	2	03-03-1996	+470.0	+36	+
13	07043	2	25-08-1996	-850.5	+211	-
14	11051	2	01-06-1997	-459.5	+491	+
15	12554	2	14-09-1997	-83.5	+596	+
16	13055	2	19-10-1997	-23.5	+631	+
17	16061	2	17-05-1998	+395.0	+841	+
18	19067	2	13-12-1998	-1001.0	+1051	-
19	26582	2	21-05-2000	+549.0	+1576	-
20	27083	2	25-06-2000	-865.0	+1611	-

Table 1: Used data set. All with respect to master. 27-01-1996, orbit 23710, ERS-1. Last column indicates usage in PS-method.

The temporal and perpendicular baselines (Bt, Bp) have been used to make following plot:

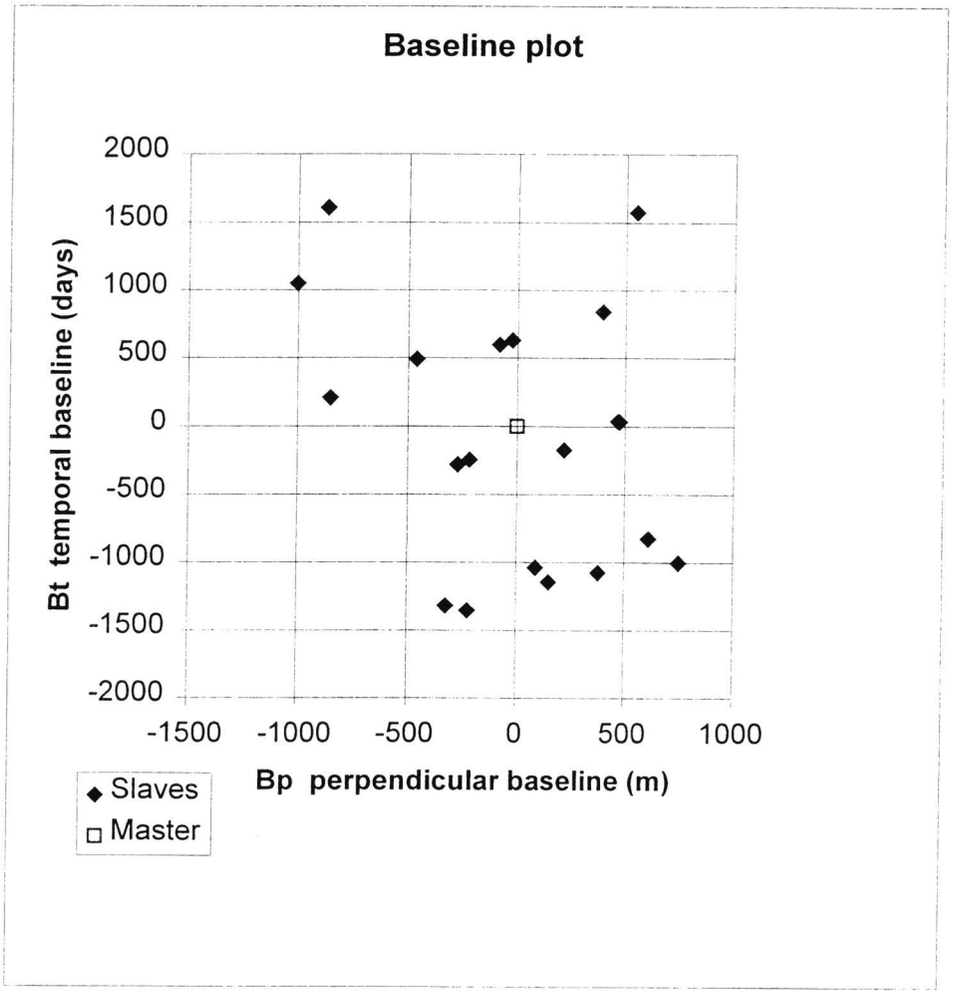

Figure 25: Baseline plot of final ERS data set

Future ERS data acquisitions are unlikely to be of any use. Due to mechanical problems, in January 2001, the tunnel width of the ERS-orbit has been increased to 5 km. As for radar interferometry the maximum baseline is about one kilometer suitable image pairs will only occasional be acquired. The possibility exists to use data of other satellites, however this data cannot be fully integrated with ERS data.

4 SUBSIDENCE MAPPING IN TIANJIN

In this chapter an overview of the measurements in Tianjin using different methods. Section 4.1 describes the processing of leveling and GPS data, followed by a description of traditional InSAR (section 4.2), section 4.3 deals with the PS method.

4.1 Subsidence measurement in Tianjin using GPS and leveling data

Processing of the leveling and GPS data is done by TSM. The final product is a database that lists all point measurements and subsidence contour maps. Note that as mentioned in the section 3.1, the GPS data is only acquired for testing purpose. Data were made available for this project in table and map format.

4.1.1 Subsidence in time

The leveling data are processed into yearly subsidence maps. Before discussing the processing steps as performed at Chinese side, a closer look at the data as available in table form will be taken. The data set available was not complete, only measurements of 252 points were available, located all over Tianjin area. By taking the yearly average for all these point an indication of the overall behavior of the subsidence is obtained. This averaged subsidence over the whole Tianjin area is almost linear, as can be seen in Figure 26.

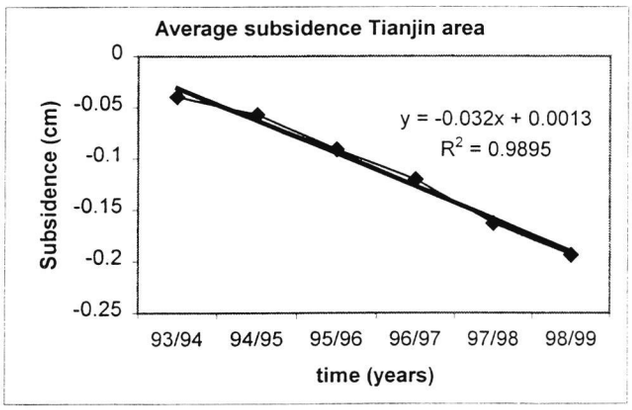

Figure 26: Average cumulative subsidence over the whole measurement area

This almost linear behavior is common as illustrated by Figure 27. Note that for proper visualization the graph was restricted to some random samples out of the 252 points.

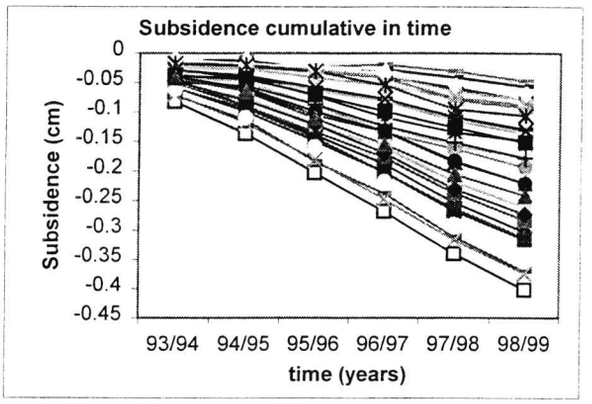

Figure 27: Cumulative subsidence for randomly selected points

It is possible that the subsidence has a seasonal character, if the subsidence would be related to groundwater extraction, this would imply that in dry years the subsidence should increase. This is not the case. It is likely that the subsidence effects due to water extraction are leveled out so much in time that the result is an almost linear behavior.

4.1.2 Processing of leveling data

Data processing is started in December. The processing is done along the following steps:

1) Link coordinates to the measurement ID
2) Convert leveling data into subsidence data
3) Enter data into database
4) Contour map production

Ad 1) Link coordinates to the measurement ID
Every year some points are lost for some reason (e.g. a new building is built at a measurement point, etc.). To compensate for these losses new points are added to the leveling network. This work is very important to update the subsidence database. Of course it is also important to name all points using the same convention.

Ad 2) Convert leveling data into subsidence data
Error analysis is done at this point. For the first degree leveling measurement the maximum error between fore measurement and back measurement is plus or minus $1.8K^{1/2}$; for the second degree leveling measurement this error is plus or minus $4K^{1/2}$ mm. (K is length of measurement in kilometer). There are some other error limitations and these must be calculated for all leveling lines. If the result of error calculation of some leveling line exceeds the limitation then the leveling measurement must be redone. The error compensation is done when all kinds of error are less than some limitation. The values of all points are recorded in terms of absolute height. So to calculate the new subsidence value simply the difference with the previous year is taken.

Ad 3) Enter data into database
The subsidence database is updated each year.

Ad 4) Contour map production
The contouring is done using dedicated computer software. After this calculated contouring, the result is enhanced manually. The contouring of a map usually takes 3 days. The contouring and printing group consists of 8 people.

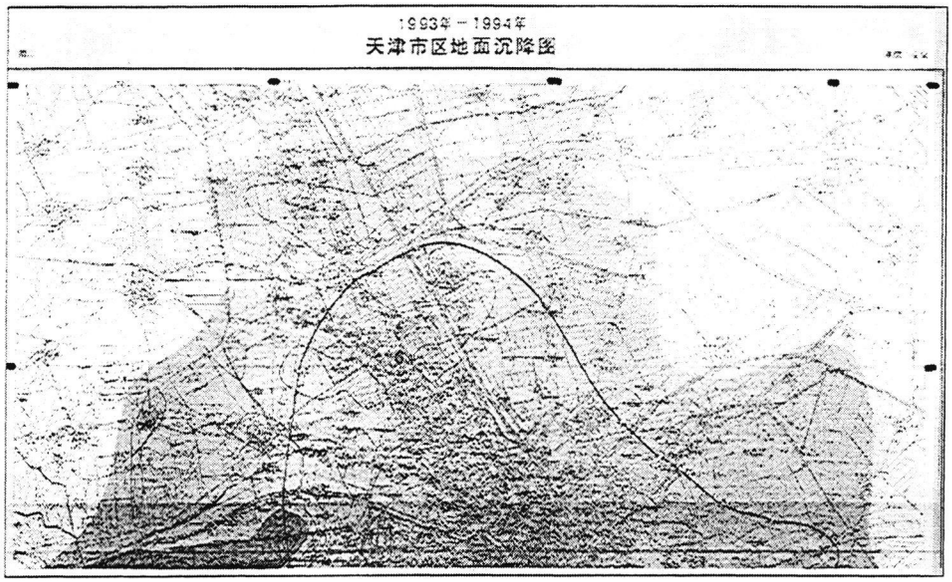

Figure 28: Example of a subsidence contour map of Tianjin as prepared by TSM

The whole procedure - from data gathering until contour map production - takes about five months. The results are handed over to TCLO around May.

The maps provided by TCLO have been digitized for reason of comparison with results derived by radar interferometry. An average subsidence map was generated from the yearly maps and was geo-referenced onto the radar map. The standard deviation of the geocoding, denoted by sigma, was less then 25 meters. The digitized subsidence maps of the Tianjin city over the period 1992-1999 were averaged, so a comparison with the average subsidence as determined by interferometry could easily made. In figure 29 the averaged subsidence data is shown. Note that the dark center covers the city, the subsidence increases to the border of the urban area. The black color is used to indicate that no data is available.

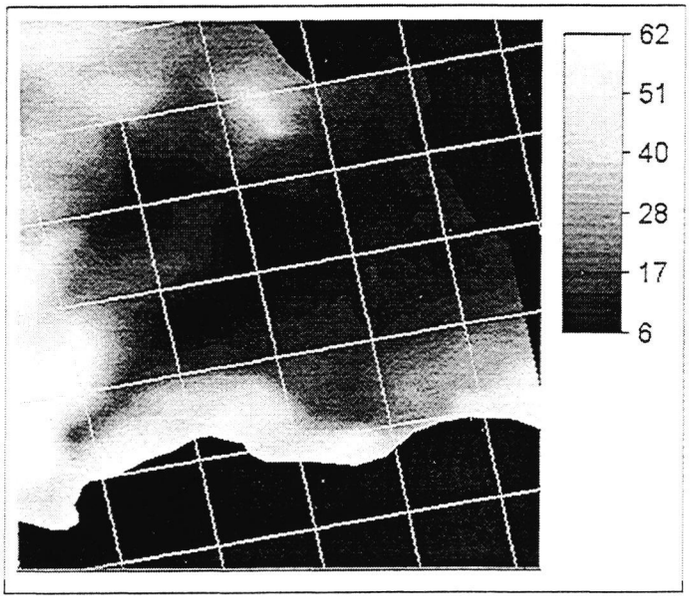

Figure 29: Subsidence map of the Tianjin city area with averaged over 1992-1999, overlain with a 5 km grid. The area displayed is the same as the magnitude image of Figure 40.

4.2 Subsidence measurement using InSAR

4.2.1 Introduction

Temporal decorrelation is a major limiting factor if one wants to apply InSAR for the whole Tianjin municipality area (100 x 100 km). Already after a time span of only 35 days, most of the (rural) area is decorrelated due to plant growth etc. Only urban parts, mainly the cities of Tianjin and Tangu, remain coherent. Therefore, we have selected the city of Tianjin as area to apply the "classical" InSAR method to derive a subsidence map. Topographic signal can be neglected for this area, since the maximum topographic difference is only 10 meters, resulting in approximately one third of a fringe difference at the perpendicular baselines used here (an example is provided in section 4.2.3).
Another limiting factor, besides temporal decorrelation, is atmospheric disturbance. This can be a significant signal over larger areas, depending on the weather conditions during the acquisitions (may be approximately 1 fringe over Tianjin area). In order to show this effect we processed an interferogram with a small perpendicular and temporal baseline. Averaging over a number of interferograms has reduced the atmospheric signal in the final deformation map.

4.2.2 Processing overview

Table 2 shows an overview of the images used in this analysis. Also check the baseline plot (Figure 25) that shows the distribution of the interferograms in time and space. The orbit and frame number of the SLC images, the perpendicular and temporal baseline, and Doppler centroid frequency are given. The first five interferograms are averaged to produce the deformation map. Interferogram 24122-23710, with a short temporal baseline and large spatial one, is used to obtain the topographic signal. Interferogram 24122-04538, with a short temporal and spatial baseline, is used to show atmospheric signal.

Interferogram	Bperp [m]	Btemp [days]	fDC diff [Hz]
21205-24122	255	210	50
21205-04538	250	211	330
21205-23710	-210	175	30
20203-23710	215	217	40
19702-23710	270	280	65
24122-23710	-465	35	-
24122-04358	-5	1	-

Table 2 Interferograms used for deformation analysis

Our goal is to produce a deformation map for 1996. The processing is performed with the Delft Doris software [Kampes, 1999]. Visualization has been done with the utility program "cpxfiddle" (www.geo.tudelft.nl/doris/).
Range filtering based on precise orbit information was performed for the five interferograms used in the analysis. This spectral filter removes the non-overlapping parts of the range spectra of master and slave image caused by a different viewing geometry. The algorithm based on the orbits can be used since the terrain is very flat. The expected increase in coherence due to this filter is approximately 20 percent for baselines of 200 meters. Non-overlapping parts in the azimuth spectrum can be filtered as well. This non-overlap is caused by different Doppler centroid frequencies, which result from different squint angles. This filter was only performed for interferogram 21205-04538 (see Table 2), as the Doppler centroid difference is only significant for that interferogram.
The complex interferogram is computed and filtered with the Goldstein algorithm (alpha 0.5; block size 32; overlap 3) [Goldstein, 1988]. The ground resolution of the interferogram is approximately 100 meters by 100 meters, due to complex multilooking with factors 25 in azimuth and 5 in range.
Multilooking and phase filtering is performed to reduce noise, which aids phase unwrapping, that easily breaks down in noisy areas. Unwrapping is performed to obtain absolute phase (deformation) differences. After unwrapping the interferogram contains a bias, which can be regarded as caused by the unknown integration constant. The interferograms are unwrapped using the tree algorithm obtained [Goldstein et al, 1998]. Note that not the entire interferogram can be unwrapped due to (temporal) noise, despite the filtering. Also it should be noted that unwrapping is less reliable at the edges of the unwrapped area, in the sense that almost isolated patches can have a phase jump of 2π.
The unwrapped phase is interpreted as a vertical deformation signal. The conversion formula is:

$$\Delta H = \frac{\lambda}{4\pi \cos\theta}\phi \qquad \textbf{(equation 14)}$$

Where ΔH is vertical deformation, λ is the wavelength, θ the angle of incidence, and φ is the unwrapped phase.
Finally, the radar coordinate system was transformed to WGS84 coordinates.
For a more detailed description of the processing check the InSAR cookbook in the appendix 'Recipe for InSAR processing with DORIS'.

4.2.3 Results

In this section we show the results of the processing. A magnitude image of the selected area is shown in Fig 36.
The phase of the six complex wrapped interferograms is shown in Figure 30 until Figure 35.

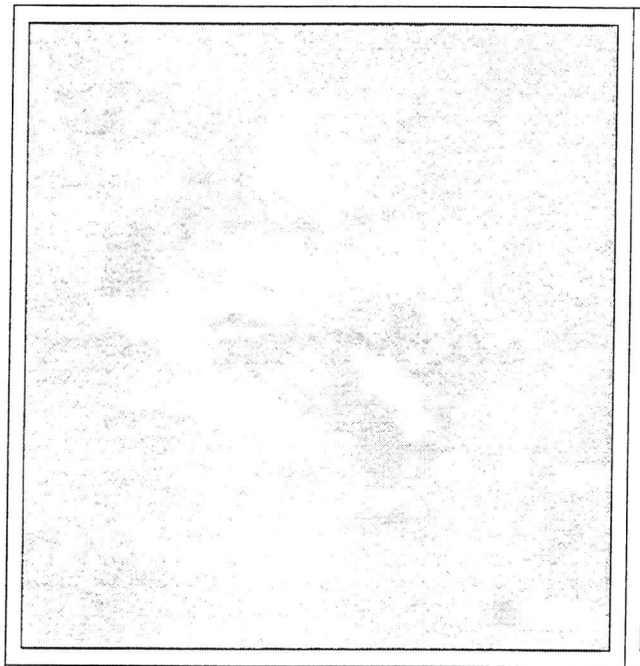

Figure 30 Phase of interferogram 21205-24122

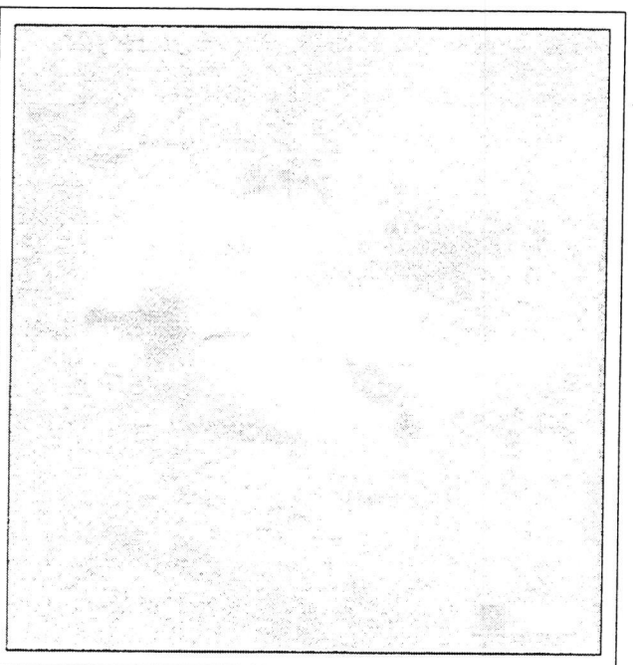

Figure 31 Phase of interferogram 21205-04538.

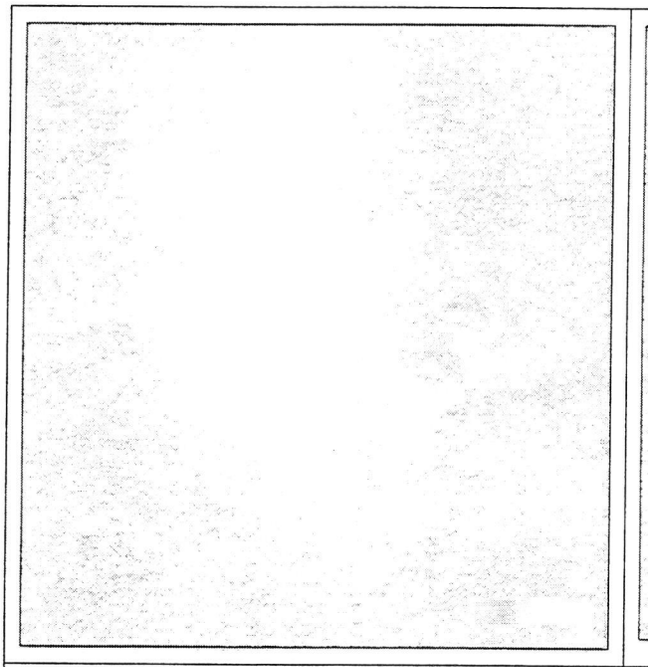

Figure 32, Phase of interferogram 21205-23710.

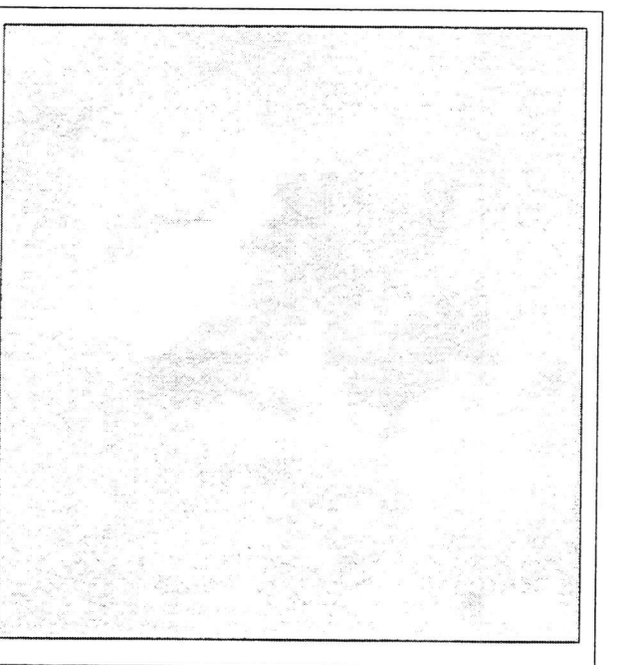

Figure 33 Phase of interferogram 20203-23710.

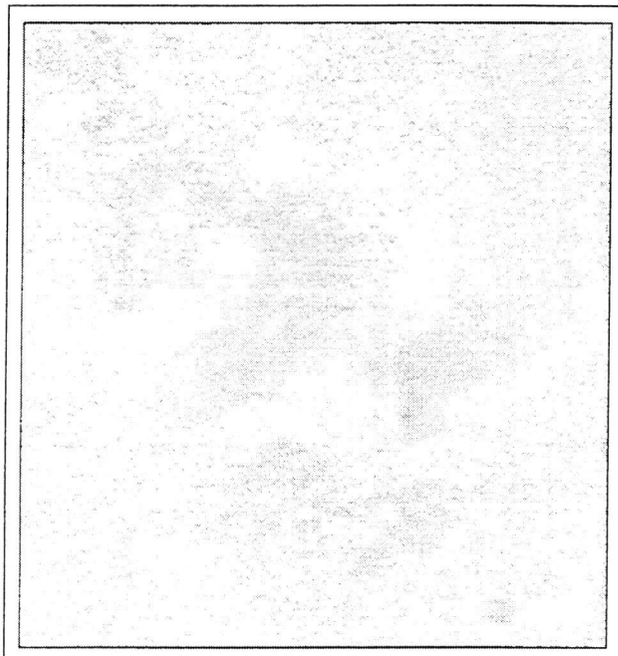

Figure 34 Phase of interferogram 19702-23710.

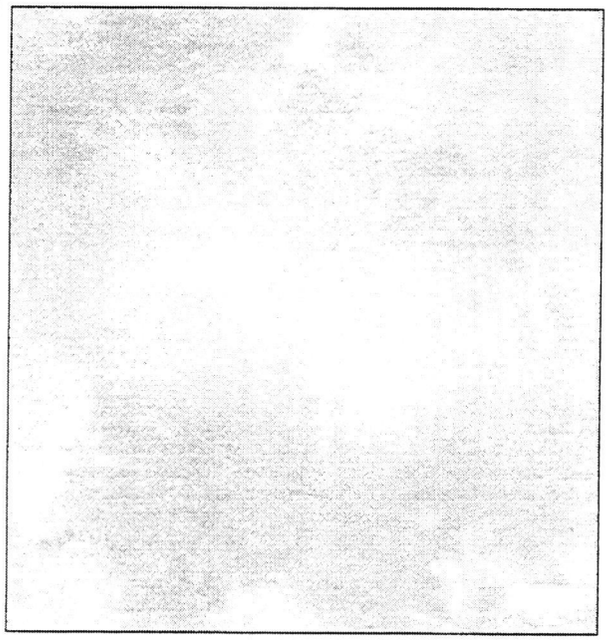

Figure 35. Topographic phase signal in the interferogram 24122-23710. This interferogram can be considered to contain only topographic signal and noise.

These interferograms contain deformation signal for approximately half a year (Aug 1995-Feb 1996). But besides this signal they may also contain topographic and atmospheric signal. Moreover, the interferograms can contain a trend due to orbit errors, and an unknown bias, since we use relative measurements.

First, we demonstrate that the topographic signal can be neglected here. Interferogram 24122-23710 (see Figure 35) with a perpendicular baseline of approximately 465 meters and a temporal baseline of 35 days mainly shows topographic signal. The height ambiguity for this interferogram is approximately 20 meters. At the most, a third fringe can be observed, centered at Tianjin city. This would imply that Tianjin center (or the buildings) is approximately 6 meters more elevated than the surroundings. Topographic signal can be neglected in the other interferograms, since in those cases the perpendicular baseline is half of this one. This interferogram has been corrected for a residual trend-caused by orbit inaccuracies-by hand It is clear from this figure that for the other interferograms with smaller baselines the effect of topography can be safely neglected.

Figure 36 Magnitude image of the Tianjin area (roughly 30 km x 30 km). This image is in the radar coordinate system, where the vertical axis is azimuth and horizontal axis is range coordinate.

The atmospheric signal in the interferograms is more difficult to eliminate. Interferogram 24122-04538 (see Fig. Figure 37) with a perpendicular baseline of approximately 5 meters and a temporal baseline of 1 day should only consist of atmospheric signal and noise terms. This figure gives an indication of the atmospheric signal in the interferograms.

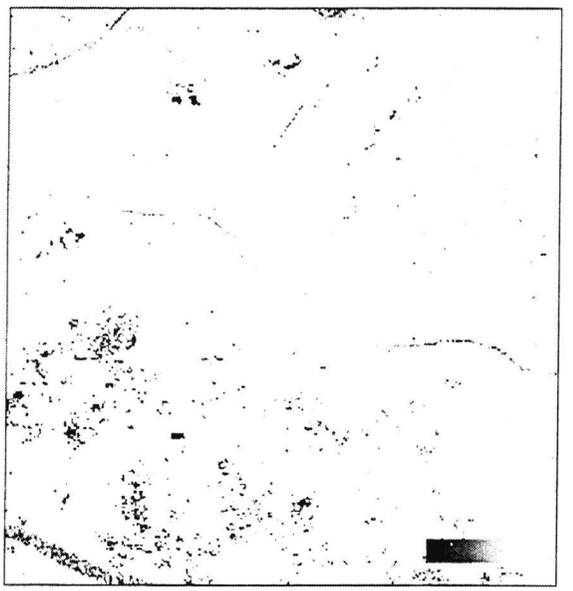

Figure 37 Example of atmospheric signal in phase of complex interferogram. Due to the small perpendicular baseline this interferogram can be considered to contain only atmospheric signal and noise. Approximately one third of a fringe can be recognized which is caused by atmospheric delays. The other interferograms can be expected to contain at least the same atmospheric signal.

For this interferogram the atmospheric signal is small, a third fringe at maximum.

However, this does not proof that atmospheric signal can be neglected, since the weather conditions are totally different during the other acquisition times. By comparing Figure 30 with Figure 31, and Figure 32 with Figure 33 (which has a different master), it can be seen that the signal in the center part (the two light blue blobs in the center of Figure 30) are most likely caused by atmospheric delays in the master acquisition. This is likely since

these two signals are not present in Figure 33, which cannot be true if it would be topography or deformation. This demonstrates the danger of interpretation of a single interferogram. In this case, the atmospheric signal, if interpreted as deformation, would result in an uplift of approximately 25 mm per year.
In order to reduce the effect of atmosphere we computed the weighted average of the five selected interferograms, see Figure 38. The weighted average is computed from the unwrapped interferograms as

$$\overline{ifg} = \frac{\sum_i ifg_i}{\sum_i B_{temp,i}} \qquad \textbf{(equation 15)}$$

This implies that interferograms with a small temporal baseline are down weighted, which is desired since they have a relative low signal to noise ratio. The assumption here is that the mean of the atmospheric signal is zero, which is not necessarily true, since the atmospheric condition during the master acquisition may be dominant. Also note that the atmospheric signal in the interferogram is caused by a difference in water vapor distribution of the two SLC images. Thus, if in the averaging interferograms are used that share a common master; the averaged interferogram still contains the atmospheric signal of the master.

The third effect in the interferograms is corrected by using ground control points. But instead of using, e.g., GPS points, we corrected the interferograms for a residual trend by computing an optimal fit with 12 points in the digitized leveling map.

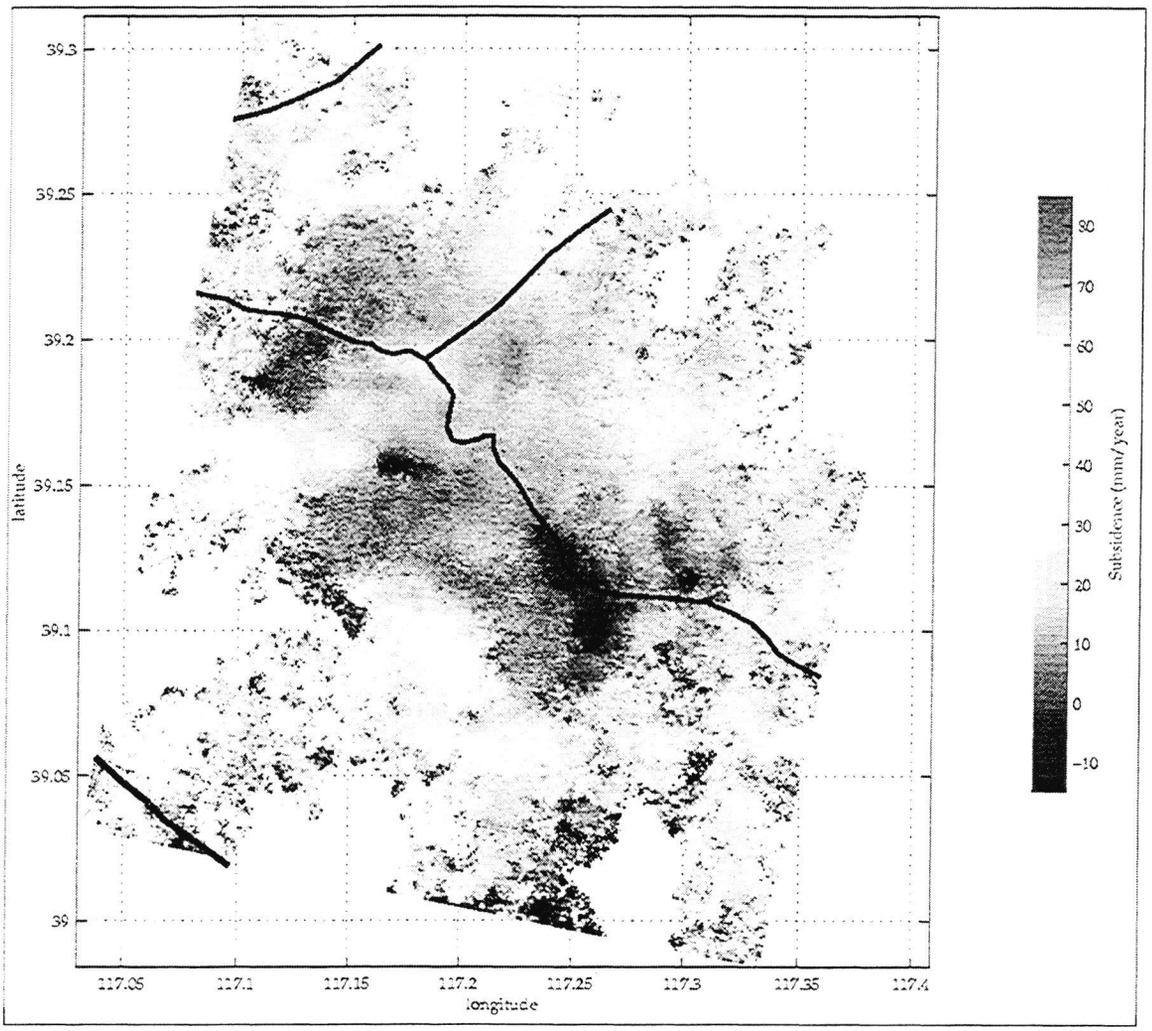

Figure 38 vertical deformation maps for Tianjin city for 1996. This is the average over five interferograms with a temporal baseline of approximately half a year, from April 1995 to March 1996. Given is the vertical deformation in mm per year. The image was geocoded from radar system into WGS-84 system.

The following picture combines the amplitude and deformation.

Figure 39, Magnitude image combined with a deformation map

In the combined picture it is clear that coherence is only maintained within the urban areas. The agricultural fields in the South never showed a useful result. This type of imagery allows rapid location of deformation sources, at the same time providing some detail on the reliability of the measurement.

4.2.4 Conclusions

Though temporal decorrelation is the major limiting factor for applying this analysis, a reliable deformation map can be formed for urban areas. This is further investigated in chapter 5 'Validation of InSAR results'.

Weighted averaging can reduce atmospheric delays. The best strategy is to combine several interferograms, using different SLC images for all of them. This satisfies the conditions that the expectation of the atmospheric signal in the interferograms is zero.
Unwrapping problems arise at the edges of the coherent areas. A different unwrapping algorithm may be able to improve this, although the real noisy parts can never be unwrapped.
Spectral filtering should be applied in azimuth and range to increase the signal to noise ratio. Phase filtering of the interferogram also should be applied.
Using larger temporal baselines can improve the results, since the deformation signal is relatively larger in that case. The drawback is that temporal decorrelation also will be larger.

4.3 Subsidence measurement in Tianjin by Permanent Scatterers

4.3.1 Introduction

With the use of the PS-method almost all interferograms from ERS-1/ERS-2 over a certain area can be used. For this method uniform baseline coverage, in time as well as spatial, is preferred. Contrary to the usual InSAR method large temporal baselines are no problem for the PS-method. If a topographic correction with accuracy of about 10m height can be applied, large perpendicular baselines can be accepted as well. The data used for this method are presented in Table 1, in the last column the interferograms used for the PS method, are marked.

4.3.2 Data selection

It was decided to use a subset covering the city of Tianjin. This decision was based on the fact that the largest subsidence was measured on the western, southern and northern borders of the city (up to 100 mm/year). The magnitude image of this subset is given in Figure 40.

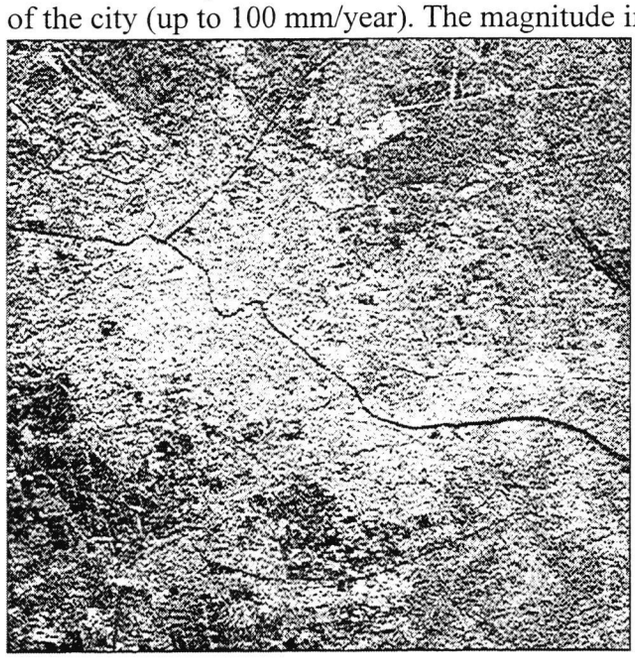

Figure 40: Magnitude image of Tianjin city (image measures ~25 x 25 km).

4.3.3 Results of PS- method

Before the results are plotted some remarks. In this data set some assumptions are made:

- There is no topographic signal in the data
- The deformations are linear in time
- The atmosphere is nearly constant over a 5x5 km radius

To find a solution a uniform distribution of PS-points is needed. (To solve the redundancy).
In relation to these assumptions, the following can be said about the real data gathered:

1) For large baselines (>600 m) topography must be corrected for.
2) Deformations could be seasonal (not linear in time.
3) Large atmospheric signals could not be corrected for.
4) The selection of PS-candidates is ambiguous and not uniform.

Ad 1) As can be seen the use of real data imposes restrictions on the result. The only thing that can be done is to try to select the most suitable interferograms. Large spatial baselines were rejected. Two cases were even rejected because of their very large temporal baselines.
Ad 2) Considering the second remark nothing can be done, the algorithm is designed for linear deformation. It is assumed that the general seasonal character of subsidence may be neglected.
In case of Tianjin this assumption seems reasonable (see paragraph 4.1.1). However, in some areas, intensive subsidence within one month was observed (Hangu), as this exceeded the yearly subsidence rate, seasonal subsidence may sometimes be present.
Ad 3) The third remark is checked visually as much as possible. If atmospheric influence was doubtful, the interferogram was not removed from the stack because as many interferograms as possible are needed.
Ad 4) The fourth remark is the trickiest one. It is of utmost importance to select the true PS points as the whole method depends on it. The selection of the PS-candidates deviates from the procedure as followed in the simulation runs, no random distribution was chosen, but the points with amplitudes above a certain level were selected. This was done for each interferogram. To see if each selected point was in each interferogram an "AND" operator was used. If a point was not in one of the 20 interferograms, the point was removed from the selection. The resulting selection of 279 PS-candidates is plotted below.

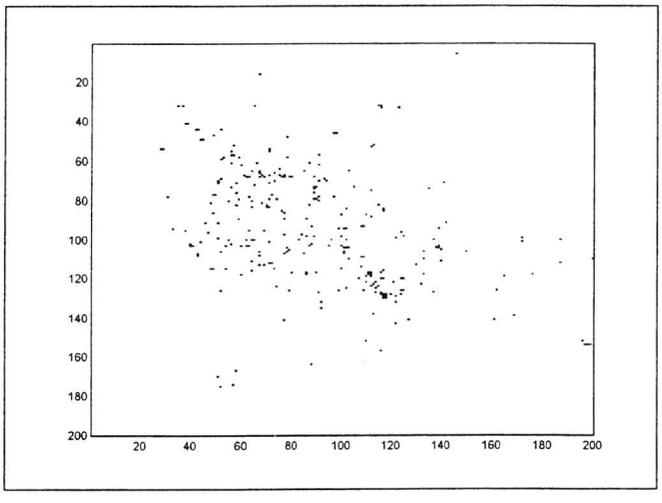

Figure 41: selection of 279 PS-candidates. Area is the same as in Figure 40

With these PS-candidates out of 14 selected interferograms the calculation was performed with a window size of 29 x 29 pixels. The subsidence limit was set to 50 mm/year as the maximum differential deformation rate between two points.

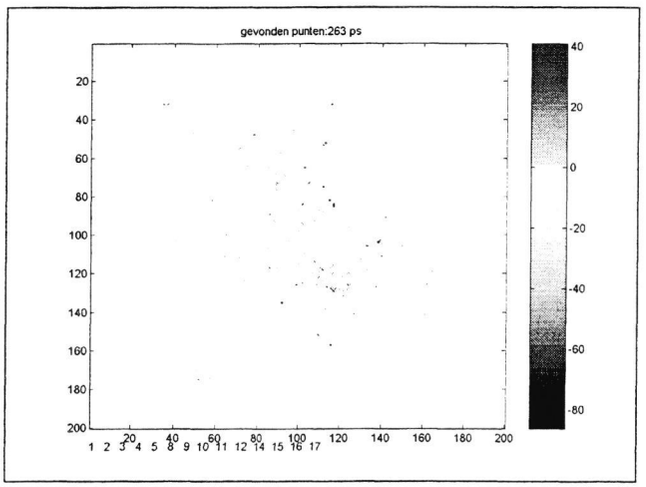

Figure 42: Result of PS software. 263 PS identified out of the initial 279 PS candidates. Deformation in mm/year over the period October 1992 / October 1998. Note that the offset allows for positive results.

The points found are then interpolated with a bi-cubic interpolation.

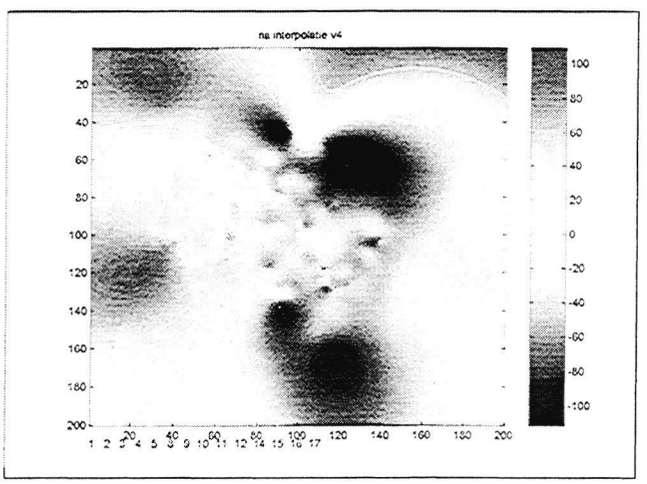

Figure 43: Interpolated (bicubic) result of Figure 42 (limit of 50 mm/year in the deformation matrix).

This interpolation method (from Matlab) causes the deformation rate to become very high to the edges of the image. The most reliable information is in the zone were the PS are densely distributed (see Figure 42). The results are not satisfactory. A comparison with the ground truth is given in chapter 5.2.

5 VALIDATION OF INSAR RESULTS

5.1 The classical interferometric approach

Introduction
In section 4.2, we described the processing with classical interferometric techniques of several interferograms to derive a deformation map for the city of Tianjin. In this section, we will compare the results of the classical interferometric approach with the TCLO leveling maps that we had to our disposal. For more detail on error analysis reference is made to Hanssen, 2001.

Deformation map generation
The deformation map, calculated from the mean of five interferograms as described in 4.2.2, was processed to accommodate the comparison with the leveling data. The map was smoothed in order to reduce noise and to obtain the same resolution as the leveling map. The resolution was reduced from 100 meters to approximately one kilometer. The deformation was scaled to half a year, because this was approximately the mean temporal baseline of the five interferograms. In this way, the atmospheric features in the interferograms, which are not proportional to the temporal baseline, are prevented from being up scaled (Figure 44).

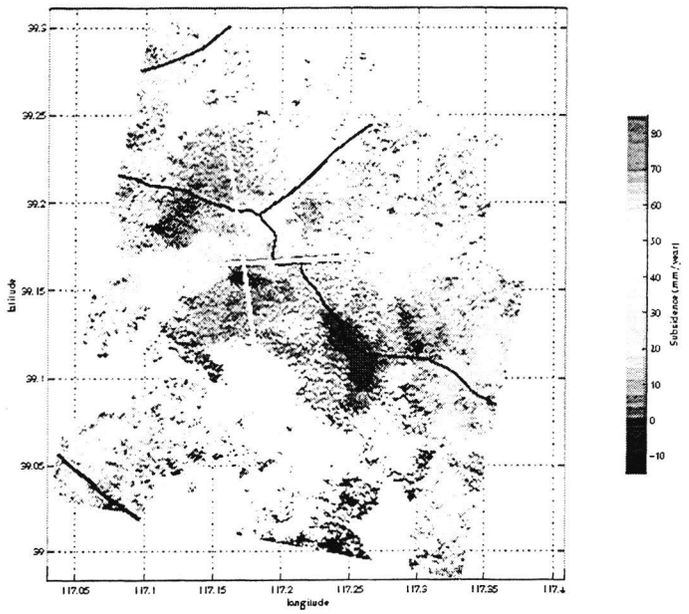

Figure 44 Vertical deformation maps for Tianjin city for 1996. Shown is the weighted average over five interferograms with temporal baselines of approximately half a year, from April 1995 to March 1996. Atmospheric signal remains present in this average, particularly visible in the blue (uplift) areas in the center. The data is georeferenced in the WGS84 system. For orientation the "Yongding He" and "Hai He" rivers are sketched on top. The white lines indicate the location of the two profiles shown in Figure 45 and Figure 46.

Two profiles have been extracted from the deformation map. The white lines in Figure 44 indicate the locations of the profiles. These profiles were drawn over characteristic features in the interferogram, one from the Northwest to the South, containing the Northwestern bowl (Figure 45).

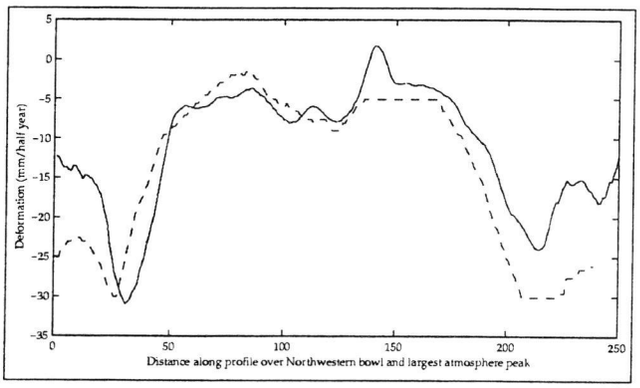

Figure 45 Profile along line from Northwest to South.

The other profile was taken from West to East (Figure 46). The advantage of the use of profiles is that one can get an impression of the deviation of the interferometric deformation map with respect to the leveling map.

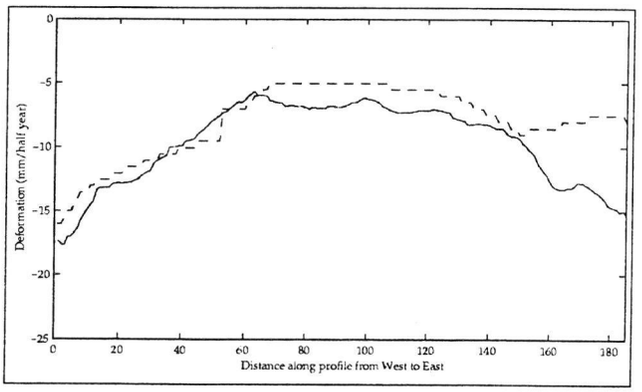

Figure 46 Profile along line from West to East.

To compare the interferometric deformation map with the leveling map, the leveling map was transformed to the radar coordinate system. In Figure 39, we presented a map of the amplitude of an interferogram, with the color-coded deformation map overlaid. With this map, the location of the deformation features can easily be interpreted.

Leveling map preparation

In order to be able to interpret the comparison results, the processing of the leveling data to yield the leveling map will be described. The Tianjin Control Landsubsidence Office (TCLO) stores the leveling data in a database. The coordinates of the leveling points are in the Chinese system. Sporadically, these coordinates contain errors. However, the leveling heights themselves almost certain do not contain errors. From these point data, TCLO calculated an interpolated map and plotted this as a contour map on paper, superposed on the leveling points and a map of Tianjin. EARS digitized the contours of the TCLO leveling map and calculated an interpolated map. EARS transformed the interpolated leveling map

to the radar coordinate system. This was done by fitting the Chinese background map on a high-resolution interferometric amplitude image.

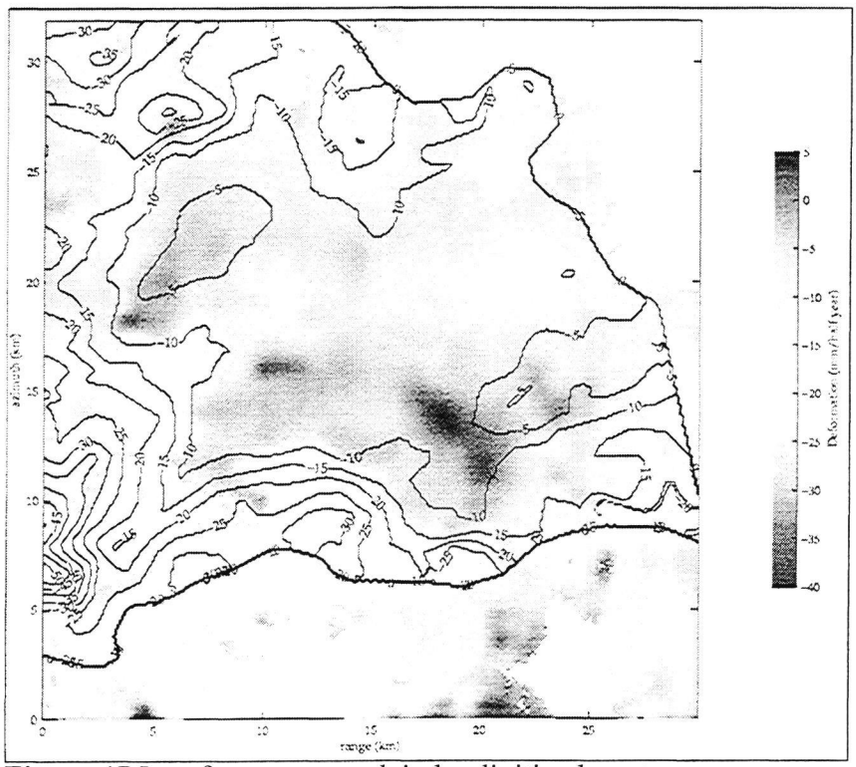

Figure 47 Interferogram overlain by digitized contours

The interpolation is not free of errors, as can be seen from the profiles in Figure 45 and Figure 46 where the interpolation is cut off in the extremes of the profiles. In the digitization of the other maps this effect was emphasized by adding extra points where needed.

Comparing interferometric deformation vs. subsidence leveling measurements

As described before, the deformation map of Figure 47 contains only data where two to five of the interferograms were reliable; in the white regions at most one interferogram contained unwrapped data. The leveling data do not cover the whole subset of the radar image, resulting in a thick black contour at the edge. In general, the features visible in the interferometric deformation map are also present in the leveling data (Figure 45). For example, the deformation present in the South and Southwest coincides very well with the leveling contours. The presence of a strong deformation bowl in the northwest is in good accordance with the leveling data. However, the subsidence bowl in the leveling data does not coincide in location with the bowl in the interferometric map. It is well possible that the original leveling data contains coordinate errors like this as the leveling points are spaced at about 1500 meters.

The bowl in the leveling contour map is based only on one leveling point with a subsidence rate of 63 mm/year, surrounded by four points with rates of about 50 mm/year. In the original map (1995) a point to the south of the bowl is visible with a subsidence of 69 mm/year, which seems not to have been included in the contour calculation for the Chinese map.

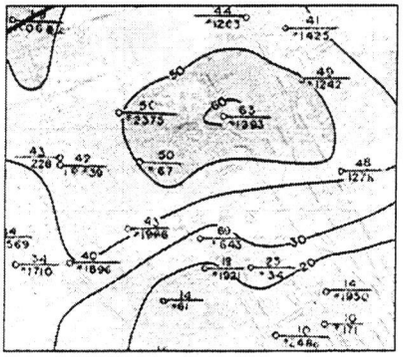

Figure 48 Contouring error, the 69 mm subsidence point was not used, this is obvious if we compare the same area with the InSAR result (next figure)

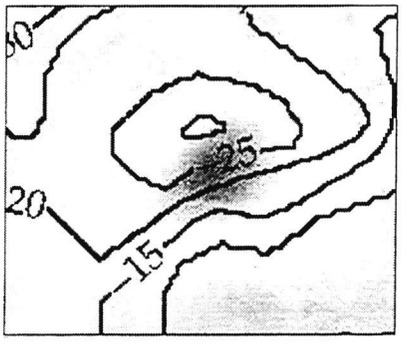

Figure 49 Leveling contours over InSAR result. The contour map was not annotated correct (apply factor 2), the shape of the lines clearly deviates from the InSAR result.

Although it is possible that the registration of the digitized and interpolated leveling map with the radar amplitude image was not performed very well, this is not likely. Errors can also be made when transferring the leveling data to the map, or during the manual drawing as applied during the contouring process. Therefore the interferometric deformation map is regarded to be more reliable as compared to the leveling map.
The deformation was scaled to half a year instead of to a full year in order to prevent the atmospheric features from being up scaled. Nevertheless atmospheric delays are still visible. The dark blue features in the middle of the city of Tianjin show a deformation of zero to an uplift of a few millimeters per half year. The leveling data show a minimum subsidence of a few millimeters per year on these locations. It must be noted that in particular in these areas, the interpolation of the leveling data is erroneous, being cut off at the level of minus 10 mm/year. This is also demonstrated by the profile of Figure 46. These atmospheric features were caused by a single SLC image, which was used as a master for three of the five interferograms. This shows that better results, i.e., less atmospheric errors, can be expected if the averaging is performed over independent interferograms.
In the North-South profile in Figure 45, the atmospheric feature is visible as a peak 5 mm higher than the leveling data (dashed). However, as described before, the leveling data have been erroneously interpolated in this area, as can be seen from the cut-off. The North-South profile shows the deep bowl. Very well it has exactly the same subsidence rate as the bowl shown by the leveling data. This is not due to scaling the interferometric deformation map, but an intrinsic feature. Averaging five interferograms, of which each was fitted to twelve leveling tie points by application of a plane correction, generated the deformation map. Although this fit can contain errors, e.g., where the patch coincided with an area where atmospheric delay is present, it cannot cause scaling of the deformation features. The map,

and in particular the profiles show clearly that the interferometric deformation map underestimates the deformation at the edges. This can be due to fitting errors, but the by far most important reason for these are unwrapping errors. Due to the temporal decorrelation of the non-urban areas of Tianjin, the interferograms show more noise, hampering the unwrapping. Although we corrected a few regions at the edges, it is very likely that the borders show erroneous unwrapping results. However, for the urban area itself, the unwrapping, and hence the deformation, will be reliable. The standard deviation of the deformation signal has a lower bound due to atmospheric delay. This can be estimated by calculating the standard deviation over a patch of the deformation map where no topography and no deformation are assumed. For this deformation map, the estimated standard deviation due to atmosphere is 2 to 3 mm per half year. On patches with a strong atmospheric signal, however, the standard deviation is several times larger. The standard deviation of the deformation map with respect to the interpolated leveling was determined from the regions were no unwrapping errors, no large atmospheric delays and no mayor influence of the leveling co-registration error were expected. This standard deviation is approximately 3 to 4 mm per half year. Note that for interpretation of the interferometric deformation, the difference of the deformation between two neighboring points is a more valid measure than the absolute deformation rate itself. Also the standard deviation of the deformation difference between two points is decreasing if the distance between the two points is decreasing.

5.2 PS method results

Introduction

The results of the PS method were that much limited that it was decided to restrict the validation of the result to a visual comparison. Data delivered by TCLO have been digitized and visualized for this purpose.

Validation

The PS point measurements have been interpolated in Matlab. As no PS were found at the border of the image the interpolation results outside the PS cloud should be ignored. The data used for validation is based on the yearly subsidence contour maps as made by TCLO. The map produced by the PS method was made under the assumption that the subsidence was linear. By calculating the average of the yearly subsidence over the same period as the input used for the PS method, two maps would be obtained that should be directly comparable. This was achieved by calculating the average subsidence using the subsidence maps made by TCLO.

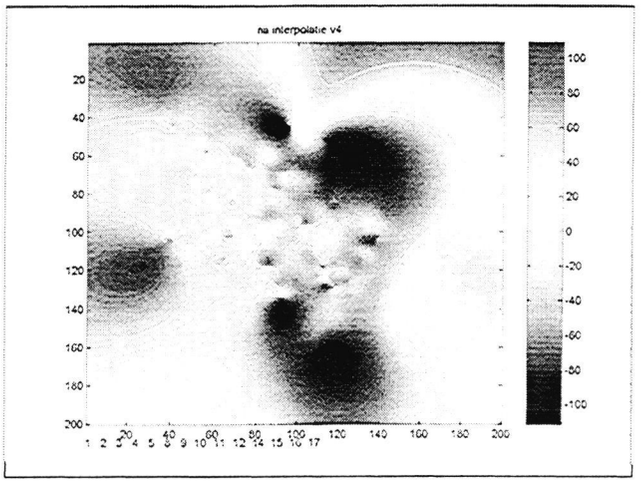

Figure 50: Interpolated (bi-cubic) result as already shown in Figure 42

The image in Figure 50 is projected on the same grid as the images of Figure 51. The grid size of the latter is 5000 meters. Subsidence is given in mm per year.

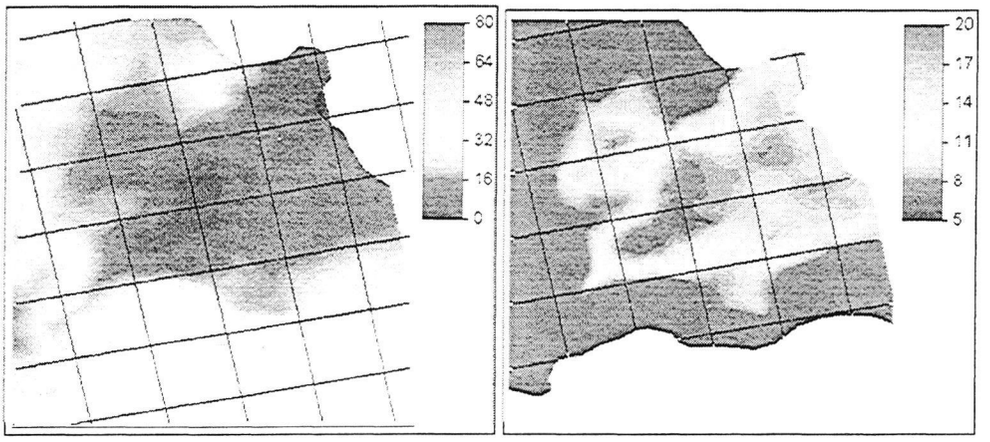

Figure 51: Left mean deformation GPS/ leveling 1992-1999 (0-80 mm/yr), on the right side the same data, but scaled to enhance details in the urban area.

Comparing Figure 50 with Figure 51, we see that some deformation areas coincide. In the West and Northwest areas, deformation zones are found but with the wrong values. In the northeast a large zone is found which is absent in the GPS / leveling data. This pattern may be due to subsidence but could also be due to atmospheric disturbance.

We see that the most reliable information is in the zone were the PS are concentrated (see Figure 20). A peculiar thing about these results is that they give mostly positive deformation rates instead of negative ones. Looking at the position of the "deformation zones" in the figures, roughly the same areas are found at the edges of the city (as expected), but(!) they seem to be formed by the interpolation method. If we look at the individual PS results of Figure 42 it is clear that almost no points are found at the edge of the city.

Conclusions

The primary goal of this study was to demonstrate that the PS-method can be used in non-urban areas with low coherence and with low deformation rates. The result is not a success,

but a promising start has been made. Simulations showed that this method has potential. The first results from the use of this PS-method seem very promising, but caution is needed. Still a lot of problems around the method exist and quite some study must be done to obtain a solid and commercial method. If the calculations are set up more carefully and notice is taken of the remarks listed below better results are likely.

Recommendations

1) A better way must be found to select PS-candidates. The method applied within this project is easy but results in an overwhelming number of points in the city and almost no candidates in the suburban areas. By selecting the top percentage in highest amplitudes we may miss important candidates in non-urban areas. A solution could be to select smaller areas or areas around Tianjin city. This was after the choice of our sub area due to lack of time not possible in this project.
2) If a suitable DEM is available, topography should be subtracted with an accuracy of 10 meters or better. If this is possible more interferograms can be used. These data did exist, but could not be made available under current governmental regulations. The interferograms with large baselines (>600 meter) caused serious disturbances in the deformation measurements; these were therefore not used in the calculations for the PS-method.
3) Non-linear deformations caused by seasonal effects can disturb the fitting with linear deformation rates. It is not clear in which areas the assumption of linear deformation is reasonable (see paragraph 4.1.1).

Large local delays caused by the atmosphere are problematic. Although small delays can be accounted for (5x5 km scales), large thunderstorms and other large water vapor disturbances can cause significant errors in the measurements. The solution is to use as many interferograms as possible so the atmosphere averages out or can be estimated and subtracted [Ferretti et al., 1999].

6 COST BENEFIT EVALUATION

In this section a brief evaluation of the commercial feasibility of interferometry in the Tianjin area.

6.1 Present cost of subsidence mapping

The total cost of subsidence mapping in Tianjin is approximately 1.000.000 US$ per year. TCLO serves as the main contractor and is paid by the Tianjin Construction Union that directly represents the Tianjin government. The costs involved for TCLO are unknown. The share in costs of each participant is nearly equivalent to the amount of people involved.

Company	Function	No. of persons	Cost in US-$
TGM	Management of geothermal water extraction and monitoring of subsidence	15	225.000
TSM	Monitoring and mapping of subsidence	35	550.000
NDMC	Monitoring of subsidence	15	225.000

To evaluate cost benefits of InSAR for application in Tianjin subsidence it is important to understand that the situation cannot be compared with that in Europe. For a person with a university degree a net salary of 1000 RMB (U.S.$ 125, -) per month is not uncommon. For labor that requires lower education only, the net monthly salary can be in the order of 300 RMB. In contradiction to these figures the cost for hardware, software and satellite data is comparable to European level. Consequently the cost of hard- and software is a decisive factor when evaluating the cost benefits of InSAR.

6.2 Benefits InSAR subsidence measurement

The application of InSAR in the urban areas of Tianjin was successful. A number of possible benefits of applying InSAR to measure surface deformations in Tianjin can be formulated:

- Enhancement of the leveling result
  Leveling is based on point measurements. These point measurements are interpolated to produce a subsidence contour map. The interpolation is based on assumptions. Using interferometry these assumptions can be replaced by measurements. The speed and accuracy of the production of contour maps may thus be increased.

- Instantaneous data capture of whole Tianjin area
  The leveling campaign is a one yearly repeated job that takes about three months, including measurements and mapping. Although data availability cannot be guaranteed, interferometric measurements can be repeated easily with shorter intervals. The radar data acquired within a few seconds. Therefore the result is not influenced by the possible deformations during the leveling campaign.

- Large coverage and high resolution of SAR data
  The scale of a full ERS image is about 100 km x 100 km. The ground resolution of the pixels is approximately 4 x 20 meter. Note that for the reduction of noise, the SLC images are multilooked to a resolution of 100 x 100 meters. Nevertheless, this resolution is higher than required for subsidence measurements. Small subsidence events may be recognized, subsidence pits missed by the leveling network may be detected, and the location of subsidence phenomena can be pinpointed with a high precision.

- High accuracy measurement
  Provided that a DEM is present the relative precision of InSAR subsidence measurements can be very high (in the order of one cm). This is comparable with GPS measurements, but better than traditional leveling.

- Simple and low priced operational set up is possible
  Basic requirements for an operational InSAR system are relatively cheap. The hardware requirements are low cost, e.g. a Pentium processor of 500 MHz, hard disk >40Gb, RAM >128Mb will do fine. Low priced software or freeware for processing of SAR SLC data is available (Linux, Doris package). In addition it should be mentioned that the use of the Doris package allows a highly flexible and verbose approach, in which different algorithms can be used of which the settings can be tuned to fit the user's needs.

- Fast result
  Provided that an operational interferometric system is implemented in the subsidence measurement procedures, the processing and integration of one set of new interferometric data should be possible within 5 working days.

- PS methodology
  With the relative new development of the PS method, possibilities exist to measure deformation of individual (artificial) point reflectors. In the future this method may be very useful outside the urban areas. See section 2.2 or [Ferretti et al., 1999] for more detail.

6.3 Limitations of InSAR subsidence measurement

The results of the InSAR techniques applied within this project for the measurement of subsidence in the city of Tianjin were successful. However, for the area outside these areas whole the measurements were not very satisfactory.

- Temporal decorrelation is problematic. Only in the urban areas coherence is maintained over longer periods. Consequently only these areas can be unwrapped. Outside the urban area only small distinctive coherent features are present (railways, tiny communities).

- The perpendicular baseline decorrelation may be problematic. Out of the 23 images derived only 20 independent interferograms suitable for subsidence mapping could be produced.

- Atmospheric influence on the images can be high. It is sometimes difficult, if not impossible, to indicate the atmospheric disturbances. Even when weather satellite data is available it is difficult to foresee problems; i.e. water in gas form also adds to the signal delay.

- Acquisition of data is based on requests. No guarantee can be given on the acquisition or the availability of SAR data. For instance three data captures of ERS data covering Tianjin were cancelled during the past year.

- Data is not very cheap. ERS data requested for commercial purpose is priced at 1000 Euro per image, an alternative provider like RADARSAT is more expensive with prices of about 2000 Euro.

- The PS method demonstrated in this project is not yet operational. Results were promising but no satisfying results have been achieved yet.

- At this moment availability of SAR data applicable for deformation measurement is restricted! In the near future satellites will become available like ENVISAT (2001), RADARSAT2 (2003).

6.4 Conclusions on cost benefit of InSAR measurements in Tianjin

Though the results of InSAR in urban areas can be used to replace part of the leveling work, it is difficult to predict to what extend the possible benefits, as listed in paragraph 6.2, can be applied. One reason is that authorities outside this project should answer this question, another reason is that more investigation is needed, in particular for the PS method.

Useful results of interferometry for Tianjin are possible at present for the urban areas, in particular Tianjin city. The subsidence maps derived from the interferometric imagery showed close correlation with the subsidence mapped using leveling. These subsidence maps present a relative estimate. After calibrating with the ground truth as provided either by a few of the leveling points, or by at least 3 DGPS points, these maps can be transformed into absolute subsidence maps. These results are useful as an aid during the contouring of the subsidence maps and may well be used to reduce the number of leveling points in the Tianjin city area. The detection of small local phenomena is another direct improvement. The results may also be used to indicate where additional leveling should be done, or where the leveling network should be adapted to include specific small subsidence features.

The cost for implementing an InSAR system for measurement of subsidence in Tianjin does not have to be very high. The processing and implementation of InSAR data can be done within a few days provided that an operational set up is available. Relatively simple hardware can be used, and cheap –if not free– software is available. Commercial software is expensive but the use may be justified when compared to the total cost of the leveling campaign. A cost factor that can be of concern is the cost for data, at present new data is relatively expensive as acquisition can only done by RadarSat. The low budget set up within this project works well and may well be preferred above commercial packages for reason of higher level of user control and better performance.

7 CONCLUSIONS AND RECOMMENDATIONS

The demonstration of the conventional InSAR in Tianjin was successful in the urban areas. It was made clear that in the urbanizations interferometry is useable to reduce cost of the leveling campaign and improve its results. It is possible to reduce the amount of benchmarks of the leveling network, to simplify the interpretation of the leveling results into contour maps and to indicate where extra leveling measurements might be required. Outside the urban areas coherence was lost, and consequently conventional InSAR were of no use.

The demonstration of the relatively new method of "Permanent Scatterers" (PS) on the Tianjin data was not satisfactory, though some of the results were promising. The results of this methodology when applied to simulated SAR data were good. Successful application of a similar method is known [Ferretti, 1998]. In the near future this technique will be developed further, because it promises to be an important direction for the development of InSAR processing. This method provides individual measurements over the whole SAR image, even for scenes showing decorrelation in the classical approach, and thus will be a major improvement when compared with the conventional InSAR. already during the final editing of this report, further research into the PS-method showed successful measurements outside the urban areas in Tianjin.

During the project the orbit of the ERS-2 satellite became less stable; the future ERS data are therefore less applicable for interferometry. At the moment the only other satellite available is RADARSAT. In the coming years several other radar satellites will be launched that can be used for interferometry like RADARSAT2 (April 2003), ENVISAT (autumn 2001), or LightSAR. With the result of this study it should be possible to do a quick inventory whether or not the data provided by these new satellites can be used.

As discussed in section 6.2 several possibilities may be of commercial interest. To what extend these can be applied should be investigated.
To improve the results of the conventional InSAR method as applied here, the following is recommended:

- improve the validation of the InSAR results by using the available geological data, well locations and water extraction data to have a more clear idea on local subsidence features and the temporal behavior of the subsidence.
- Apply a DEM correction
- Include a stochastic model of the atmosphere
- Validate the precision of the InSAR results based on the various error distributions

For the future measurements on subsidence the PS-method should have our attention, if successful this will be a very useful tool for subsidence mapping of Tianjin area. Especially when reasonable priced SAR data becomes available on a regular basis.

8 REFERENCES

Bree, van R.J.P., Gens, R., Groot, J.S., Halsema, van D., Hanssen, R.F., Hout, van den P., Klees, R., Min, de E.J., Schrama, E.J.O., Usai, S, 1999, Deformation measurements with SAR, BCRS report no. 99-16, BCRS, Delft, The Netherlands.

Ferretti, A., Prati, C., and Rocca, F., 1999, Permanent Scatterers in SAR interferometry, Proc. IGARSS 1999, pp1528-1530, Hamburg, Germany.

Ferretti, A., Prati, C., and Rocca, F., 2000, Non-lineair subsidence rate estimation using permanent scatterers in differential SAR interferometry, submitted to IEEE Transactions on Geosience and Remote Sensing.

Hanssen, R.F., 1998, Atmospheric heterogeneities in ERS tandem SAR interferometry, DEOS report no. 98.1, Delft University Press, Delft, The Netherlands.

Hanssen, R.F., 2001, Radar interferometry: Data interpretation and error analysis, Kluwer, Dordrecht, the Netherlands, ISBN 0-7923-6945-9.

Haynes, M., Capes, R., Lawrence, G., Smith, A., Shilston, D., and Nicholls, G., 1997, Major urban subsidence mapped by differential SAR interferometry , Proc. of the 3rd ERS Symposium (ESA), 18-21 March 1997, Florence, Italy.

Goldstein,R.M., H.A.Zebker and C.L.Werner, " Satellite Radar Interefrometric: Two dimensional phase unwrapping", Radio Sci, Volume 23, No.4, July, 1988.

Kampes B., S. Usai, Doris: the Delft Object-oriented Radar Interferometric Software, 2nd International Symposium on Operationalization of Remote Sensing, 1999.

Kooij, M.W.A. van der, 1997, Land subsidence measurements at the Belridge oil fields from ERS InSAR data. Proc. of the 3rd ERS Symposium (ESA), 18-21 March 1997, Florence, Italy.

Prati, F. Rocca, A. Monti Guarnieri, E. Damonti, 1990, "Seismic migration for SAR focusing: Interferometrical applications," *IEEE Transactions on Geoscience and Remote Sensing*, vol. 28, no. 4, pp. 627-640.

Scharroo R., P. Visser, Precise orbit determination and gravity field improvement for ERS satellites, J. Geophys. Res. 103, 8113-8127, 1998.

Swart, L.M.Th., Spectral filtering and over sampling for radar interferometry, Master thesis, Delft University of technology, 2000.

Stow, R. J., and Wright, P., 1997, Mining subsidence land surveying by SAR interferometry. Proc. of the 3rd ERS Symposium (ESA), 18-21 March 1997, Florence, Italy.

Valkengoe, E., S. Boks, 2000, Airborne InSAR demonstration for urban and rural applications, BCRS project 3.1/DE-06, BCRS report 00-01.

Wegmuller, U., Strozzi, T. and Werner, C., 1998, Land subsidence in the Po river valley – Italy Proc. IGARSS 1998, vol. 3, pp. 1376-1378.

APPENDICES

A Recipe for InSAR processing with Doris

B Recipe for stack SAR-processing with ESARP

C Internet links

D Figures in full color

Appendix A: Recipe for InSAR processing with Doris

with special interest to permanent scatterers

Rens Swart and Bert Kampes
Version 2.0 • 10 May 2001

This recipe is intended as a guide for the interferometric SAR processing as performed at the department of Geodesy of the Delft University of Technology. For the processing we use our public domain scientific interferometric processor *Doris* and some auxiliary software or scripts we developed. Not all software used below will be generally available, but nevertheless the interferometric processing will become clear from the description.

The recipe will describe the interferometric processing with special interest to permanent scatterers, but the steps to perform the classical interferometric approach will be described as an alternative. Also the use of SLC images processed from raw SAR images with the ESARP SAR processor will be described as an alternative to the use of generally available SLC images.

1. Acquire SLC-images

Assume that the full scene single look complex (SLC) images are present on CD-ROM, e.g., ordered from ESA or processed from raw images with the ESARP SAR processor (cf. our *Recipe SAR processing*).

2. Select master image and set up environment

Select master image of stack:
Should be central in time/baseline plot.
Preferably tandem to be able to apply a differential topography correction.
Orbits must be present (/home/fmr/d4/delftorbits/ers.., webpage http://www.deos.tudelft.nl/ers/precorbs/), otherwise select different master.
Naming and environment:
Make directories for each interferometric pair following the naming scheme masterorbit_slaveorbit.
Name the interferometric products masterorbit_slaveorbit.dorisstep, e.g., 32728_18934.srp.
Still to discuss: how to rename for a reliable, platform-independent writing to CD.
Remarks:
Do not use tandem pair for estimation of deformation.
Keep track of bad regions (e.g., bad azimuth compression due to missing lines), possibly by means of a flag; include a term for this in the covariance model.

3. Determine region of interest

Determine region of interest in master coordinates.
If no image is present to select the region of interest, first run the initial steps of Doris (see below) in order to generate a raw (and cropped) SLC image that can be viewed with, e.g., 'disp'. The SLC-images processed with the ESARP SAR-processor are already raw SLC (without file- or record headers) and can be viewed with 'disp' (the width of a line is 6144 pixels).
Print a magnitude plot for full master for future reference.

Write down the coordinates of the region of interest.
Around the region of interest in the master image, a border of about 40 pixels in range and 250 lines in azimuth should be present to assure that the (shifted) slave images do still contain the whole selected region of interest. If the baseline is very long, the range shift can be up to 80 pixels; if the Doppler centroid frequency is very high (e.g., due to ERS-2 operating with one gyroscope), the shift in azimuth can be up to 600 pixels. While cropping the slave images, a similar border should be taken into account. After coregistration, the region of interest will then be in the master and slave images.
(If region is small, consider oversampling the master and slave image by factor of 2 to obtain double(?) resolution / half pixel spacing. Divide PRF and RSR in parameter files by two, does this work?)

4. Start InSAR processing with Doris
Doris documentation:
http://www.geo.tudelft.nl/fmr/research/insar/sw/doris/Usersmanual/index.html.
script helpdoris.
Use Doris auxiliary program "run" to generate template input files for Doris interferometric software in directory masterorbit_slaveorbit.
See "run -h" for help.
Generate the inputfiles to the Doris processing step families in subdirectory Inputfiles and make subdirectory Outdata and Outinfo with run -g. Use, e.g., 'run -g -M 23710 -S 07334 -A "Rens Swart" -R "Tianjin Land Subsidence Observation project"'. If the baseline is approximately known, add "-B baselinelength", just for information.
With run -s#, Doris step number # can be performed; before running the processing step, run -e# will open the Doris input file in your editor.

If the SLC images were locally processed from raw images with ESARP: refer to steps a below
If the SLC images were acquired from a PAF: refer to steps b below
5a. Prepare the master image
Keep the master SLC image, generated with the ESARP processor, on CD. This is a raw image, i.e., without file and record headers, that can be directly processed by Doris.
According to our *Recipe SAR processing*, the precise orbits have been determined and recorded in the Doris result file orbit.res, written to CD. Copy this master result file to the directory masterorbit_slaveorbit and change the parameter Data_output_file in section _Start_crop to the location of the master SLC image.

5b. Prepare the master image
Because the SLC-images acquired from the Processing and Archiving Facility (PAF) has a file header and record headers, Doris must extract the header information to the master result file and extract the image to a raw SLC format without headers.
The reading of the parameter files, the acquirement of the precise orbits and the cropping to disk is performed with "run -s1". Check the parameters for this step with "run -e1" as follows, editing the Inputfiles/input.m_initial file.
To copy the region of interest in the master image generated by the (PAF) in a raw SLC format to disk, set the M_DBOW to the region to crop. Extend the region of interest determined in step 3 with a border in order to assure that all cropped slave images fall within this selection.

For the determination of the precise orbits with processing step m_porbits, change the question mark in parameter M_ORBDIR into the ERS number. Set the stepsize for the evaluation of the orbit (S_ORB_INTERVAL) to 15 seconds and the time before and after the acquistion of the SAR image (S_ORB_EXTRATIME) to 150 seconds.
After running Doris with "run -s1", check the orbit data in orbit.res.

6. Prepare the slave image
Prepare the slave data in directory masterorbit_slaveorbit. Determine the section of the slave image which contains the region of interest, determined from the master image in step 3. The region cut out from the slave image must be large enough to contain at least the region of interest of the master, in order to prevent problems during the resampling of the slave to the master grid, with a border as stated in step 3.

6a. Prepare the slave image
Use program 'bkcrop' to crop the slave SLC image from CD to disk. ('cpxfiddle' is not able to output complex two-byte integer as till now.) Name this file Outdata/slaveorbit.raw, e.g.
'bkcrop -i ../24122/24122.SLC -f 2 -q -w 6144 -c 1201 -r 5401 -R 26600 -o Outdata/24122.raw'.
Retrieve the resultfile with the SLC parameters and the precise orbit, generated in step 5 of the *SAR recipe*. Place this file "slaveorbit.res" in directory masterorbit_slaveorbit.
Otherwise, prepare the Doris input files and do 'run -s1' as in step 6b.
Edit the parameters in the crop section in "slaveorbit.res": set parameter Data_output_file to the location of the cropped slave image Outdata/slaveorbit.raw; edit first_line etc. according to the cropping operation.

6b. Prepare the slave image
This step is similar to the step for the master image, 5b.

7. Coarse coregistration
The coregistration is performed in three steps: coarse coregistration based on orbits, based on correlation and the fine coregistration based on correlation. The three steps can be run with 'run -s3' and then use template input file Inputfiles/input.coregistration. They can be run in one step the first time, but will be described separately.
Run Doris to obtain the coarse coregistration at pixel level. The first guess is made based on the orbits and has (if precise orbits are used) an accuracy of a few pixels in range and about 30 pixels in azimuth. This step coarseorb does not use input cards in Inputfiles/input.coregistration.
If the Doppler centroid frequency difference is high, e.g., for a pair with ERS-1 and an ERS-2 image acquired after February 2000, the offset estimated from the orbits is bad in azimuth direction. This is due to the large difference in antenna pointing (the perpendicularity condition is not met any more). We hope to improve this in the future.
Check offset in masterorbit_slaveorbit.res. Offset is positive if slave is to the upper left of the master, or, if the images are displayed on top of each other, if a point in the slave is to the lower right w.r.t. the same point in the master. If you want to check or if coarse coregistration is a problem, display the two images on top of each other with, e.g.,
'disrgfiles -w6144 -fci2 -Fci2 -l14000 -L16000 ../23710/23710.SLC /cdrom/scene1/24122.SLC'
and estimate offset on screen.

Denote perpendicular baseline in result file.
Estimate coarse coregistraton on data with step coarsecorr. Comment PROCESS coarseorb in input.coregistration out if necessary. Set CC_NWIN to 21 and CC_WINSIZE to 512 128. Use 'run -s3' to run Doris.
If (due to a large baseline, a large difference in Doppler centroid frequency or a large temporal separation) the estimates in masterorbit_slaveorbit.res are very dissimilar, estimate the offset visually from the two images displayed on top of each other as described above. Specify the initial offset by commenting 'CC_INITOFF orbit' out and adding 'CC_INITOFF azimoffset rangeoffset' with the visually estimated offset. Alternatively, increase the estimator window size CC_WINSIZE, although for this the initially estimated offset must be not too bad and this increases processing time considerably.

8. Spectral filtering
Basically do NOT apply spectral filtering to the data if the *permanent scatterer* technique is used.

If the classical interferometric approach is used, filter the master and slave in range if the perpendicular baseline is longer than about 150 meter and filter them in azimuth if the Doppler centroid frequency differs more than about 150 Hz. For the master, this means that as many versions of the master image are calculated as there are slave images.

Spectral filtering must be applied after the coarse coregistration has been performed, in order to calculate the fringe frequency based on the right combination of patches of the master and slave image. Apply range filtering before azimuth filtering, because as till now Doris takes the extent of the result of azimuth filtering to be equal to the largest of the previous images, which can be the whole SLC image.
For range filtering, use the method based on orbits (*porbits*) if the fringe frequency cannot be estimated from the interferogram, due to the large temporal separation or the large baseline. Otherwise, use the method based on the fringe frequency in the interferogram (*adaptive*). The orbit method can also be used if almost no topography is present.
For the orbit method, use a FFT-length of 1024; for the adaptive method, use a length of 64. Set RF_HAMMING to the appropriate Hammingweighing, being one for no weighing or a rectangular spectrum.
The extent of the range filtered images is taken equal to the part the master and slave have in common. Doris takes into account the offset between the master and slave image, determined by the coarse coregistration.
For azimuth filtering, set the FFT-length to 1024 and the Hammingweighing to the appropriate value.
The extent of the azimuth filtered images is taken equal to the consisting master or slave image by Doris as till now. Therefore, apply range filtering before azimuth filtering.

9. Fine coregistration estimation
Perform the fine coregistration to estimate the offset between master and slave image within approximately one fifth of a pixel. The integer offset estimated with the coarse coregistration steps (cf. 7 above) must be within a few pixels, otherwise the result will be erroneous.
Generally, follow the steps below:
Estimate with FFT-method based on magnitude.
Depending on the extent of the images and their coherence, use a grid of 1001 patches (FC_WIN = 1001) to obtain subpixel offset vectors and their correlation. By default use FC_WINSIZE = 64 64 and accL, accP = 8, 8. Plot vectors above correlation 0.4 and with

amplitude background (BG) with FC_PLOT 0.4 BG. Alternatively, comment out or set BG to NOBG. Run Doris with run -s3.
The offsets above the given correlation are drawn. This can be run separately to assess the offsets with a different correlation threshold or after some lines from the result file have been changed with the command 'plotoffsets 23710_24122.res 1 28000 1 6144 0.25 23710/23710.SLC &' or, if no background image is to be plotted, with 'plotoffsets 23710_24122.res 1 28000 1 6144 0.25 &'. With this program a sensible threshold for the correlation can be estimated.
If coregistration is a problem, consider azimuth and range filtering to improve it (but do not use these files to detect permanent scatterers!). In this case use FORMAT_CI2.
If a stack of images has to be coregistered, do not use a grid of estimation windows, but make a file with estimation window positions of highly coherent features in the following way.
For the first interferogram of the stack, use a dense grid (FC_WIN = 2001 or even 10001) and perform fine coregistration estimation as above.
Based on its output in the result file, create a file with master line/pixel coordinates of locations with expected high correlation. After selecting only the vectors from the res file in temporary file e1.res, this can be done for correlations > 0.25 with, e.g., "awk '$6 > 0.25 {print $2, $3, $6, $4, $5}' e1.res > coregwindows".
For the rest of the interferograms of the stack, use these windows by adding card 'FC_IN_POS coregwindows'. Card FC_NWIN then is ignored. In this way, within a limited computing time the fine registration is determined on the most coherent features.
If the classical interferometric approach is used, the production of a *stack*, coregistered on a central master, is not necessary. Instead, process all image pairs optimally by spectral filtering them and coregistering them separately. After calculation of the interferogram, for which the coregistration must be determined within a fifth of a pixel, several interferograms can be combined by calculating the offset with a one-pixel accuracy and resampling or coregistrating them.

10. Fine coregistration parameter modelling
Determine a model through the offset vectors determined by FINE (step 9), applying a threshold on the correlation of the individual windows with step coregpm.
Use a polynomial of degree 1 and set the threshold on the correlation.
Check solution/stability/stats in logfile. Check errors for individual points in plots of errors or in file CPM_data (based on which the plots are made). Check translation of corners in logfile out.resample.
Select points with large errors in azimuth or range with, e.g., "awk '{if (abs ($7) > 0.4 || abs ($8) > 0.3) {print $1, $2, $3, $7, $8}}' CPM_Data". Disable suspect points with large errors in res-file by giving them a very low correlation (e.g., 0.001).
Iteratively, run this step again with these points disabled. Possibly change the correlation threshold. (If repeating a Doris step: delete previous results from result file and set processing flag to 0.)
Repeat this until no outliers are present any more in the determination of the model. The largest error normally is larger for azimuth than for range. It depends on the coherence, thus on geometrical and temporal baseline. The largest error must be smaller than approximately 0.4 in range and 0.7 in azimuth. However, accomplishing this by keeping to delete points from the res-file is equivalent to adapting the data to the model.
In our experience, increasing the degree of the model from 1 to 2 or 3 is useless.

Alternatively, use our script coregpm.fast. This script is performing the above steps iteratively.
Run 'coregpm.fase Inputfiles/input.resample', after commenting keyword CPM_PLOT out.

11. Resampling
Interpolate the slave with the coregistration model determined in the previous step and crop it to the region of interest (step resample).
For the resampling, use a 6 points cubic convolution kernel (RS_METHOD cc6p).
Set output window to the region of interest, selected in step 3; choose this identical for all slave images (card RS_DBOW). Coordinates are in the original master image system.
If the Doppler centroid frequency differs more than 300, use SHIFT_AZI card. We have still to check this.
If Doris crashes, check variable FORSURE in code.
Probably use RS_OUT_FORMAT ci2. We have still to check the extent of data.

12. 'Raw' interferogram calculation
Calculate the interferogram by complex multiplication of the master and the coregistered slave image (step interfero). The interferogram will contain fringes because the reference phase was not yet subtracted.
Calculate the complex interferogram to a file named in card INT_OUT_CINT. Include a identification of the multilook factor in the name and add extension '.cint'., e.g.,
Outdata/21205_04538.25x5.cint.
Do not use INT_OUT_INT, which calculates the real valued interferogram.
Basically do NOT apply multilooking to the data if the *permanent scatterer* technique is used.
If the classical interferometric approach is used, multilook with 5 in azimuth to obtain square pixels of 20 x 20 meter and reduce noise.

13. Model reference phase
Model the reference phase (step comprefpha).
Use the precise orbits to calculate the phase of the reference body for a number of windows in the image. Use 'FE_METHOD porbits'
Use a polynomial of degree 5, 'FE_DEGREE 5'.
Use approximately 501 points, 'FE_NPOINTS 501' for full scene.
Check stability/solution/stats of solution in log file.

14. Calculate interferogram corrected for reference phase
Subtract the reference phase from the interferogram calculated in step 12.
Use 'SRP_METHOD polynomial' to evaulate the reference phase determined in step 13. 'SRP_METHOD exact' calculates the reference phase based on the orbits for each pixel individually.
If the classical interferometric approach is used, multilook with at least 20 x 4 (80 m pixels) or 25 x 5 (100 m pixels) to reduce noise and improve unwrapping. The multilooking factor in this step is multiplicative with that of the interfero step (12), so specify 'SRP_MULTILOOK 5 5' etc.
Specify a filename as 'SRP_OUT_CINT Outdata/21205_04538.25x5.srp'.
The reference phase image can be written to a file named in SRP_OUT_REFPHA by setting card SRP_DUMPREFPHA to ON.

Alternatively, one can skip the raw interferogram calculation of step 12. If step interfero is performed with the results of step 13 (comprefpha) already available, then the interferogram is calculated with the reference phae immediately subtracted. If doing this, account for the multilooking factor, that is not the product of the multilooking of step 12 and 14 any more but is specified directly.

15. Possibly subtract topography
Topography pair or digital elevation model should be good. Baseline ratio should be favourable. There should be topographic signal in interferograms.
Format: complex real4.
Filename: orbitmaster_orbitslave.srd.

16. Possibly check other interferogram combinations
Im1 .* conj (Im2) = I12 (m is master slc). ...

17. Multiply all images (permanent scatterers only)
If all images are coregistrated, multiply all images (mind the integer*2 range. Do with cpxmult?). Result according to Ferretti: mean amplitude, better resolution??

18. Filter interferogram (classical interferometry only)
To amplify the fringes in the interferogram and to reduce the noise, apply filtering to the interferogram (step filtphase).
Use the Goldstein filter for amplification of the fringe peak in the interferogram spectrum, 'PF_METHOD goldstein'. Use an alpha factor of 0.2 to 1 (preferably 0.5), a rectangular 5 wide filter as a smoothing kernel ('PF_KERNEL 5 1 1 1 1 1'), a overlap of 3 to 15 and a blocksize of 32.

19. Unwrap phase (classical interferometry only)
Unwrap the phase to remove the 2_-phase ambiguity. This cannot be done in Doris.
Use the tree algorithm of Stanford university, 'treefbk 320', where 320 is the number of lines.
Assess the unwrapping and extend it by supplying additional seeds. Write the result to a .hgt- and a .region-file.
Use Bert's Matlab-program manuwbk to split or join unwrapping regions and correct the 2_-ambiguity level.

20. Convert the slant range to height (classical interferometry only)
Can be done by Doris (step slant2h). Not used for processing of the Tianjin data.

21. Geocode the unwrapped interferometic image
Based on the orbits, the location of the radar pixels in an earth reference system can be calculated (step geocode).
A file with the height of each pixel is needed to correct for the slant range differenc height makes. For very flat areas, this height might be taken zero. Then a zero file is needed as till now.
This step results in a file with geographical longitude and latitude for each interferogram pixel.

22. Convert to deformation (classical interferometry only)

We projected the interferometric phase to vertical deformation, using the incidence angle and the assumption that the interferometric unwrapped phase is totally due to vertical deformation and no atmospheric delay nor uncorrected topography is present in the interferogram.
Possibly average over several independent interferograms by adding the unwrapped signal and divide by the sum of the temporal separations.
Present the deformation for a timespan that makes sense. If the time span is chosen larger than the consisting interferograms span, the atmospheric signal is undesirably amplified.

29. Store results
Store interferogram on CD-ROM.
Print plot of multilooked magnitude/phase. Check for interesting areas, use spinmap feature of disp -fcr4. Write down what you see or any possible problems.

Appendix B: Recipe for stack SAR-processing with ESARP

Rens Swart and Bert Kampes
Version 1.3 • 14 March 2001

This recipe is intended as a guide for the SAR processing as performed at the department of Geodesy of the Delft University of Technology. The processing of raw SAR images to SLC images is performed with the ESARP SAR processor of the Scripps Institution of Oceanography of the University of California, San Diego. This SAR processor is not in the public domain. For the interferometric processing with our public domain scientific interferometric processor *Doris*, refer to the *recipe InSAR processing*.

1. Make overview

entries:
#; orbit; platform; acquisition date; Btemp; Bperp; Doppler centroid frequency; #clipped points in esarp; #lines raw; #lines missing; #lines fixed; written on CD?; coregistration paramaters; remarks

2. Generate PRM file

Make directory for processing of this orbit.
Mount cd-rom with mountcd.
Check orbit number and date in /cdrom/scene1/vdf_dat.001.
Use pre_proc_dpaf /cdrom/scene1 orbit;
(see for script pre_proc_dpaf file '/home/fmr/opt/Siosar/Documents/RUNNING')
If ersbaseline fails: check www for new orbits or email Bert; if there are no orbits (e.g., for ers-1 between 6 Jun 1996 and 18 Jun 1999), use appropriate values for earth radius, spacecraft velocity, etc.: copy from other or use preliminary

3. Check line fixing

Missing lines are fixed by ers_line_fixer (in script pre_proc_dpaf, run in previous step).
Check this:
Calculate number of raw lines: divide file size by line length 11644. The number of actual data lines (n_record in orbitdat.log) is 1 less because the first line is a header.
Denote number of lines after fixing (calculate from file size) and number of reported missing lines in log file (use grep missing orbitfix.log).
ers_line_fixer replaces lines with a garbage counter with a copy of a previous line (file is not growing) and inserts a copy if the counter steps (file is growing). If you do not trust the fixing: use checkln around the line numbers ers_line_fixer reported missing, use: checkln orbit.fix 11644 startline 10 210 y 0
Write small script/use awks?
If number of lines is smaller than 28000, assure that num_patches in orbit.PRM is 10.

4. Generate SLC image from linefixed image with ESARP

Use the Scripps Institute of Oceanography SAR processor to process the linefixed raw ERS image to an integer*2 SLC (single look complex) image.

Process in such a way that the last lines are in the SLC image. This is normally the case if the previous steps were performed as prescribed. If not, assure that in file orbit.PRM:

num_valid_az = 2800
numpatches = 10
firstline = 1

Run with "esarp orbit.PRM orbit.SLC I2 >& orbitsar.log &" to write standard error messages to log file. Takes 3 minutes per patch or half an hour in total on the Baarda.
In general the Doppler centroid frequency is not known. If orbit.PRM contains fd1 = 0.0, fdd1 = 0.0 and fddd1 = 0.0, the linear term of the Doppler centroid is calculated for the first patch and written to screen. This value is used to focus the raw image in azimuth for all patches.
Write down estimated Doppler centroid and number of clipped points from log file.
Resulting image orbit.SLC is complex 2-byte integer, 28000 lines of 6144 pixels wide (688.128.000 bytes).
If fixing was OK and SLC-file is OK, delete file orbit.fix.

5. Generate Doris input file *orbit.res*

In Doris we skip the steps to read the SLC image and parameter files, because the SLC image was calculated with esarp. We have to generate the parameter file that Doris outputs in its reading steps from the PRM-file of esarp. Doris uses this file as input file and appends results of processing steps to it, as far as the results are typical for one of the interferometric pair of images.
Run "esarp2doris orbit s" to generate the Doris input/output file "slave.res" in the current directory. Rename it to "orbit.res" (with "orbit" the orbit number).
If the image is the master, omit the 's': run "esarp2doris orbit". In this case, no flag for the Doris processing step resample will be included.
In fact I ran my adaptiation /home/fmr/rswart/Progr/Verwerking/esarp2doris_rs, which takes the Doppler centroid from orbitsar.log if it is 0.0 in orbit.PRM and which calls the parameter file orbit.res instead of slave.res. Probably we will include this in script esarp2doris.
Check file orbit.res, especially the Doppler centroid frequency and the file names and folders.

6a. Make input files and subdirectories for Doris; get precise orbits

If only an SLC image for later use has to be made and no interferometric processing is performed, refer to step 6b. Otherwise:
Make directory for interferometric pair "masterorbit_slaveorbit", e.g., 23710_07334. If only one master is used, one could stay in directory "slaveorbit", e.g., 07334.
Use the run script, an auxiliary script to ease use of Doris. Get help with "run -h". First, generate the inputfiles to the Doris processing step families in subdirectory Inputfiles and make subdirectory Outdata and Outinfo. Use, e.g.,
run -g -M 23710 -S 07334 -A "Rens Swart" -R "Tianjin Land Subsidence Observation project". If the baseline is approximately known, add "-B baselinelength", just for information.
Check the Doris input file for the precise orbit generation for the slave (file Inputfiles/input.s_initial) with "run -e2". Comment the processing cards s_readfiles and s_crop out, because we intend to run Doris only to get the precise orbit, not to read the SLC-image from CD. In parameter S_ORBDIR change the question mark in the ERS number. Our last experiences indicate that the orbit should be interpolated with a piecewise

polynomial with only one piece over the image: set S_ORB_INTERVAL to 15 seconds and S_ORB_EXTRATIME to 150.
Run Doris step precise orbits with "run -s2". Check the orbit data in slaveorbit.res.
If you process the master image, do this for the input.m_initial file ("run -s1").
In the directory "masterorbit_slaveorbit", make a symbolic link named "masterorbit.res" to the file with the same name in the directory "masterorbit" with ln -s. Alternatively, change the location of the master result file in the Doris input files.

6b. Make input files and subdirectories for Doris
If only an SLC image for later use has to be made and no interferometric processing is performed, step 6a can be replaced by this step 6b.
No Doris directories and input files are necessary. Make a Doris input file to process the precise orbits. No other cards are necessary except PROCESS, S_RESFILE, S_ORBDIR, S_ORB_EXTRATIME and S_ORB_INTERVAL.
If you need this for several slaves, you can use a csh-script like /home/fmr/rswart/Progr/Verwerking/precorbits_rs. Probably we will include this in script esarp2doris.

7. Write all SLC-related files to CD-ROM
Obtain a 700 MB CD-ROM and make iso-CD-image with CDEveryWhere on PC (room René Reudink). Select only ISO9660 standard platform, level 2, no other platforms. This program downloads (network) files during making the iso-image. Write the image to CD with Adaptec Easy CD Creator.
Alternatively, use Easy CD Creator to write to CD after FTP-ing the files to the local PC. Use 8.3 conventional filenames. File naming conventions: orbit.SLC, orbit.res, orbit.PRM and the log files orbitldr.log, orbitdat.log, orbitfix.log, orbitsar.log.
Problem still to fix: case of filenames is not consequent. Probably select support for all platforms while using CDEveryWhere.

Appendix C: Internet links

http://www.geo.tudelft.nl/fmr/research/insar/dig/dig.html
Site of the Dutch Interferometry Group (DIG), here a full color copy of the report can be found.

http://www.deos.tudelft.nl/ers/precorbs/)
DEOS site of precise orbits.

http://www.geo.tudelft.nl/doris/
Site of Doris and additional software.

Appendix D: Figures in full color

In the following pages the most important graphics were selected for a full color print. The figures have not been printed in sequence of appearance, but were grouped by topic instead. The figures are printed in following order:

Figure 42: Result of PS software. 263 PS identified out of the initial 279 PS candidates. Deformation in mm/year over the period October 1992 / October 1998. Note that the offset allows for positive results.

Figure 43: Interpolated (bicubic) result of Figure 42 (limit of 50 mm/year in the deformation matrix).

Figure 51: Left mean deformation GPS/ leveling 1992-1999 (0-80 mm/yr), on the right side the same data, but scaled to enhance details in the urban area.

Figure 30: Phase of interferogram 21205-24122

Figure 31: Phase of interferogram 21205-04538.

Figure 32: Phase of interferogram 21205-23710.

Figure 33: Phase of interferogram 20203-23710.

Figure 34: Phase of interferogram 19702-23710.

Figure 35: Topographic phase signal in the interferogram 24122-23710. This interferogram can be considered to contain only topographic signal and noise.

Figure 39: Magnitude image combined with a deformation map

Figure 44 Vertical deformation maps for Tianjin city for 1996. Shown is the weighted average over five interferograms with temporal baselines of approximately half a year, from April 1995 to March 1996. Atmospheric signal remains present in this average, particularly visible in the blue (uplift) areas in the center. The data is georeferenced in the WGS84 system. For orientation the "Yongding He" and "Hai He" rivers are sketched on top. The white lines indicate the location of the two profiles shown in the figures 45 and 46.

Figure 47: Interferogram overlain by digitized contours

Figure 49: Leveling contours over InSAR result. The contour map was not annotated correct (apply factor 2), the shape of the lines clearly deviates from the InSAR result.

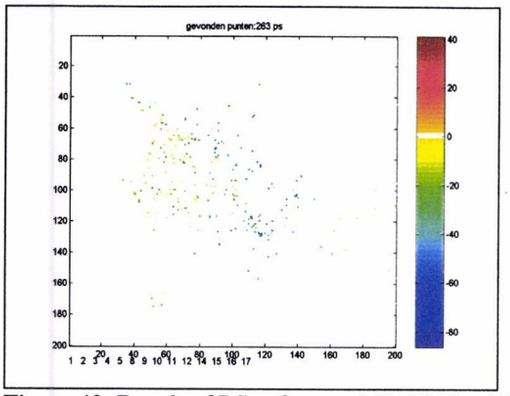

Figure 42: Result of PS software. 263 PS identified out of the initial 279 PS candidates. Deformation in mm/year over the period October 1992 / October 1998. Note that the offset allows for positive results.

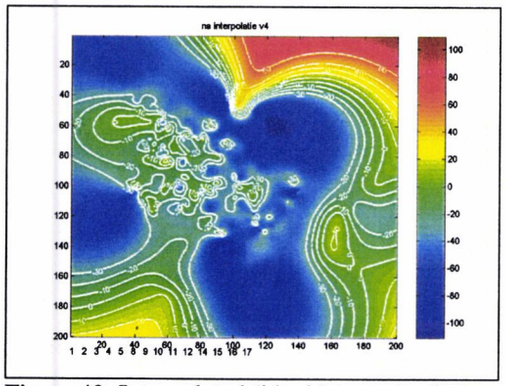

Figure 43: Interpolated (bicubic) result of Figure (limit of 50 mm/year in the deformation matrix).

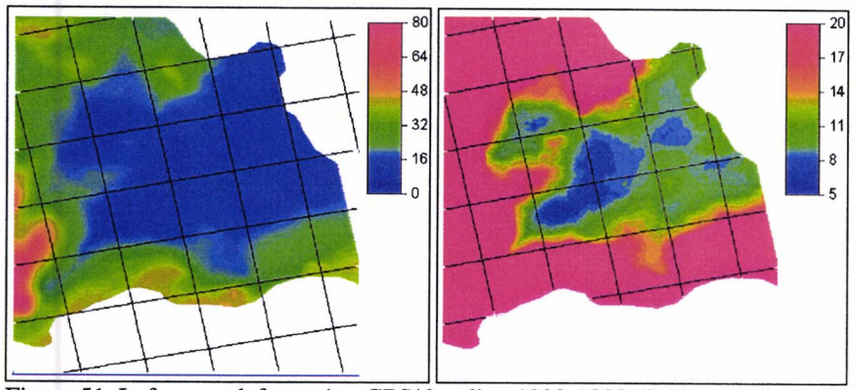

Figure 51: Left mean deformation GPS/ leveling 1992-1999 (0-80 mm/yr), on the right side the same data, but scaled to enhance details in the urban area.

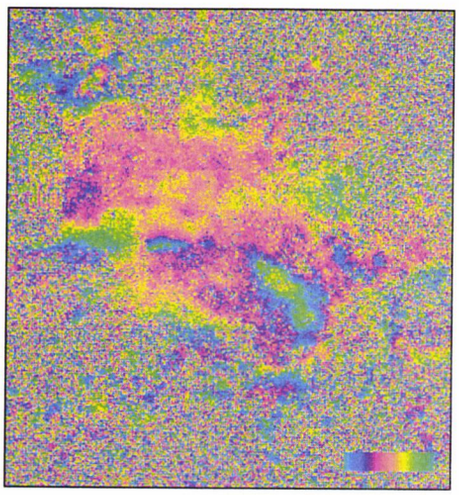

Figure 30 Phase of interferogram 21205-24122

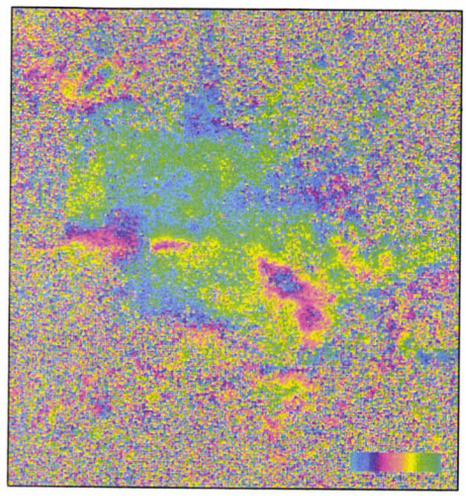

Figure 31 Phase of interferogram 21205-04538.

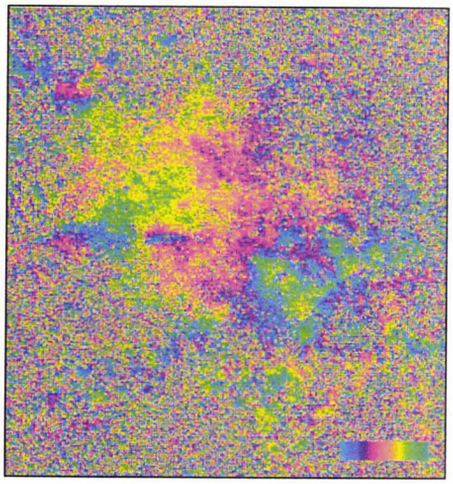

Figure 32 Phase of interferogram 21205-23710.

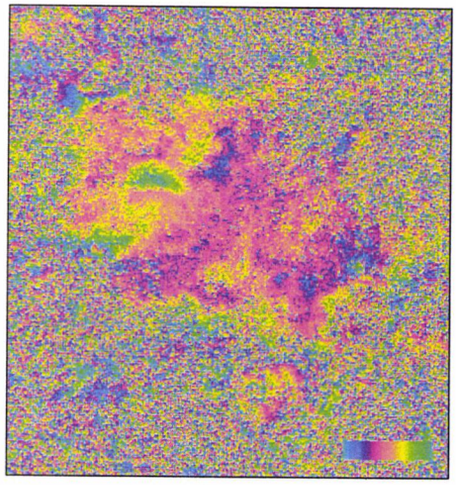

Figure 33 Phase of interferogram 20203-23710.

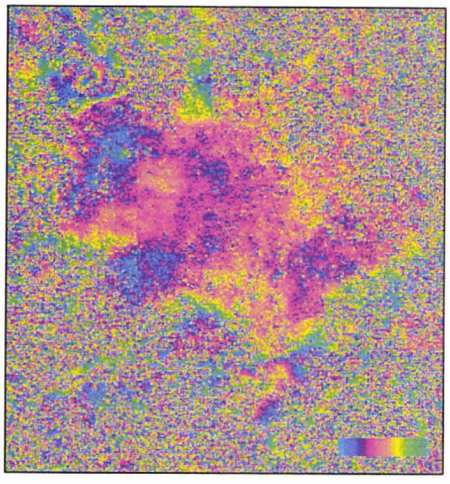

Figure 34 Phase of interferogram 19702-23710.

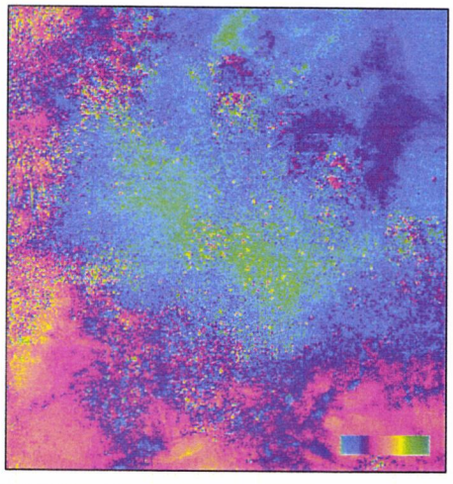

Figure 35 Topographic phase signal in the interferogram 24122-23710. This interferogram can be considered to contain only topographic signal and noise.

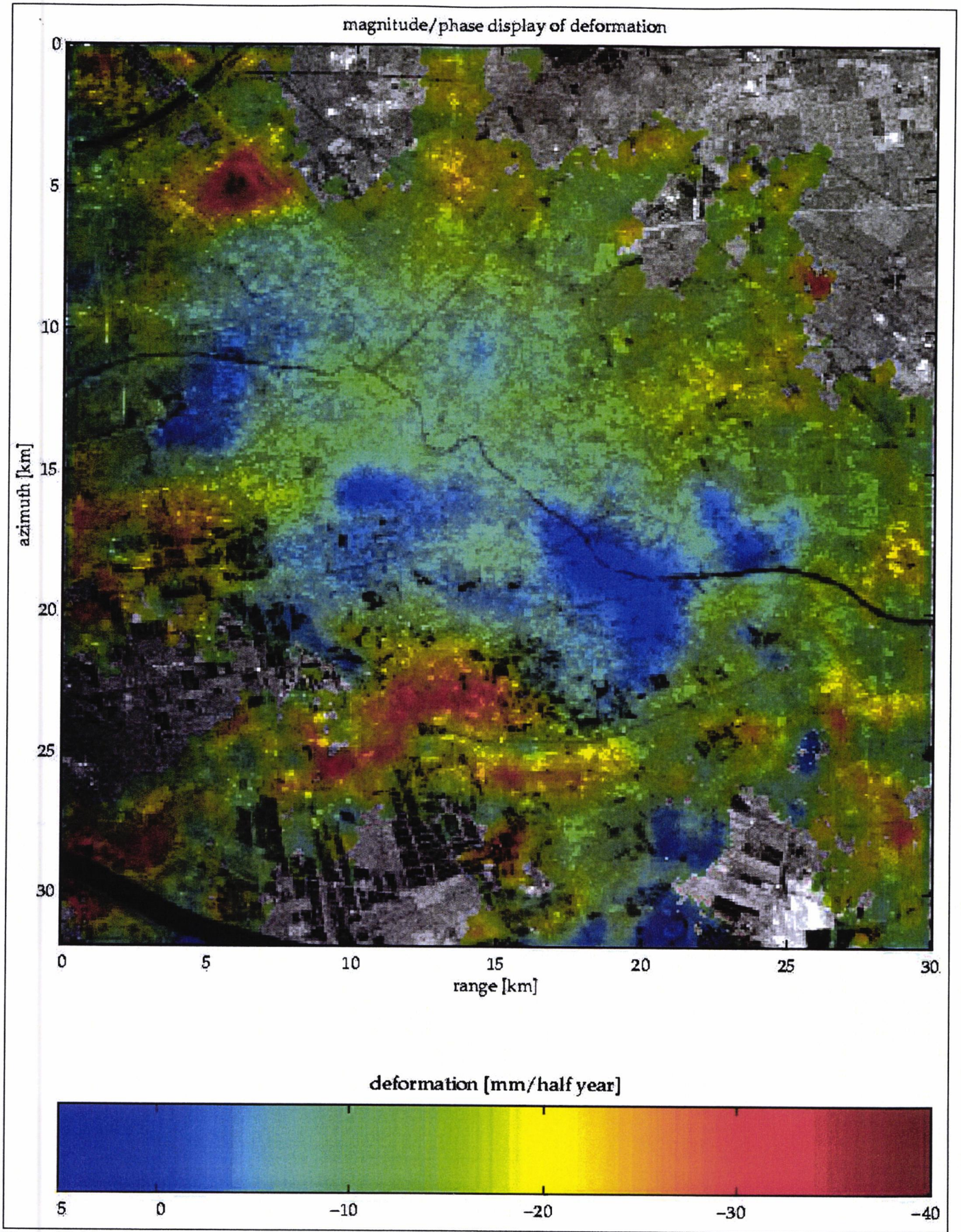

Figure 39, Magnitude image combined with a deformation map

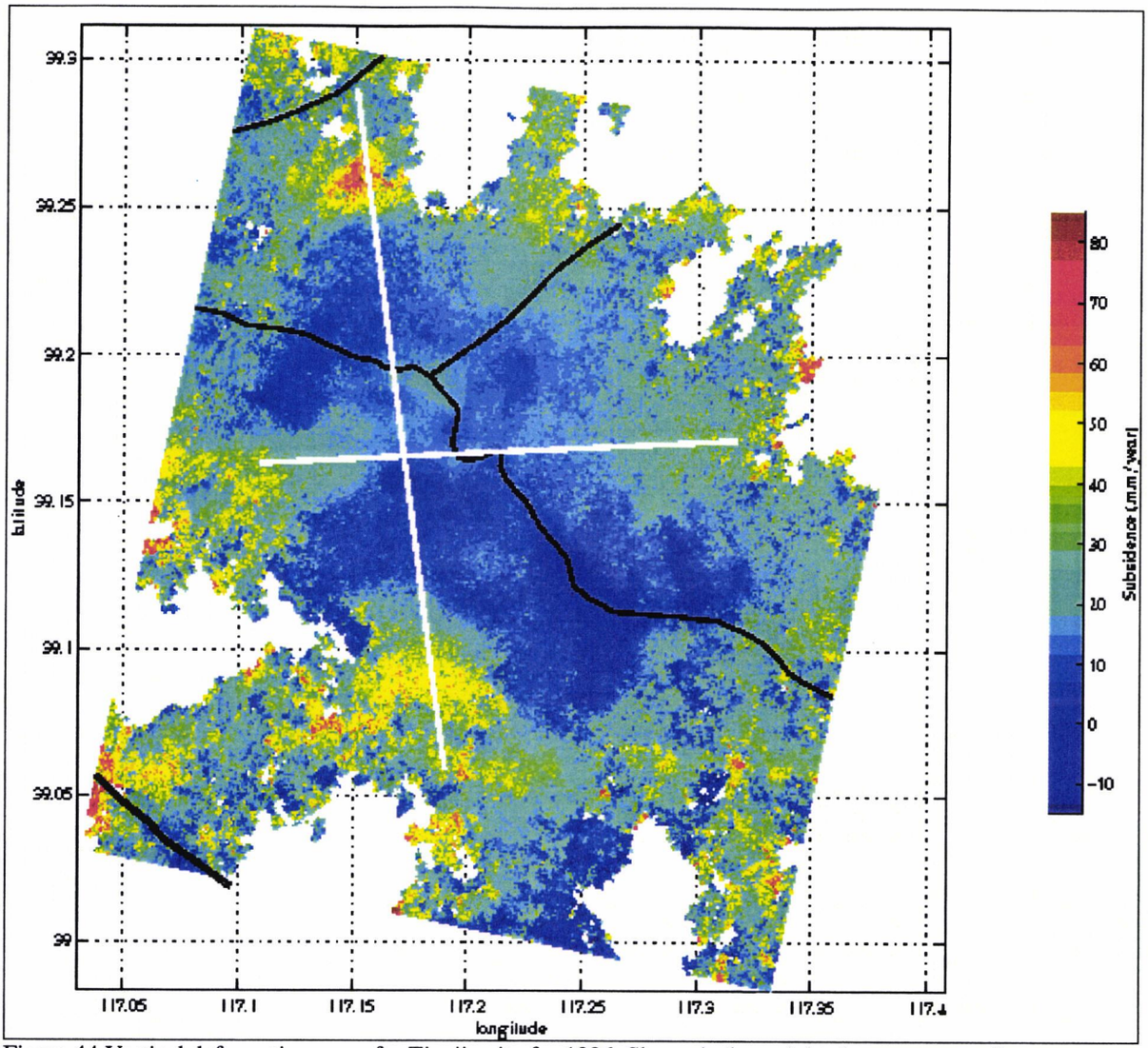

Figure 44 Vertical deformation maps for Tianjin city for 1996. Shown is the weighted average over five interferograms with temporal baselines of approximately half a year, from April 1995 to March 1996. Atmospheric signal remains present in this average, particularly visible in the blue (uplift) areas in the center. The data is georeferenced in the WGS84 system. For orientation the "Yongding He" and "Hai He" rivers are sketched on top. The white lines indicate the location of the two profiles shown in the figures 45 and 46.

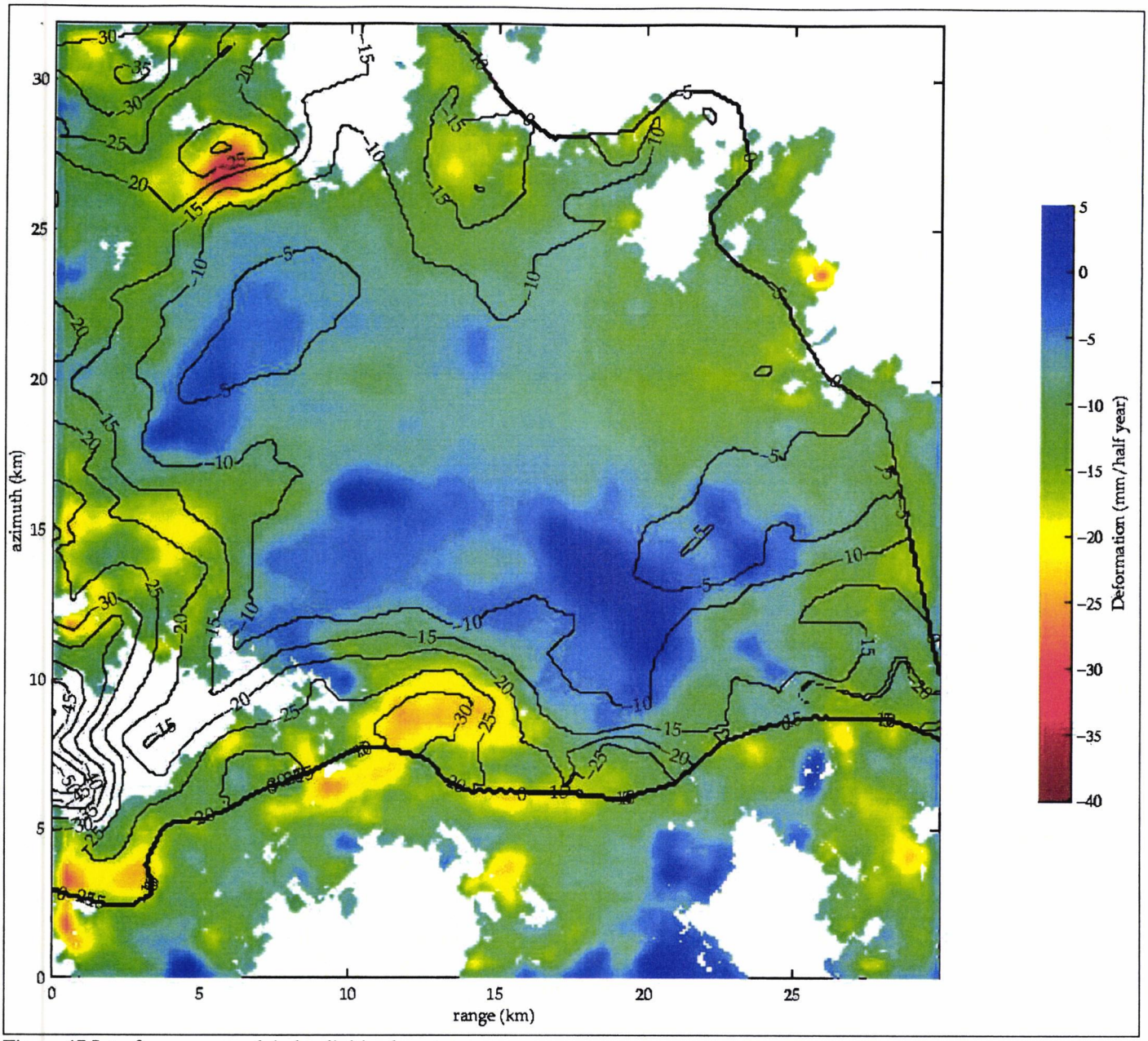

Figure 47 Interferogram overlain by digitized contours

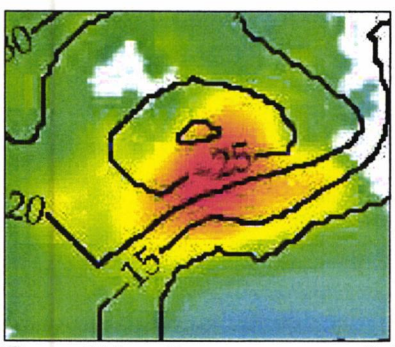

Figure 49 Leveling contours over InSAR result. The contour map was not annotated correct (apply factor 2), the shape of the lines clearly deviates from the InSAR result.

The National Remote Sensing Programme 1990-2000, (NRSP-2) is implemented under the responsibility of the Netherlands Remote Sensing Board (BCRS) and coordinated by the Ministry of Transport and Public Works.

The objectives of the NRSP-2 are: to secure the long-term integration of the operationel use of remote sensing through temporary stimulation in the user-sectors of government and industry, to strengthen the development of remote sensing applications and the expansion of the national infrastructure.

Publication of:

Netherlands Remote Sensing Board (BCRS)
Programme Bureau
Rijkswaterstaat Survey Department

P.O. Box 5023
2600 GA Delft
The Netherlands
Tel.: +31 (15) 269 11 11
Fax: +31 (15) 261 89 62
E-mail: p.b.bcrs@mdi.rws.minvenw.nl
BCRS homepage: http://www.minvenw.nl/rws/mdi/bcrs